TECHNISCHE UNIVERSITÄT MÜNCHEN
Lehrstuhl für Leichtbau

Parametric Model Order Reduction for Structural Analysis and Control

Eun Jung Yoo

Vollständiger Abdruck der von der Fakultät für Maschinenwesen der Technischen Universität München zur Erlangung des akademischen Grades eines

Doktor-Ingenieurs (Dr.-Ing.)

genehmigten Dissertation.

Vorsitzender:	Univ.-Prof. Dr.-Ing. Wolfgang A. Wall
Prüfer der Dissertation:	1. Univ.-Prof. Dr.-Ing. Horst Baier
	2. Univ.-Prof. Dr.-Ing. habil. Boris Lohmann

Die Dissertation wurde am 15.09.2010 bei der Technischen Universität München eingereicht und durch die Fakultät für Maschinenwesen am 16.11.2010 angenommen.

Gedruckt mit Unterstutzung des Deutschen Akademischen Austauschdienstes

Abstract:

For the analysis and control of large complex structures, many methods have been developed and are used. Finite element (FE) techniques fulfill a substantial role in structural analysis, furthermore in designing or controlling the structure. As finer methods are and the more accurate results they can provide, the required modeling and computational effort is larger. In particular, in space structures such as reflectors or solar array panels, size and complexity is increasing and structural requirements are getting stringent. Therefore, a large amount of simulation is required during the design and analysis stage. To increase computational efficiency, furthermore to enable an analysis with extremely high computation, model order reduction (MOR) techniques are developed and used; once the model has been transformed to low order space, computational effort for each analysis diminishes. Additionally MOR is required to design a proper controller especially in modern controller design, where the order of controller is increased with the order of system. However, the changes in thickness, material properties, and other design parameters can alter static and dynamic properties of the structure completely. Therefore the reduced model is no longer valid after parameter changes. In this dissertation, a method providing parameterized reduced models is developed so that parameter changes can be directly applied in the reduced space. The challenging part is considering physical and geometrical parameters directly from a large FE model, so that the application of reduction method is not limited for a controller design with chosen input/output configuration, instead, it extends to the overall static and dynamic analysis and control. The main reduction process is based on Krylov subspace iteration so that very large matrices are applicable. The parametric model order reduction (PMOR) method is developed for both static and dynamic analysis, and can be used for further application whenever a large number of analyses subject to parameter changes are required: for instance a design optimisation problem. A large reflector model and its shape control are examined as an example of static analysis. An active truss structure with piezo stack actuators and solar array panel with piezo patch actuators are shown for dynamic analysis and vibration control. Design optimizations of a composite plate and a mirror segment from the overwhelming large (OWL) telescope model are demonstrated using PMOR.

Kurzfassung:

Für die Analyse und Handhabung von großen komplexen Strukturen wurden viele Methoden entwickelt und eingesetzt. Finite Element (FE) Techniken nehmen eine wesentliche Rolle in der Strukturanalyse, im Design und der Reglung der Struktur ein. Je genauer die Methoden sind, desto exakter sind die Ergebnisse, die sie liefern, jedoch steigt der benötigte Modellierungs- und Berechnungsaufwand. In Raumfahrtstrukturen wie z.B. Reflektoren oder Solarkollektoren nimmt die Größe und Komplexität zu, sodass sich die strukturellen Anforderungen verschärfen. Dies macht eine große Anzahl von Simulationen und Auswertungen während der Design- und Analysephase erforderlich. Um die Recheneffizienz zu erhöhen und darüber hinaus Analysen mit sehr großen Berechnungen durchführen zu können werden Modellreduktionstechniken (Model Order Reduction, MOR) entwickelt und angewendet. Sobald das Model in einen Raum geringerer Ordnung reduziert wurde, wird der Berechnungsaufwand pro Analyse geringer. Zusätzlich benötigt man MOR für die Entwicklung von Reglern für moderne Steuerungen, bei denen die Ordnung des Reglers mit der Ordnung des Systems zunimmt. Trotzdem kann die Veränderung der Wandstärke, Materialeigenschaften und weiterer Parameter die statischen und dynamischen Eigenschaften einer Struktur vollständig verändern. Deshalb ist das reduzierte Modell nach Parameterveränderungen nicht mehr gültig. Im Rahmen dieser Dissertation wird eine Methode erarbeitet, die es ermöglicht, reduzierte parametrisierte Modelle zu erstellen, sodass Parameter direkt im reduzierten Raum verändert werden können. Der schwierigste Teil ist die Berücksichtigung physikalischer und geometrischer Parameter direkt aus einem großen FE-Modell, sodass die Reduktionmethode nicht nur für das Regler-Design mit ausgewählten Input/Output-Konfiguration, sondern auch für statische und dynamische Analysen und Kontrollen des Gesamtsystems angewendet werden kann. Der Hauptprozess der Reduktion basiert auf der Krylov-Unterraum-Iteration (Krylov subspace iteration), sodass sehr große Matrizen anwendbar sind. Die parametrischen Modellreduktionsmethode (Parametric Model Order Reduction, PMOR) wird sowohl für statische als auch dynamische Analysen entwickelt und ferner benutzt, wenn umfangreiche Analysen durch Parameteränderungen benötigt werden: zum Beispiel ein Design-Optimierung Problem. Ein großes Reflektormodell und seine Formkontrolle als ein Beispiel der statische Analyse untersucht. Eine aktive Fachwerkkonstruktion mit Piezoaktoren und Solarkollektoren mit Piezo-Patch-Aktuatoren werden für die dynamische Analyse und Schwingungsreduktion aufgezeigt. Die Designoptimierung eines Faserverbundplattemodell und eines Spiegel-Segments des Overwhelming Large (OWL) Teleskop-Modell werden anhand PMOR demonstriert.

Contents

List of Figures

List of Tables

1. Introduction

1.1. Motivation

Modeling and Simulation of structures are fundamental steps in engineering. The system is turned into an ordinary differential equation (ODE) analytically or numerically, and solved via various algorithms. The general approach to solve high derivative order of ODE is transforming it into the first derivative order matrix equation. Although the size of matrix is increased proportional to the number of variables and order of derivatives, in the end the problem is simplified to a large first-derivative matrix equation. After this transformation, the main problem of solving it is how large the matrix is, not how high the derivative order is. Therefore the term 'order' in model order reduction (MOR) means the size of the matrix, not the order of derivatives. As the structure or system becomes more complex, the required order of the model becomes higher. Therefore, reducing the order of model is an useful and practical idea to improve the computational efficiency of analyses. What Model Order Reduction (MOR) aims for is diminishing the computational effort while the accuracy of result remains same.

The concept of MOR is founded mathematically in eigen-value problems. Because eigen-analysis requires considerable amount of computation, $O(n^3)$, it would be very helpful if one could reduce the size of the model while keeping the accuracy of the eigen-values and vectors. Fundamental ideas and theories which are used in MOR are developed from solving eigen-problems. The application of MOR in physical problems is done in the control engineering field because reduced order models are very convenient to design a controller: in general the order of controller increases with the order of system, and considerably high order of controller is complicated to design because there are many poles and zeros which affect the stability of the system. Sometimes exceedingly high order of controller cannot be physically built. Systems with relatively small order, around a hundred, also need MOR because modern control methods such as linear quadratic regulator (LQR) generates a controller which has the same order as the system. Therefore, reducing the order of the system is necessary to design a physically feasible and robust controller.

The demands for MOR also arises from structural analysis, especially in these days as the finite element (FE) analysis is widely used. The principle of FE method is approximating a continuous physical structure by a summation of discretized elements. As the model is divided into finer elements, the approximated model is closer to the real structure. Therefore, to increase the accuracy of structural analysis, a complex large structure should be divided into small elements in FE analysis. Consequently the model has very large size, for instance several hundred thousand degrees of freedom. Such a large model increases computational time and effort, which is undesirable in

structural analysis, optimization as well as controller design.
From the above needs, model reduction techniques are studied and used in many fields of engineering and mathematics. Although they work well in each of their purpose, there still remain hurdles such as parametric MOR. When parameters of a system change, the entire system is changed. Consequently the reduced model is no longer valid. Every time parameters of the system alter, modeling, reduction, and analysis should be repeated as illustrated in Fig. 1.1. Since the reduction process itself requires a considerable amount of computation, up to $O(n^3)$, parameter changes could make MOR meaningless.
Parametric model order reduction (PMOR) makes not only the model smaller but also the reduced model managible to its parametric effects, so that once the reduction is done, the reduced model with different parameter values can be induced from the reduced space only, regardless of its original large model; this ability is expected to be very useful in optimization problems. Its concept is shown in Fig. 1.2. PMOR is a relatively new topic and several different approaches are being investigated intensively. Depending on what types of parameters are interested, for example, frequency band, material properties, and geometrical parameters, the approaches differ, which will be covered in the following chapters. Despite of such attempts to develope PMOR method, there have been general difficulties: first, the computational effort required for the reduction itself and second, the accuracy of reduced model including parametric changes. The effectivity of a method is not only how much it is mathematically correct, but also how much the time and cost efficiency it has. Therefore in this dissertation the computational cost and accuracy of the results from real structural models are observed, not only the level of operational numbers. The targetted model itself also not a state-space model which is already once formulated and reduced, but a raw structural model from FE software. Since most previous studies focus on first order dynamic systems in a state-space form, how to induce parameterized reduction procedure for second order dynamic systems and static systems, which are used more often in structural analysis, is more challenging and valuable work.

In this thesis, previous studies and theories concerning model order reduction and parametric model order reduction are introduced. Furthermore, improved PMOR methods for second order dynamic analysis as well as static analysis are suggested and investigated through numerical examples. A distinguishable contribution of this thesis is the improvement and modification of existing PMOR theory and real application of it. A method suggested here is realized in MATLAB, a numerical algebra software. As models, large finite element models from ANSYS, a commercial FE software, are examined. As a result, the algorithm for practical and larges scale structures is provided.

1.2. Literature survey

During the recent several decades, model order reduction has been investigated for simulation, control, and optimization of mechanical and electrical systems. As mentioned in section 1.1, the use of the finite element method helps us to analyze complex

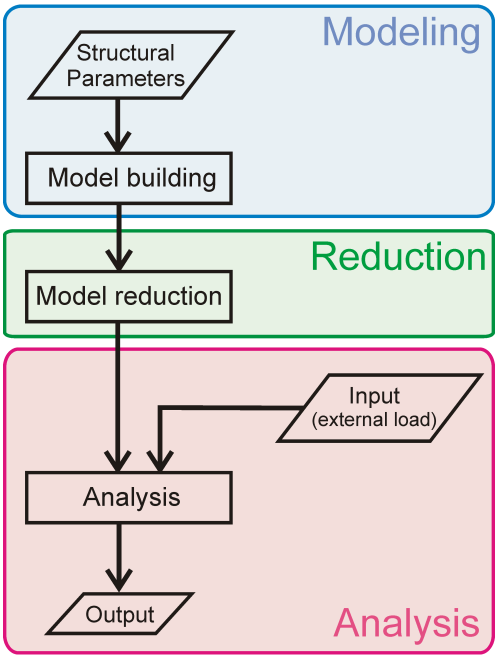

Figure 1.1.: Analysis procedure with general Model Order Reduction (MOR)

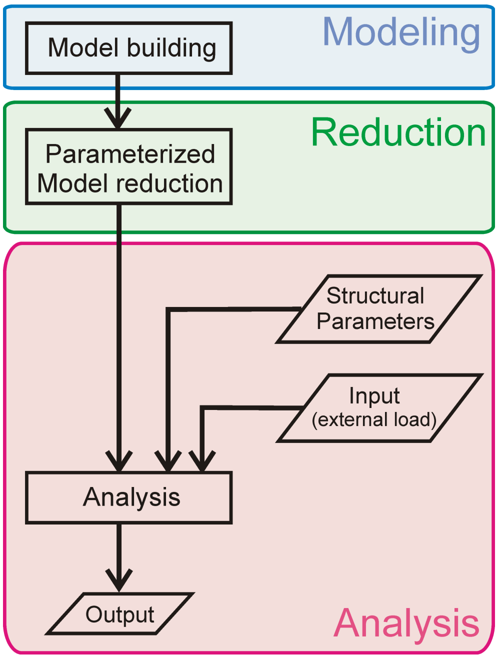

Figure 1.2.: Analysis procedure with Parametric Model Order Reduction (PMOR)

structures; however, the high computational effort associated with large models brings the needs to study model order reduction.

In this chapter, previously studied model order reduction (MOR) and parametric model order reduction (PMOR) theories are introduced. The flow and trend of MOR are shown here while the essential theorems and proofs are provided in chapter 2 and chapter 3.

1.2.1. Model order reduction (MOR)

1) Static systems

Since most of MOR theories are developed for a controller design of a dynamic system or eigen-value problems in linear algebra, the static problem is not actively studied. The fact that computational effort for static problem is much less than dynamic one is another reason why MOR for static analysis is rarely investigated. However, when the required number of analysis is high, model order reduction is helpful in static analysis as well. There exist two basic methods: Guyan reduction and Krylov subspace reduction. Note that these are not limited to the static problem, and applicable to the dynamic problem as well.

- **Transformation methods**

Guyan[Guy65] developed simple static reduction by integrating some dependent(slave) degrees of freedoms(dofs) or states into independent(master) dofs or states, so that a system is represented by master dofs or states only. Guyan reduction can be represented as a transformation from the space with full dofs or states to the space of master dofs or states only; hence it is often called transformation based reduction.

- **Projection methods**

Another type of reduction mostly used in these days is a projection method. The basic idea is projecting an original system onto a low order, compact mathematical space reflecting all the information we want to keep. Definition and usage of the projection matrix are written on page 11. By multiplying with the projection matrix, the mirror image of the system or matrix is obtained as a reduced model. The main differences between the transformation method and the projection method is that the reduced space can be re-reflected to the full space with the projection method, which is not possible with the transformation matrix. In [YB09], it is explained that the Krylov subspace from a stiffness matrix is a column space where the solution of the static problem lies; threefore, the Krylov subspace can be used as a projection space in static MOR.

2) Dynamic systems

Since a dynamic system requires much more computational effort coping with eigenanalysis, while a static analysis solves matrix-vector problems, order reduction for dynamic model have been actively investigated. In early stage, methods based on transformation are developed. But later projection based methods are preferred because of its capability to keep more information than transformation method and the capability to bring the model back to its original space.

- **Transformation methods**

Guyan reduction can be also used for dynamic problems[Guy65]. The slave dofs or states expressed with master dofs or states as in the static system are applied to the dynamic system. The limitation of the Guyan method is that the slave dofs or states are represented only by stiffness terms. Therefore some important terms from the inertia matrix might be omitted in the reduced model. To solve this problem, improved reduced system (IRS) has been developed. The IRS method uses both inertia and stiffness terms to represent slave dofs or states by master ones. It shows more accurate result than Guyan reduction[Fla90]. However, IRS method still has a limitation in its accuracy; when the selection of master dofs or states are not appropriate to reflect some modes of interest, the result is not correct.

- **Projection methods**

In modern MOR methods, projection is mainly used to overcome the disadvantages of Guyan and IRS methods. The most common method is the modal truncation method projecting the physical coordinates into modal coordinates. The most important advantages of the modal truncation method are (1) a direct relation to the physical system, and (2) decoupling of the system of the ordinary differential equations under some assumptions on damping behavior. The modal truncation method is good to preserve dynamic properties; however it cannot preserve boundary conditions. Craig and Bampton[CB68] combined Guyan reduction and modal truncation to keep both boundary condition and dynamic properties of a structure. Though its original intention was to connect substructures effectively, the basic idea is widely used in MOR. These four methods, Guyan, IRS, modal truncation, and the Craig-Bampton method, are adapted in many of commercial finite element programs such as ANSYS and NASTRAN.

Singular value decomposition (SVD) based method
In control engineering, on the other hand, different approaches have been investigated. Because controllability and observability of a system play important roles in controller design, their gramians are used in many MOR theories. One of the ideas which is called balanced truncation (BT) reduction is omitting uncontrollable and unobservable states of a system. After transforming a system into a balanced form, which has the same controllability and observability gramians, states with small Hankel singular values are eliminated[Moo81]. Another reduction method based on Gramians is Hankel norm approximation suggested by Gragg and Lindquist[GL83]. In [GL83], optimal reduction based on the largest Hankel singular value which is defined as a Hankel norm is suggested. Both BT reduction and Hankel norm approximation methods are based on singular value decomposition (SVD). As a benefit, the reduced system has a global error bound, and the stability from the original model is preserved[Glo84, Enn84]. Their application is limited to the low dimension up to several hundreds because the solution of two Lyapunov equations which causes computation order of $O(n^3)$ is included during the reduction. Nevertheless, BT reduction is used in many academical or practical examples[ASG01, FI01, GAB01, Ben06, YRS04]. Its limitation on the number of dimensions can be solved by applying modal truncation before BT reduction. Many attempts exist to diminish the high computation during BT reduction; for example, Gawronski [Gaw98] suggested an approximation of balanced representation. From the observation that gramians have low numerical rank in many cases, low-rank Cholesky factors are used to approximate gramians. The Smith method is used to iteratively solve Lyapunov equations in [GSA03]. However, the computational order increases to $O(n^3)$ for Schur decomposition shown later.

Krylov subspace based method
Apart from SVD, the Krylov subspace method is another big topic in modern model order reduction study. The idea is to find a proper approximation of a transfer function of a system, matching the coefficients of the transfer function. Because the low frequency range is more interested in general, the coefficients with low order Laplace variable s are preserved.
The Padé approximant, developed by Henri Padé, is adapted for approximation. Ville-

magne and Skelton[VS87] transformed moments of a transfer function, which is coefficients of Padé approximation of a transfer function, into a Krylov subspace form. Oblique projection is applied to obtain reduced model, and moment matching properties are also proved.

Three representative algorithms for Padé approximation exist: Asymptotic waveform evaluation (AWE), Arnoldi algorithm, and Lanczos algorithm. Furthermore, many variations of them are developed for higher accuracy or multi-input multi-output (MIMO) application or passivity preservation or computaional efficiency. Asymptotic waveform evaluation proposed by Pillage[PR90] is an explicit moment matching method; it is easily understandable and implementable. But the order of transfer function which guarantees good accuracy is very limited because of the numerical instability.

The others, Arnoldi and Lanczos, are based on the Krylov subspace. Lanczos developed an iteration method for the eigenvalue problem in 1950[Lan50]. The Lanczos algorithm is computationally cheap, and applicable to a higher order system. However it is not always numerically stable. To prevent a break down during the iteration, a look-ahead method is suggested by Freund[FGEM93], and a deflation technique is also used for better orthogonality in many cases where Lanczos algorithm is used[LS96]. Feldmann and Freund[FR95] applied a look-ahead lanczos algorithm for Pade approximation of a transfer function, which is called Pade via Lanczos (PVL) method. It shows higher numerical stability and high accuracy near the Pade expansion point(frequency) keeping computational cost low. For multi-input multi-output (MIMO) system, the block Lanczos algorithm as in [GLO81, KCJ88] and matrix Pade via Lanczos (MPVL) have been developed[SL99]. As a further improvement, Wittig[WMSW02] suggested a two-step Lanczos method to reduce computational cost further. After a system is reduced via normal Lanczos iteration, PVL is applied as the second step.

The Arnoldi algorithm is another representative iterational method for Krylov subspace computation. Like the Lanczos algorithm, it was initially developed for eigenvalue analysis by Arnoldi[Arn51]. Silveira et al.[SKEW99] used the Arnoldi algorithm to generate a Krylov subspace for moment matching model reduction. The Arnoldi algorithm is based on the Gram-Schmidt process and is a one-side method unlike the Lanczos method, which is a two-sided method. For a MIMO system the block Arnoldi algorithm is suggested by Boley[Bol94]. Many attempts to improve the Arnoldi method have also been followed. To overcome the major disadvantage of the Krylov subspace method, loss of stability, Odabasioglu et al.[OCP98] developed passive reduced-order interconnect macromodeling algorithm (PRIMA). It is designed to preserve passivity during the model reduction of a RLC circuit via a block Arnoldi algorithm, and congruence transformation. PRIMA is superior to MPVC because of passivity preservation; however this property is limited to RLC circuit systems. On the other hand, Salimbahrami et al.[SBLK03] achieved performance similar to Lanczos method by developing the two-sided Arnoldi algorithm. The two-sided Arnoldi algorithm uses the Arnoldi iteration twice: one for the input Krylov subspace and the other for the output Krylov subspace. Consequently the reduced model can match twice as many moments than the general Arnoldi method can. With the same reduced order, there is also no numerical instability which Lanczos has. It can be further applied to the second order dynamic system, as the most of the structural models. Several MIMO examples are also presented[Sal05]. Bai and Su[BS05] also presented the second order Krylov method based on Arnoldi algorithm, which is called second order Arnoldi reduction (SOAR). Lampe and Voss[LV] demonstrated numerical examples with SOAR. Meanwhile Lin et al.[LBW07] extended SOAR to MIMO system calling it as the block second order Arnoldi reduction (BSOAR). Chu[CLF06] proposed global Arnoldi algorithm to prevent numerical ill-conditioning due to deflation. Instead of Gram-Schmidt process, the Frobenius process is used for orthonormalization.

In [MM03] Prony's least square approximation method is adapted instead of Pade approximation to build a reduced model. With bilinear transformation, Prony's method results in smaller model matching more poles and zeros.

Proper orthogonal decomposition (POD) method
The POD method is a sampling based reduction. From snapshots of the states, the optimal bases to describe these snapshots are found. The relation between POD and SVD makes POD applicable for model order reduction. It is used for dynamic analysis of structures[FK98, KF00a, KF00b, MVB01, GS99], and Micro Electro-Mechanical Systems (MEMS)[LLL$^+$01]. Since POD is applicable to nonlinear systems, it is desirable to the field of fluid dynamics or aerodynamics. In 80s Sirovich[Sir87] showed a possible use of POD in analyzing coherent structures of a turbulent flow. Willcox and Peraire[WP02] applied POD method to a two-dimensional airfoil model for the computational fluid dynamics (CFD) analysis. However, the accuracy of reduced model is significantly dependent on the choice of snapshots.

1.2.2. Parametric model order reduction (PMOR)

Parametric model order reduction (PMOR) is motivated from the needs of designing structures or controllers more efficiently. During the designing process parameters of the structure are varied; however, with general model order reduction (MOR) the reduced model is no longer valid under parameter changes. Therefore many studies to overcome this limitation have been investigated. The goal is including parametric effects into the reduced space based on general MOR methods, such as SVD and Krylov. The approaches are divided first by what kind of parameters are considered and secondly how to treat their effects. For the case when the frequency range is considered as parameter, rational MOR methods are developed. Focusing on system parameters, mainly two approaches are suggested: first, extracting parametric effects before the reduction and finding a reduced space which can keep parameter effects; second, reducing sample models individually and approximating the reduced model with different parameter values based on interpolation.

1) Rational model order reduction

Because Padé approximation provides high accuracy near the reference point of the Padé expansion, the reference point which represents an interesting frequency range could be an important parameter in some studies. Rational reduction methods are studied for changing reference frequency after the reduction. Ruhe[Ruh84] suggested the rational Krylov method for eigenvalue computation in 1984. The column space for the projection is collected from Krylov subspaces of various frequencies. Subsequently Ruhe and Skoop[RS98] used a rational Krylov algorithm based on shifted and inverted Arnoldi iteration for model reduction. As a further application, Weile and Michielssen[WM01] added two system parameters to general rational Krylov method. Rational reduction has also been applied for optimal H_2 model reduction by Gugecrin et al.[GAB08] In the field of SVD based reduction, Phillips and Silveira[PS05] designed Poor Man's Truncated Balanced Representation (PMTBR) applying multipoint rational approximation technique to BT reduction. Rational reduction is used in controller design[Gil06]; however, rational reduction changes the expansion points, not the system matrix itself. Consequently it should be treated as a different field of study from PMOR concerning system parameter changes.

2) PMOR with system parameters

Parameters of interest here can alter the system matrix, such as physical or geometrical parameters of structures, or parameters from electric circuits, etc. Shi et al.[SHS06] studied Symbolic MOR; however, its application is very limited to simple analytical models. Apart from that, two major approaches exist: one is finding a common projector, and the other is interpolating various parameter cases.

Multiparameter moment matching method
Daniel[DSC+04] suggested a multiparameter moment matching reduction method finding a common projection space which contains parametric effects as well as the characteristics of the original system. This method requires knowledge about how parameters affect the system, and provides an accurate result. In recent years, it has been actively applied, especially in multi-disciplinary problems such as electro-thermal systems or electro-mechanical systems, for instance Micro Electro-Mechanical Systems (MEMS)[MRG+05, RFS+, FRK05, FKRK05, BD05]. For the application to mechanical structures, there are some disadvantages due to the existance of inversions and limitations from the Gram-Schmidt process: Calculating and multiplying the inversion matrix cause very high computational effort as well as a memory problem, and the round-off errors and badly chosen basis during Krylov iteration bring the loss of orthogonality in the Gram-Schmidt process, which ends up with singularity of reduced model. Through this dissertation, these problems are observed and improved.

Interpolation based method
The interpolation based PMOR method does not substract parametric effects before reduction and preserves them during reduction as Daniel's method does, but approximates parametric effects after reduction. The models with various parameter values are reduced individually and transformed to a proper manifold for interpolation. According to the space where interpolation occurs and the interpolation algorithm itself, different methods are presented. Lohmann and Eid[LE09] suggested the state transformation to have a common physical interpretation and performed linear approximation with weight functions. Degroote et al.[DVW09] proposed spline interpolation among the reduced models from proper orthogonal decomposition. Both ouput space and tangential Riemann manifolds have been tested as an interpolation space. Amsallem

et al.[ACCF09] used modal truncation for order reduction and applied generalized matrix interpolation. This is quite a new field of study, and there are still many open questions, for instance which space will be optimal for the interpolation, and which interpolation algorithm is computationally cheap but still accurate. Another concern is the computational cost when many parameters are involved; if the required number of reference parameter sets increases, then computation for each reduction and interpolation will be very high. Because the interpolation method is independent from the reduction method itself, numerous combinations of reduction algorithm and interpolation method seem to be possible.

1.2.3. Outlook from literature survey

As the demanding computational effort in analysis, design, and control of structures increases, model order reduction methods are widely used: for instance, for faster dynamic analysis or controller design. Responding to those needs various methods and algorithms are developed to fulfill specific requirements, for example accuracy of reduced model, or robustness of reduction algorithms, or preservation of controllability/observaility. The challenge in MOR is the adaptation of parameter changes. Because of the high demands on parameter studies during structural design and control, the ability to change parameter values after reduction is emphasized, especially from the fact that a reduction procedure requires considerable amount of calculations. Therefore in recent studies, various attempts to include parametric effects in the reduced model are made. The limitation so far is that only simple models with a few parameters are tested, and the parameters considered in previous studies are not structural parameters such as material properties, but system parameters which are easily seperable from structural models. Interpolation based PMOR method may have better opportunity to use various typse of parameters; but the models from each parameter set needs to be reduced and to which space they should be subjected and interpolated is not clearly found yet. Therefore parametric model reduction method which enable to track down the structural parameters merged in FE model is still in demand and needed to be investigated.

1.3. Thesis outline

This thesis aims to develop practically efficient parametric model order reduction (PMOR) method and show its results using some exemplary structures. First, detailed theories in model order reduction (MOR) are shown in chapter 2. Since advanced methods are derived from existing ones keeping its properties, it is necessary to know fundamental theorems and proofs to support the validity of new ones. Among the numerious variations of MOR theories, fundamental ones such as modal truncation, balanced truncation, and the Krylov subspace method are presented.

PMOR theories are followed by chapter 3. Two main approaches, common projector development and the interpolation based method, are presented.

The improved method investigated in this dissertation will be shown in chapter 4 theoretically. Even for the theoretical development, methods how to handle each physical or geometrical parameters in FE model are covered with high importance, because the final goal is practically useful method. Improvements of methods to solve the problems occurred during applications are also shown in chapter 4. Both methods for static and dynamic analyses are presented. The method based on LU decomposition is introduced to prevent calculating inversion of a matrix.

The application of the method is provided in chapter 5. In the static case, a large reflector is used as an example. Material properties such as modulus and density, and geometrical property such as thickness of the shell are considered as parameters. Deflection under an arbitrary loading is observed and shape control is performed by calculating optimal actuations. Both an active truss structure and a solar array panel model are taken as examples for dynamic problems. Parameters are properties of the composite material, nonstructural masses, and thicknesses. Natural frequencies and mode shapes are examined, vibration control is performed using a positive position feedback controller or linear quadratic regulator. Various parameter sets are applied to examine whether the reduced model can successfully be influenced by parameter changes or not. The potential use of PMOR in design optimization is prospected in chapter 5 as well. Considering design variables as parameters, designing material properties and geometrical properties of mirror panels from overwhelming large telescope (OWL) model is shown as well as designing a composite plate.

Conclusion follows in chapter 6. The models and theories requested to develop the numerical models are provided in an Appendix A. Additional results from chapter 5 are provided in Appendix B.

2. Theories of Model Order Reduction

As introduced in section 1.2, there are many model order reduction (MOR) methods and variations of them. Most recent work is based on projection technique, because it is easy to reconvert the reduced states to the full order states by back-projection. A projection transforms a target vector or vector space into the vector or vector space consisting only the elements in the projection space. From the target vector or vector space, the elements which are parallel to the projection space are kept and the elements which are orthogonal to it are removed as illustrated in Fig. 2.1.

The projection matrix P consists of row vectors which represent the projection space. When the row vectors of P are orthogonal to each other, the projection matrix becomes an orthogonal projector as defined in equation (2.1).

$$P^2 = P,\ P^T P = I \tag{2.1}$$

When the row vectors of P are not orthogonal to each other, it becomes an oblique projector as defined in (2.2).

$$P^2 = P \tag{2.2}$$

If the projected space has lower dimension than the original space such that $P \in \mathbb{R}^{r\times n}$ where $r \ll n$, we can reduce the system A by multiplying P, $A_r = PA \in \mathbb{R}^{r\times n}$. The question remains is how to properly choose the projection matrix P to preserve the most important information of the original system A. In this chapter, the kinds of MOR techniques are reviewed according to on which space and with which method the model is projected. The characteristics of each method are followed as well.

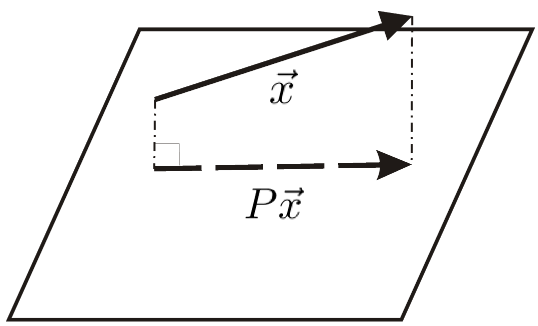

Figure 2.1.: Projection

2.1. Modal truncation method

For the physical system, an equation of motion is defined as in (2.3) in time domain.

$$M\ddot{x}(t) + D\dot{x}(t) + Kx(t) = f(t) \tag{2.3}$$

where M is a mass matrix, D is a damping matrix, K is a stiffness matrix, x is a vector of physical degrees of freedom(dofs), and f is an external force. It can be rewritten as the first order state space equation in physical domain as in (2.4).

$$\begin{bmatrix} M & 0 \\ 0 & I \end{bmatrix} \dot{z} + \begin{bmatrix} D & K \\ -I & 0 \end{bmatrix} z = \begin{Bmatrix} f \\ 0 \end{Bmatrix} \text{,where } z = \begin{Bmatrix} \dot{x} \\ x \end{Bmatrix}$$

$$\dot{z} = \begin{bmatrix} M^{-1} & 0 \\ 0 & I \end{bmatrix} \begin{bmatrix} -D & -K \\ I & 0 \end{bmatrix} z + \begin{Bmatrix} f \\ 0 \end{Bmatrix} \tag{2.4}$$

$$\dot{z} = Az + b$$

In continuous structures, M, K, and D are generally not diagonal; therefore the degrees of freedom in x are coupled with each other.
The solution x is a combination of a homogeneous solution x_c and particular solution x_p such that $M\ddot{x}_c + D\dot{x}_c + Kx_c = 0$ and $M\ddot{x}_p + D\dot{x}_p + Kx_p = f$. The dynamic characteristics of a structure are contained in x_c, the free vibration solution; therefore we will focus on x_c. Assuming that there is no damping, x_c is as shown in equation (2.5).

$$x_c(t) = \sum_i a_i \phi_i e^{\lambda_i t} \tag{2.5}$$

where a_is are scalars, λ_is are eigen-values, and ϕ_is are corresponding eigen-vectors

The idea of the modal truncation method comes from above equation; the dynamic response of a structure is a linear combination of eigenforms. It means that the mode shapes are the bases of the reponse space of a structure. Using those eigenforms as bases of a projector, the model in physical space can be projected onto a modal space. When damping is involved, eigen-frequencies are shifted but mode shapes remain almost same especially when damping is small or modeled as modal damping or proportional damping. To reduce the size of the model, not all modes but only some of the modes are selected and the projection matrix P has chosen eigenvectors as row vectors as shown in equation (2.6).

$$P = \begin{bmatrix} \phi_1^T \\ \phi_2^T \\ \vdots \\ \phi_r^T \end{bmatrix} \tag{2.6}$$

Since eigen-vectors(ϕ_is) are orthogonal to each other, P becomes an orthogonal projector. When this projector is applied to the equation of motion as in equation (2.3), system matrices such as mass, damping, and stiffness matrices will be reduced as in equation (2.7).

$$M_r\ddot{x}_r(t) + D_r\dot{x}_r(t) + K_r x_r(t) = f_r \tag{2.7}$$

$$\text{where } M_r = PMP^T, \quad D_r = PDP^T, \quad K_r = PKP^T$$
$$P^T x_r = x, \quad f_r = Pf$$

It keeps the eigen-values (natural frequencies) and eigen-vectors (mode shapes) of the original model for the chosen corresponding modes. As the columns of the projector represent physically deformed form on each mode, it is easy to see how the structure will respond even after the reduction. The challenging part in the modal truncation method is which modes are important or not. Depending on target structures some interesting modes are selected: for instance, the lowest some modes, or modes near a target frequency, or modes which have high effective mass, which is explained in A.2. The main drawback of the modal truncation method is the spill-over problem, which is an instability caused by neglected high frequency eigenmodes. Spill-over may bring significant structural instability when the control system excite high natural frequency which is omitted in the reduced model. Additionally, high order of computation, $O(n^3)$, and some boundary conditions which are not preserved in the reduced model are other problems.
The Craig-Bampton method is a modification of modal truncation method to release the last limitation. Degrees of freedoms (dofs) are first divided into dofs assigned for boundary dofs x_B and dofs of internal area x_I. x_I is expressed as a summation of mode shape and rigid body vectors as in equation (2.8).

$$x_r = \begin{Bmatrix} x_B \\ x_I \end{Bmatrix} = \begin{bmatrix} I & 0 \\ \phi_R & \phi_m \end{bmatrix} \begin{Bmatrix} x_B \\ q_I \end{Bmatrix} = T_{cb} \begin{Bmatrix} x_B \\ q_I \end{Bmatrix} \tag{2.8}$$

where x_B : boundary dofs
x_I : internal dofs
ϕ_R : rigid body vectors from each boundary dofs
ϕ_m : fixed base mode shapes
q_I : modal dofs in internal area
T_{cb} : Craig-Bampton transformation matrix

By multiplying T_{cb}^T as a projector, mass, stiffness, and damping matrices also can be reduced as follows.

$$M_r\ddot{x}_r(t) + D_r\dot{x}_r(t) + K_r x_r(t) = f_r \tag{2.9}$$

$$\text{where } M_r = T_{cb}^T M T_{cb}, \quad D_r = T_{cb}^T D T_{cb}, \quad K_r = T_{cb}^T K T_{cb}$$
$$T_{cb} x_r = x, \quad f_r = T_{cb}^T f$$

Modal truncation method and Craig-Bampton method are widely used in these days. They can provide direct insight to the physical states, and high accuracy for the chosen modes. The high computation effort for eigen-analysis is alleviated by iterative methods such as Lanczos method or subspace method. However, spill-over problem still remains.

2.2. Balanced truncation method

While modal truncation method and Craig-Bampton method dominate in structural analysis, different approaches are investigated based on controllability and observability from control engineering side. Controllability is defined as the ability to send any initial state to any finite state within finite time, and observability is defined as the ability to determine a current state from the output. Their mathematical definitions are described in Theorem 2.1 and in Theorem 2.2 accordingly.

Theorem 2.1 *The following continous-time system in equation (2.10) is controllable, when the rank of matrix of controllability matrix R is the same with the size of A, n.*

$$\dot{z} = Az + Bu \quad A \in \mathbb{R}^{n\times n} \tag{2.10}$$

$$R = \begin{bmatrix} B \,| & AB\,| & \cdots | & A^{n-1}B \end{bmatrix} \tag{2.11}$$

□

Theorem 2.2 *The following continous-time system in equation (2.12) is observable, when the rank of matrix of observability matrix O is the same with the size of A, n.*

$$\begin{aligned} \dot{z} &= Az + Bu \quad A \in \mathbb{R}^{n\times n} \\ y &= Cz + Du \quad C \in \mathbb{R}^{m\times n} \end{aligned} \tag{2.12}$$

$$O = \begin{bmatrix} C \\ CA \\ \vdots \\ CA^{n-1} \end{bmatrix} \tag{2.13}$$

□

Controllability and observability represent the possible effectiveness of a controlled system. Therefore, in controller design, controllable and observable states are desired to be preserved during the reduction. As a means of quantifying, gramians are introduced. The word gramian means a matrix composed of inner products of two vector spaces, however in control theory it is used to show energy level of output vector, E_c, or energy level of state of a system, E_o. For instance, the controllability gramian is defined as an inverse of the minimum energy required to send an initial state to a certain final state. Since the state $z(t)$ under input $u(t)$ is calculated as in equation

(2.14), the required input energy E_c to drive a system to initial state $z(0)$ is as shown in equation (2.15).

$$z(t) = \int_0^t e^{A(t-\tau)} Bu(\tau)d\tau = e^{At}B \tag{2.14}$$

$$\begin{aligned} E_c &= \int_0^\infty u(\tau)^T u(\tau)d\tau = z_0^T \left(\int_0^\infty e^{A^T t} BB^T e^{At} dt \right)^{-1} z_0 \\ &= z_0^T W_c^{-1} z_0 \qquad \text{,where } z_0 = z(0) \end{aligned} \tag{2.15}$$

The controllability gramian W_c is defined as in equation (2.16), and its property is directly related to the controllability of a system as described in Theorem 2.3.

$$W_c = \int_0^\infty e^{At} BB^T e^{A^T t} dt \tag{2.16}$$

Theorem 2.3 *If the controllability gramian W_c is positive definite, then a system (A,B) is controllable.*

□

For the observability, a similar definition can be drawn. Since the output $y(t)$ is calculated as in equation (2.17), the output energy E_o is as shown in equation (2.18).

$$y(t) = Ce^{At}z_0 \tag{2.17}$$

$$\begin{aligned} E_o &= \int_0^\infty y(\tau)^T y(\tau)d\tau = z_0^T \left(\int_0^\infty e^{A^T t} CC^T e^{At} dt \right) z_0 \\ &= z_0^T W_o z_0 \qquad \text{,where } z_0 = z(0) \end{aligned} \tag{2.18}$$

The observability gramian W_o is derived from E_o and defined in equation (2.19) satisfying Theorem 2.4.

$$W_o = \int_0^\infty e^{A^T t} CC^T e^{At} dt \tag{2.19}$$

Theorem 2.4 *If the observability gramian W_o is positive definite, then a system (A,C) is observable.*

□

By differentiating each of the gramians from equation (2.16) and equation (2.19), the following equations are obtained.

$$\dot{W}_c = AW_c + W_c A^T + BB^T \tag{2.20}$$

$$\dot{W}_o = A^T W_o + W_o A + C^T C \tag{2.21}$$

For a stable system, stationary solutions satisfy $\dot{W}_c = \dot{W}_o = 0$. Then, equations (2.22)-(2.23) are derived, which are called the Lyapunov equations. Gramians are obtained generally from solving the Lyapunov equations instead of integration as in equation (2.16) and equation (2.19).

$$AW_c + W_c A^T + BB^T = 0 \tag{2.22}$$
$$A^T W_o + W_o A + C^T C = 0 \tag{2.23}$$

As described, gramians are indicators of controllability and observability; therefore they can be used as a criterion whether certain states should be preserved or not during the reduction. A model can be reduced by removing uncontrollable and unobservable states. However, in general, controllability and observability gramians of the system are not the same. Therofore, which states are undesirable or desirable is not clear. To solve this problem, a system is first transformed into balaced system, which has same controllability and observability gramians as defined in Definition 2.1, and then reduced. The balancing transformation algorithm suggested by Laub[LHPW87] is described in Algorithm 2.1.

Definition 2.1 *A system Σ is balanced, if $W_o = W_c = diag(\sigma_1, \sigma_2, \cdots, \sigma_n)$. where $\Sigma = \begin{pmatrix} A & B \\ C & D \end{pmatrix}$ from equation (2.12), and σ_i's are Hankel singular values.*

□

Algorithm 2.1 *For gramian matrices W_c and W_o, the following algorithm finds a transformation matrix T which transforms a system Σ into balanced system $\Sigma_{balanced}$.*

Step 1. *Compute Cholesky factors of Gramians such that*

$$W_c = L_c L_c^T, \quad W_o = L_o L_o^T \tag{2.24}$$

Step 2. *Compute singular value decomposition of $L_o^T L_c$.*

$$L_o^T L_c = U \Lambda V^T \tag{2.25}$$

Step 3. *Form a balancing transformation T.*

$$T = L_c V \Lambda^{-1/2}, \quad T^{-1} = \Lambda^{-1/2} U^T L_o^T \tag{2.26}$$

Step 4. *Form a balanced system $\Sigma_{balanced}$.*

$$\Sigma_{balanced} = \begin{pmatrix} T^{-1}AT & T^{-1}B \\ CT & \end{pmatrix} = \begin{pmatrix} A_{,bl} & B_{,bl} \\ C_{,bl} & \end{pmatrix} \tag{2.27}$$

After the transformation, controllability and observability gramians from the transformed system, $W_{c,bl}$ and $W_{o,bl}$, can also be calculated from the Lyapunov equation; and both of them are equal to a diagonal matrix Λ in equation (2.25). The diagonal elements, called singular values, represent the controllability and observability level of each state. Consequently, states which have small singular values are eliminated for the order reduction. Since the algorithm is based on singular value decomposition, it has an important benefit on the error bound as described in Theorem 2.5.

Theorem 2.5 *Let $G(s) = C(sI - A)^{-1}B$ be a stable transfer function with Hankel singular values $\sigma_1\ \sigma_2\ \cdots\ \sigma_n$, and let $G_r(s)$ be the balanced realization of $G(s)$ for the first r states. Then,*

$$\left\|G(s) - G_r(s)\right\|_{L\infty} \leq 2\Sigma_{i=r+1}^{n}\sigma_i \tag{2.28}$$

$$\left\|G(s) - G_r(s)\right\|_{H} \leq 2\Sigma_{i=r+1}^{n}\sigma_i \tag{2.29}$$

□

On the other hand, applications of balanced truncation method are limited upto several hundreds order model because of solving the Lyapunov equation, which requires a computation of $O(n^3)$. Both balancing transformation and the Lyapunov equation solver need $O(n^3)$ of computation; therefore a large finite element model cannot directly use the balanced truncation method. Instead, it is reduced with modal truncation first, and the balanced truncation is applied. Eigen-analysis to find proper modal space is generally order of $O(n^3)$. But with a sparse matrix, which most of the structural matrices from a finite element model are, the order of computations is reduced to $O(kn^2)$ or $O(k^2n)$ depending on its sparsity. Another solution to reduce the computational order of balanced truncation method is approximating the gramians instead of calculating them. Gawronski[Gaw98] suggested approximate Hankel singular values in modal space as in equation (2.30), and Smith method and its variations suggest iteratively solving the Lyapunov equation in [GSA03, GL].

$$\gamma_i \cong \frac{\left\|B_i\right\|_2\left\|C_i\right\|_2}{4\xi_i\omega_i} \tag{2.30}$$

where $A \cong diag(A_i)$, $B = \begin{bmatrix} B_1 \\ B_2 \\ \vdots \\ B_n \end{bmatrix}$, $C = \begin{bmatrix} C_1 & C_2 & \cdots & C_n \end{bmatrix}$.

$$A_i = \begin{bmatrix} -\xi_i\omega_i & \omega_i \\ -\omega_i & -\xi_i\omega_i \end{bmatrix}$$

In the end, the system is projected onto the eigenspace of W_cW_o for some important(largest) eigenmodes.

2.3. Krylov subspace method

The motivation of Krylov subspace reduction comes from using the Rayleigh quotient to build a reduced column space. Similar to many other reduction methods, it aims to find a proper projection matrix $V_r \in \mathbb{R}^{n\times r}$ $(r \ll n)$ such that $V_r^TAV_r \approx A$. According to Cauchy's interlacing theorem, $V_i \in \mathbb{R}^{i\times r}$ $(i = 1, 2, \cdots)$ composed of orthonormal columns satisfies following equation.

$$\lambda_{max}\left(V_1^TAV_1\right) \leq \lambda_{max}\left(V_2^TAV_2\right) \leq \cdots \leq \lambda_{max}\left(V_r^TAV_r\right) \leq \lambda_{max}\left(A\right) \tag{2.31}$$

Therefore, finding V_r which maximizes $\lambda_{max}\left(V_r^T A V_r\right)$ will be a solution for good approximation. Since a Rayleigh quotient $\rho\left(\gamma_i\right)$ is defined as in equation (2.32), V_{i+1} containing $\nabla\rho\left(\gamma_i\right) = \frac{2}{\gamma_i^T\gamma_i}\left(A\gamma_i - \rho(\gamma_i)\gamma_i\right)$ will maximize $\lambda_{max}\left(V_{i+1}^T A V_{i+1}\right)$.

$$\rho\left(\gamma_i\right) = \frac{\gamma_i^T A \gamma_i}{\gamma_i^T \gamma_i} = \lambda_{max}\left(V_i^T A V_i\right) \tag{2.32}$$

where $\gamma_i = a_1 v_1 + \cdots + a_i v_i$, v_is are columns of V

Consequently,

$$span\left\{col\left[v_1\,,\,\cdots\,,\,v_i\,,\,v_{i+1}\right]\right\} = span\left\{col\left[v_1\,,\,Av_1\,,\,\cdots\,,\,A^i v_1\right]\right\} \tag{2.33}$$

The right hand side of equation (2.33) is defined as a Krylov subspace.

Definition 2.2 *The ith order Krylov subspace is defined as*

$$\mathbb{K}_i(A,b) = span\left\{b, Ab, \cdots, A^i b\right\} \tag{2.34}$$

where $A \in \mathbb{R}^{n\times n}$, and starting vector $b \in \mathbb{R}^{n\times 1}$

□

The algorithms to find Krylov subspace bases are developed for eigen-analysis first. After it is known that some dominant spaces of the system dynamics are preserved in Krylov subspace form, the usage of Krylov vectors are extended to the model order reduction area.
For the following dynamic system in equation (2.35),

$$\begin{aligned} E\dot{z} &= Az + Bu \\ y &= Cz \end{aligned} \tag{2.35}$$

the transfer function in Laplace domain $G(s)$ is

$$\begin{aligned} G(s) &= C(s)\left(sE(s) - A(s)\right)^{-1} B(s) = -C(s)A(s)^{-1}\left(I - sE(s)A(s)^{-1}\right)^{-1} B(s) \\ &= -C(s)A(s)^{-1}\sum_{i=0}^{\infty}\left(sE(s)A(s)^{-1}\right)^i B(s) \\ &= -C(s)\sum_{i=0}^{\infty}\left(sE(s)A(s)^{-1}\right)^i A(s)^{-1}B(s) \\ &= \sum_{i=0}^{\infty} m_i s^i \qquad \text{where } m_i = -C(s)\left(E(s)A(s)^{-1}\right)^i A(s)^{-1}B(s) \end{aligned} \tag{2.36}$$

The coefficients m_i for each s^i are called the ith moment of a transfer function. Transfer function can be expanded from a certain frequency point s_0, by replacing s with $(s - s_0)$. In most cases $s_0 = 0$ is observed as in equation (2.35) because the behavior in a low frequency range is important in dynamic systems. Focusing on high frequency range, the moments around infinity, $s_0 = \infty$, called Markov parameters are considered as shown in equation (2.37).

$$m_i = -C\left(A^{-1}E\right)^i E^{-1}B \tag{2.37}$$

In both cases, it is clear that moments m_is are represented as iterative forms and the column space of m_is are represented as a Krylov subspace as in equation (2.38) and equation (2.39) accordingly.

$$span\left\{m_0, m_1, \cdots, m_i\right\}|_{s_0=0} = C\,\mathbb{K}_i\left(A^{-1}E, A^{-1}B\right) \tag{2.38}$$

$$span\left\{m_0, m_1, \cdots, m_i\right\}|_{s_0=\infty} = C\,\mathbb{K}_i\left(E^{-1}A, E^{-1}B\right) \tag{2.39}$$

Consequently, if the projection space is chosen as above Krylov subspace, the reduced model is expected to the keep moments. The exact statement and proofs will be provided in section 2.3.1. Two representative algorithms to calculate Krylov subspaces are the Arnoldi algorithm and the Lanczos algorithm. Both use Matrix-vector multiplication only; therefore they are computationally effective.

2.3.1. Lanczos algorithm

The Lanczos method which was originally developed by Cornelius Lanczos in 1950 is to solve eigenvalue problems of a symmetric matrix efficiently. Starting from an initial vector v_0, the column vector of A is extracted as being orthogonal to all previously chosen vectors, v_0, v_1, $\cdots$,v_k, and named as v_{k+1}.

$$\begin{aligned}
r_{k+1} &= Av_k - \sum_{i=1}^{k}\left(v_k^T A v_k\right) v_i && (2.40)\\
&= Av_k - V_k\left[V_k^T A v_k\right] \quad \text{,where } V_k = [v_1\; v_2\; \cdots\; v_k] \\
&= \left[I - V_k V_k^T\right] A v_k \\
v_{k+1} &= \frac{r_{k+1}}{\|r_{k+1}\|} && (2.41)
\end{aligned}$$

On the other way, it can be expressed as follows,

$$\begin{aligned}
Av_k &= \sum_{i=1}^{k}\left(v_i^T A v_k\right) v_i + \|r_{k+1}\| v_{k+1} && (2.42)\\
&= \sum_{i=1}^{k} \alpha_{i,k} v_i + \|r_{k+1}\| v_{k+1} \qquad \text{where } \alpha_{i,j} = v_i^T A v_j
\end{aligned}$$

Because of the orthogonality of v_i's, $\alpha_{i,j} = 0$ for $i > j+1$, and because of the symmetricity of A, $\alpha_{i,j} = 0$ for $j > i+1$. In the end, the matrix V_k satisfies equation (2.43).

$$\begin{aligned} AV_k &= V_k H_k + r_k e_k^T \\ \text{where } H_k &= V_k^T A V_k \\ &= \begin{bmatrix} \alpha_1 & \beta_2 & & \\ \beta_2 & \alpha_2 & \beta_3 & \\ & \beta_3 & \alpha_3 & \\ & & & \ddots \end{bmatrix} \text{,tridiagonal matrix} \end{aligned} \tag{2.43}$$

If r_k is small enough, H_k becomes a good approximation of A, and its tridiagonality provides great benefits on eigenvalue calculation. And the condition for good approximation is released from V^T to any biorthogonal matrix W^T, satisfying moment or eigenvalue matching properties as proved in Theorem 2.6.

Theorem 2.6 *If the columns of matrix $V \in \mathbb{R}^{n\times q}$ are bases of $\mathbb{K}_q(A^{-1}, b)$ from system Σ , and the biorthogonal matrix $W \in \mathbb{R}^{n\times q}$ is chosen such that $W^T AV$ is nonsingular, then the first q moments of the original system Σ and those of the reduced order system Σ_r match.*

$$\begin{aligned} &\Sigma \quad : \dot{x} = Ax + bu, \quad y = c^T x \\ &\Sigma_r \quad : \dot{x_r} = W^T AV x_r + W^T bu, \quad y = c^T V x_r, \quad \text{where } x = V x_r \end{aligned}$$

Proof. *Based on the definition of $m_i = c^T (A^{-1})^{i+1} b$, $i = 0, 1, \cdots$, 0th moment of reduced model becomes,*

$$m_{0,r} = c_r^T A_r^{-1} b_r = c^T V \left(W^T AV\right)^{-1} W^T b$$

Because the vector $A^{-1}b$ lies on the Krylov subspace, $^\exists\, r_0 \in \mathbb{C}$ such that $A^{-1}b = V r_0$. Therefore $\left(W^T AV\right)^{-1} W^T b = \left(W^T AV\right)^{-1} W^T A A^{-1} b = \left(W^T AV\right)^{-1} W^T AV r_0 = r_0$

$$\therefore m_{0,r} = c^T V r_0 = c^T A^{-1} b = m_0$$

Similarly, there exists r_1 such that $(A^{-1})^2 b = V r_1$, $\quad AV r_1 = V r_0$. For the first moment,

$$\begin{aligned} m_{1,r} &= c^T V \left(W^T AV\right)^{-1} \left(W^T AV\right)^{-1} W^T b \\ &= c^T V \left(W^T AV\right)^{-1} W^T V r_0 \\ &= c^T V \left(W^T AV\right)^{-1} W^T AV r_1 \\ &= c^T V r_1 = c^T \left(A^{-1}\right)^2 b = m_1 \end{aligned}$$

The same procedure can continue until m_i, $i = q-1$. Therefore the moments $m_{0,r}$ to $m_{q-1,r}$ match to m_0 to m_{q-1}.

□

From the classical Lanczos process, Feldmann and Freund[FR95] pointed out that tridiagonal matrix H_k can be composed of two Krylov subspaces from a dynamic system, and it provides special benefits in moment matching property as follows.

Theorem 2.7 *If the columns of matrix $V \in \mathbb{R}^{n \times q}$ are bases of $\mathbb{K}_q\left(A^{-1}, b\right)$, and the columns of matrix $W \in \mathbb{R}^{n \times q}$ are bases of $\mathbb{K}_q\left(A^{-T}, c\right)$ from system Σ, then the first $2q$ moments of the original system Σ and those from the reduced system Σ_r match.*
Proof. *According to the previous theorem 2.6, the first q moments from m_0 to m_{q-1} match to the first q moments of reduced model. From the definition of W, $^\exists\ l_i \in \mathbb{C}$ such that $Wl_i = \left(A^{-T}\right)^{i+1} c$, where $i = 0, 1, \cdots, q-1$. For the next moment, m_q, following equation is satisfied.*

$$\begin{aligned} m_{q,r} &= c^T V \left(W^T A V\right)^{-1} \left(W^T A V\right)^{-q} W^T b \\ &= c^T A^{-1} A V \left(W^T A V\right)^{-1} \left(W^T A V\right)^{-q} W^T b \\ &= l_0^T W^T A V \left(W^T A V\right)^{-1} \left(W^T A V\right)^{-q} W^T b \\ &= l_0^T W^T \left(A^{-1}\right)^q b = c^T \left(A^{-1}\right)^{q-1} b = m_q \end{aligned}$$

Upto m_{2q-1}, the moment matching properties are similarly proved.
Note that $\mathbb{K}_q\left(A^{-1}, b\right)$ and $\mathbb{K}_q\left(A^{-T}, c\right)$ are called input Krylov subspace and output Krylov subspace accordingly.

□

As shown in Theorem 2.7, using the Lanczos algorithm, it is possible to include both input and output Krylov matrices matching $2q$ moments. However, there is a risk of break-down during the Lanczos iteration; if v' and w' are orthogonal to each other in Algorithm 2.2, β_{k+1} is divided by zero and the algorithm fails. To prevent this, deflation and look-ahead methods are used. When $v'^T w'$ is too small, near break down, the algorithm simply skips this ill-conditioned vector and goes to the next step. The disadvantages of the look-ahead implementation are the loss of tridiagonality of H_k and the increase of computational complexity.

Algorithm 2.2 **Step 1.** *With given starting vectors v_1 and w_1,*

$$v_1 = \frac{b}{\sqrt{|c^T b|}}, \quad w_1 = \frac{c}{-\sqrt{|c^T b|}}$$

Step 2. *For* $k = 1, 2, \cdots$

$$\alpha_k = w_k^T A v_k$$
$$v' = A v_k - \alpha_k v_k - \delta_k v_{k-1}$$
$$w' = A^T w_k - \alpha_k w_k - \delta_k w_{k-1}$$
$$\delta_{k+1} = \sqrt{|v'^T w'|}$$
$$\beta_{k+1} = \frac{v'^T w'}{\delta_{k+1}}$$
$$v_{k+1} = \frac{v'}{\beta_{k+1}}$$
$$w_{k+1} = \frac{w'}{\delta_{k+1}}$$

2.3.2. Arnoldi algorithm

The Arnoldi algorithm is designed for applications on general nonhamiltonian matrices. The fundamental idea is the same as in the Lanczos algorithm; eliminating all the components parallel to the previously chosen bases. Starting from $v_1 = b/\|b\|$, the next orthogonal vector from $\mathbb{K}_q(A, b)$ can be collected by

$$v_{k+1} = A v_k - \sum_{i=1}^{k} \left(v_k^T A v_i\right) v_i$$

The resulting matrices V_k and H_k have the same relationship as in Lanczos. The only difference is that H_k is not a tridiagonal matrix, but an upper Hessenberg matrix.

$$A V_k = V_k H_k + r_k e_k^T \tag{2.44}$$
$$V_k^T A V_k = H_k\text{: upper Hessenberg matrix}$$

In practical applications, to avoid round-off error, a normalization procedure is added. This modified method is called Arnoldi modified Gram-Schmidt method, which is shown in Algorithm 2.3.

Algorithm 2.3 *For the matrix* $A \in \mathbb{R}^{n\times n}$ *and vector* $b \in \mathbb{R}^{n\times 1}$,

Step 1. *Initial vector* $v_1 = b/\|b\|$
Step 2. *For* $k = 1, 2, \cdots$

$$z = A v_k$$

Step 3. *For* $i = 1, \cdots, k$

$$h_{i,k} = q_k^T z$$
$$z = z - h_{i,k} q_k$$

continue from Step 2.

$$h_{k+1,k} = \|z\|_2$$
$$v_{k+1} = z / h_{k+1,k}$$

As an upper Hessenberg matrix, it is computationally easy to find the eigenvalues of H_k, which are called the Ritz values with respect to $\mathbb{K}_q(A, b)$. They are good estimates of the eigenvalues of A. The error between the actual eigenvalue of A and the Ritz value determines the effectiveness of Arnoldi method. From numerical experiments it is clear that Ritz values are close to the actual eigenvalues and converge to them as the number of iterations increases. In a dynamic system it also guarantees the moment matching property as proved in Theorem 2.6.

Major advantages of the Arnoldi algorithm compared to Lanczos are its simplicity in that only single matrix is used for projection, and no risk of break down. The Lanczos algorithm is superior with respect to the number of matching moments when both input and output Krylov subspaces are used during the reduction. However, it also requires twice as much computation and there is a possibility of break down from both cases. As an alternative way, Salimbahrami[SBLK03] suggested a two-sided Arnoldi algorithm using both input and output Krylov subspaces in the Arnoldi iteration.

2.4. Proper orthogonal decomposition method (POD)

Proper orthogonal decomposition (POD), often called the Karhunen-Loéve method, has been developed to find optimal series expansions of continuous time stochastic process. From a given data set, so called snapshots in MOR theory, orthogonal bases which can describe data sets well are constructed based on optimum problem. For a Hilbert space P, let P^l be a l dimensional subspace of P ($l \leq rank(P)$) and $\Phi = \{\phi_1, \phi_2, \cdots, \phi_l\}$ be the orthonormal bases of P^l. The snapshot set $\chi = \{x_1, x_2, \cdots, x_m\}$ is expressed by bases $\{\phi_1, \phi_2, \cdots, \phi_l\}$ as in equation (2.45).

$$x_i \approx x_i^{\Phi} = \sum_{j=1}^{l} \langle x_i, \phi_j \rangle \cdot \phi_j \tag{2.45}$$

where $\langle a, b \rangle$ represents an innerproduct of two vectors $a^T b$

The goal is to find the optimum set Φ minimizing the error between x_i and x_i^{Φ}. The projection error from data set χ is represented as in equation (2.46).

$$E(\chi, P^l) = \sum_{i=1}^{m} \|x_i - \sum_{j=1}^{l} \langle x_i, \phi_j \rangle \cdot \phi_j\|^2 \tag{2.46}$$

The resultant bases become eigenvectors corresponding to l largest eigenvalues from sampled space. Based on this property, POD is applied for SVD based model reduction especially when the system identification is difficult because of the nonlinearity. Snapshot matrix χ is processed by SVD and the column vectors corresponding to some highest singular values are assumed as a proper projector.
Sampling based method such as POD provides more flexibility on its application

because no exact system equation is required. However it is not actual system reduction but a response approximation. Since POD is dealing with reflection (response) only, there is always a possibility of missing important property. The accuracy of the reduced system is exceedingly dependent on the choice of snapshots.

3. Theories of Parametric Model Order Reduction

As the model order reduction is commonly used in structural analysis and control, parametric model order reduction is needed to reduce computational efforts even more, and to enable the analysis with extremely high computation caused by parameter study. With general model order reduction methods, the projector matrix V is no longer valid when some of structural parameters are changed because projector itself is built based on the system properties. Whenever parameters are changed, from modeling to reduction procedure should be repeated. To avoid this repetition, methods to keep the parametric effects after the reduction are investigated, which are called parametric model order reduction (PMOR). Its concept is shown in Fig. 3.1. Depending on how to treat parameters and how to keep their effects during the reduction and how to reconnect them to the reduced model, there are various methods.

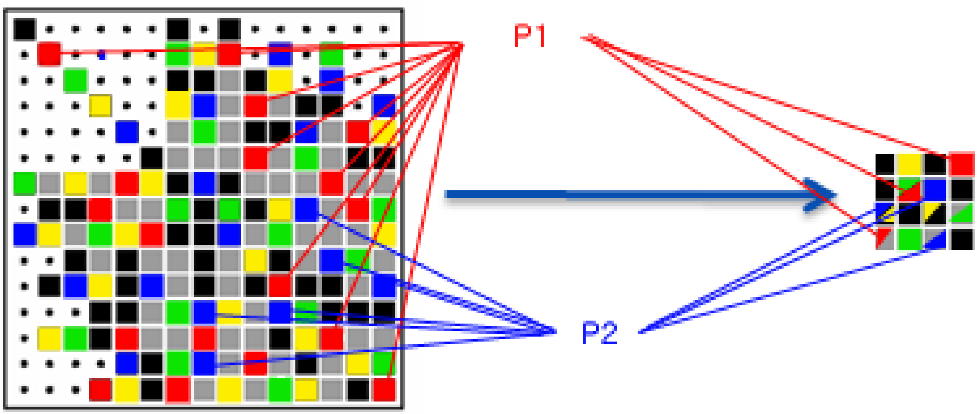

Figure 3.1.: Concept of Parametric Model Order Reduction

3.1. Symbolic method

Symbolic reduction isolates the parameters from the system as symbols, and treat them as additional states. From the following dynamic equation (3.1), the components in matrix E and A are divided into some parts according to the dependence on state

z and parameter p. Then equation (3.2) are reduced via normal reduction methods such as Pade via Lanczos or PRIMA.

$$E(p)\dot{z} = A(p)z + Bu \tag{3.1}$$

$$\begin{bmatrix} E_{11} & E_{12} \\ E_{21} & E_{22} \end{bmatrix} \begin{Bmatrix} \dot{z} \\ \dot{p} \end{Bmatrix} = \begin{bmatrix} A_{11} & A_{12} \\ A_{21} & A_{22} \end{bmatrix} \begin{Bmatrix} z \\ p \end{Bmatrix} + \begin{bmatrix} B & 0 \\ 0 & 0 \end{bmatrix} \begin{Bmatrix} u \\ 0 \end{Bmatrix} \tag{3.2}$$

$$\hat{E} \begin{Bmatrix} \dot{z} \\ \dot{p} \end{Bmatrix} = \hat{A} \begin{Bmatrix} z \\ p \end{Bmatrix} + \hat{B} \begin{Bmatrix} u \\ 0 \end{Bmatrix} \tag{3.3}$$

This approach is mathematically ideal to handle parameters; however, in reality it is seldom to find proper analytical formulation of $\hat{E}$, and $\hat{A}$ because in most cases the parameters are coupled with each other, and coupled with states. For the analysis of circuit design and MEMS simulation, symbolic method is often used but its application is very limited. Especially in a large finite element model, symbolic method is almost impossible to be applied.

3.2. Nominal projection method

In the nominal projection method, parameter changes are treated as small perturbation. Projector V is simply calculated from nominal parameter set p_0, and it is applied to the parameterized system matrices.

$$V = \mathbb{K}_q \left(A(p_0)^{-1} E(p_0), A(p_0)^{-1} b(p_0) \right) \tag{3.4}$$

$$E_r(p)\dot{z}_r = A_r(p)z_r + B_r(p)u \tag{3.5}$$

$$\text{where } E_r(p) = V^T E(p) V, \quad A_r(p) = V^T A(p) V$$
$$b_r(p) = V^T b(p), \quad V z_r = z$$

In [SHS06] parameters' effects from each of $E(p)$, $A(p)$, and $b(p)$ are linearly approximated, and applied in circuit analysis. The problem is laid in its accuracy; the range where projector V is still valid is very limited from p_0 and not exactly proved.

3.3. Multiparameter moment matching method

Lesson learned from nominal projection method is that projector V should either be independent on the parameter values or include parametric effects. The possibility on the former case is varied from model and parameters but generally rare. Changing parameters affects the model; hence, if projection matrix is independent on parameters' change, it is not reflecting the model well. Consequently the latter case is studied mainly. Daniel's method in [DSC+04] is a generalized form of PMOR concerning many numbers of parameters, not one or two as in previous studies. In the original paper, expansion frequency points are treated as parameters as well as spacing distance in a circuit; which means it is designed for the rational model order reduction. However, the same methodology can be used for structural parameters, which are covered in Chapter 4.

For the parameterized system equation,

$$E(p_1, p_2, \cdots, p_{np})x = Bu \tag{3.6}$$

where $E \in \mathbb{R}^{n\times n}$, $x, B \in \mathbb{R}^{n\times 1}$, and p_is $(i = 1, \cdots, np)$ are parameters

The effects of parameters on system matrix E can be rewritten by Taylor's expansion as follows.

$$\begin{aligned} E(p_1, p_2, \cdots, p_{np}) = \tilde{E}_0 + \sum_i \Delta\tilde{p}_i\, \tilde{E}_i + \sum_{j,k} \Delta\tilde{p}_j\, \Delta\tilde{p}_k\, \tilde{E}_{jk} \\ + \sum_{l,m,n} \Delta\tilde{p}_l\, \Delta\tilde{p}_m\, \Delta\tilde{p}_n\, \tilde{E}_{lmn} + \cdots \end{aligned} \tag{3.7}$$

where $$\tilde{E}_0 = E(\bar{p}_1, \bar{p}_2, \cdots, \bar{p}_{np}) = E(\bar{p})$$
$$\tilde{E}_i = \frac{\partial E}{\partial p_i}|_{\bar{p}}, \quad \tilde{E}_{ij} = \frac{\partial^2 E}{\partial p_i \partial p_j}|_{\bar{p}}, \quad \tilde{E}_{ijk} = \frac{\partial^3 E}{\partial p_i \partial p_j \partial p_k}|_{\bar{p}},$$
$$\Delta\tilde{p}_i = p_i - \bar{p}_i$$

The goal is to find a proper projector $V \in \mathbb{R}^{n\times r}$ $(r \ll n)$ which makes the reduced model in the form of equation (3.8) so that direct access on the parameter change $\Delta\tilde{p}_i$ is possible even after the reduction.

$$\begin{aligned} V^T E V x_r &= \left(V^T\tilde{E}_0 V\right)x_r + \sum_i \Delta\tilde{p}_i \left(V^T\tilde{E}_i V\right)x_r + \sum_{j,k} \Delta\tilde{p}_j\, \Delta\tilde{p}_k \left(V^T\tilde{E}_{jk} V\right)x_r + \cdots \\ &= \tilde{E}_{0,r}x_r + \sum_i \Delta\tilde{p}_i\tilde{E}_{i,r}x_r + \sum_{j,k} \Delta\tilde{p}_j\, \Delta\tilde{p}_k\tilde{E}_{jk,r}x_r + \cdots \end{aligned} \tag{3.8}$$

The main issue is how to calculate proper V which contains all the important information of parametric effects as well as the system. To simplify the equation, notations are altered as follows[DSC+04].

$$E_i = \begin{cases} \tilde{E}_i & i = 0, 1, \cdots, np \\ \tilde{E}_{ij} & i = 1, \cdots, np \quad j = 1, \cdots, np \\ \tilde{E}_{ijk} & i = 1, \cdots, np \quad j = 1, \cdots, np \quad k = 1, \cdots, np \\ \vdots & \end{cases}$$

$$\Delta p_i = \begin{cases} \Delta\tilde{p}_i & i = 0, 1, \cdots, np \\ \Delta\tilde{p}_i\Delta\tilde{p}_j & i = 1, \cdots, np \quad j = 1, \cdots, np \\ \Delta\tilde{p}_i\Delta\tilde{p}_j\Delta\tilde{p}_k & i = 1, \cdots, np \quad j = 1, \cdots, np \quad k = 1, \cdots, np \\ \vdots & \end{cases}$$

Then the parameterized system equation can be simplified in a linear form as in equation (3.9).

$$Ex = \left(E_0 + \sum_{i=1}^{q} \Delta p_i E_i \right) x = Bu \tag{3.9}$$

The solution x will lie on the space $E^{-1}Bu$, and it can be expressed as in equation (3.10) including parameters.

$$\begin{aligned}
x &= E^{-1}Bu = \left(E_0 + \sum_{i=1}^{q} \Delta p_i E_i \right)^{-1} Bu \\
&= \left(I + \sum_{i=1}^{q} \Delta p_i E_0^{-1} E_i \right)^{-1} E_0^{-1} Bu \\
&= \left(I - \sum_{i=1}^{q} \Delta p_i R_i \right)^{-1} B_M u \\
&= \sum_{j=0}^{\infty} \left(\sum_{i=1}^{q} \Delta p_i \; R_i \right)^{j} B_M u \\
&= \sum_{j=0}^{\infty} \sum_{k_2=0}^{j-(k_3+\cdots+k_q)} \cdots \sum_{k_{q-1}=0}^{j-k_q} \sum_{k_q=0}^{j} \left[F^{j}_{k_2,\cdots,k_q}(R_1,\cdots,R_q) B_M u \right] s_1^{j-(k_2+\cdots+k_q)} s_2^{k_2} \cdots s_q^{k_q} \\
& \text{where } R_i = -E_0^{-1}E_i \quad \text{and } B_M = E_0^{-1}B
\end{aligned} \tag{3.10}$$

$$F^{j}_{k_2,\cdots,k_q}(R_1,\cdots,R_q) = \begin{cases} 0 & \text{if } k_i \notin \{0,1,\cdots,j\}, i = 2,\cdots,q \\ 0 & \text{if } k_2+\cdots+k_q \notin \{0,1,\cdots,j\} \\ I & \text{if } j = 0 \\ R_1 F^{j-1}_{k_2,\cdots,k_q}(R_1,\cdots,R_q) + R_2 F^{j-1}_{k_2-1,\cdots,k_q}(R_1,\cdots,R_q) & \\ \;+\cdots+ R_q F^{j-1}_{k_2,\cdots,k_q-1}(R_1,\cdots,R_q) & \end{cases}$$

The resultant column space of projector V is represented as in equation (3.11).

$$\begin{aligned}
colspan(V) &= span \left\{ \bigcup_{j=0}^{j*} \bigcup_{k_2=0}^{j-(k_q+\cdots+k_3)} \cdots \bigcup_{k_{q-1}=0}^{j-k_q} \bigcup_{k_q=0}^{j} F^{j}_{k_2,\cdots,k_q}(R_1,\cdots,R_q) B_M \right\} \\
&= span \{ B_M, R_1B_M, R_2B_M, \cdots, R_qB_M, (R_1R_2+R_2R_1)B_M, \cdots, \\
& \quad (R_1+R_q)(R_q+R_1)B_M, R_2^2B_M, (R_2R_3+R_3R_2)B_M, \cdots \\
& \text{where } j* \text{ is the largest order of derivative on Taylor series approximation}
\end{aligned} \tag{3.11}$$

After the reduced model is derived by projector V as in equation (3.12), only $V^TE_iV \in \mathbb{R}^{r\times r}$ ($r \ll n$, $i = 0,\cdots,q$) are concerned and parameter change Δp_is are directly managable in $\mathbb{R}^{r\times r}$.

$$E_r(p)x_r = B_r u \tag{3.12}$$

$$\text{where } E_r(p) = V^T E_0 V + \sum_{i=1}^{q} \Delta p_i \left(V^T E_i V\right),$$
$$V x_r = x, \text{ and } V^T B = B_r.$$

When some of parameters are frequency points (s or s_i), moment matching property is still valid as shown in Theorem 3.1. Its proof is written in [DSC+04].

Theorem 3.1 *For the parametrized system equation in (3.9), if some of parameters p_is are frequency points s_is and projection matrix $V \in \mathbb{R}^{n\times r}$ is calculated from equation (3.11), The first r moments of the transfer function from the reduced model as in equation (3.12) match to the first r moments from the original model.*

□

One concern from this method is the coupled moments; if the number of parameter increases and they are coupled strongly, the number of parametric effectiveness matrices, E_is, will increase drastically. On the other hand, if the effects of each parameter are uncoupled or rarely coupled, multi-parameter moment matching method would be a powerful solution. To overcome this coupled momentum problem, some of ideas are suggested from section 3.3.1 to section 3.3.3

3.3.1. Passive reduction of multi-dimensional model

In [GN00], instead of the exact coupled moments, the moments with respect to the single parameter change are used. For the dynamic system equation in the Laplace domain, the parts concerning both Laplace variable s which represents frequency point and system parameter p_is are treated as a single function Υ as in equation (3.13),

$$\left(sE(p_1,\cdots,p_{np}) - A(p_1,\cdots,p_{np})\right) X(s) = B(s) \tag{3.13}$$
$$\text{where } p_i \quad (i=1,\cdots,np) \text{ are parameters}$$
$$\Upsilon(s,p_1,\cdots,p_{np}) = sE(p_1,\cdots,p_{np}) - A(p_1,\cdots,p_{np})$$

After setting only one parameter p_k as a variable and others as a fixed value $s=\bar{s}, p_i = \bar{p}_i, (i=1,\cdots,i\neq k)$ corresponding moments $m_i^{p_k}$ (i is the order of the moment) are calculated as in equation (3.14) and collected.

$$\Upsilon(s,\bar{p}_1,\cdots,\bar{p}_{np}) m_i^{p_j} = -\sum_{k=1}^{i} \frac{\frac{\partial^k}{\partial p_j^k}\Upsilon(s,p_1,\cdots,p_{np})|_{p=\bar{p}} M_{i-k}^{p_j}}{k!} \tag{3.14}$$
$$\Upsilon(s,\bar{p}_1,\cdots,\bar{p}_{np}) m_0^{p_j} = b$$

Then column space from all collected moments will be a projection space.

$$V = colsp\left\{m_0^{p_1}, m_1^{p_1}, \cdots, m_q^{p_1}, m_0^{p_2}, m_1^{p_2}, \cdots, m_q^{p_2}, \cdots, m_q^{p_{np}}\right\} \tag{3.15}$$

It is shown that chosen moments are preserved through the reduction as well as the passivity in [GKN+03]. Passivity preservation is very useful especially in electrical engineering and control system because the stable system can be unstable by connected into another component if the system is not passive. A drawback of this method is the calculation of derivatives. It obstructs the usage of this method to the more general cases, which do not have the analytic formula with respect to the parameters, for instance a large finite element model.

3.3.2. Random sampling of moment graph

While people are trying to use Daniel's method[DSC+04] in real complex system, they found that treating all the moments generated from many parameters are not very efficient especially they are focusing on wider frequency range rather than wider system parameter variation. The idea of random sampling of moment graph comes from taking sets of sample parameters and frequency values and derives some moments from them[ZP07]. From the parameterized system equation,

$$\left[s\left(E_0+\sum_{i=1}^{np}p_iE_i\right)-\left(A_0+\sum_{i=1}^{np}p_iA_i\right)\right]x=Bu \tag{3.16}$$

the solution x can be formulated as in equation (3.17).

$$\begin{aligned} x(s,p_1,\cdots,p_{np}) &= \left[I-\sum_{i=1}^{np}p_iA_i'+sE_0'+s\sum_{i=1}^{np}p_iE_i'\right]^{-1}B'u \\ &= \sum_{j=0}^{\infty}\left(\sum_{i=1}^{np}p_iA_i'+sE_0'+s\sum_{i=1}^{np}p_iE_i'\right)^{j}B'u \end{aligned} \tag{3.17}$$

where $A_i'=-A_0^{-1}A_i$, $E_i'=-A_0^{-1}E_i$, and $B'=-A_0^{-1}B$

The elements of this space can be renotated as follows,

$$\begin{aligned} T_0 &= B' \\ T_1 &= \left(\sum_{i=1}^{np}p_iA_i'+sE_0'\right)B' \\ T_2 &= \left(\sum_{i=1}^{np}p_iA_i'+sE_0'\right)^2B'+\left(s\sum_{i=1}^{np}p_iE_i'\right)B' \end{aligned} \tag{3.18}$$

$$\vdots \tag{3.19}$$

Then, nth moment recursion term T_n is represented by equation (3.20)

$$T_n = M_1T_{n-1}+M_2T_{n-2} \tag{3.20}$$

$$\text{where } M_1 = \sum_{i=1}^{np}p_iA_i'+sE_0' \tag{3.21}$$

$$M_2 = s\sum_{i=1}^{np}p_iE_i'$$

Randomly chosen parameters and frequency points (samples) are used to calculate M_1 and M_2. Projection space is composed of all T_ns from each samples. With this approach, the low order moments are more emphasized than higher order moments. When the number of samples is larger than the resulting columns, the moments from random sampling method are preserved as same as in normal moment matching method. The proof is shown in [ZP07]. Additionally for a given moment matching requirement, the computational complexity of random sampling method is upper bounded by that of the normal moment matching method[ZP07]. It shows dominant performance especially in computational complexity compared to PRIMA and PMTBR. The difficulties in applying this method to a large finite element model with many parameters will be the selection of samples and the valid variation of parameters' change. Because the moment matching property on sampled point does not guarantee the moment matching on other points, the accuracy is not clearly defined; it is because the original method is suggested for rational reduction maching moments on different frequency points not for structural PMOR. Moreover as the number of parameter involved is increased and as the variation of them is increased, required number of samples will be huge.

3.3.3. PMOR with Arnoldi and TBR

Another approach to handle parametric effects by sampling is suggested in [LK05]. The difference is that not only Krylov subspace reduction but also truncated balanced reduction (TBR) is applied. The former part is to extract parametric effectiveness matrices and include them into projection matrix as done in [DSC+04], and the latter part is to leave out less important subspaces based on singular values.
For the chosen k sets of parameters, $\vec{p}_i = [p_{i,1}, p_{i,2}, \cdots, p_{i,np}]^T$ $(i = 1, 2, \cdots, k)$, dynamic system equation in Laplace domain can be written as in equation (3.22).

$$sE|_{\vec{p}_i}x = A|_{\vec{p}_i}x + Bu \tag{3.22}$$

where $E|_{\vec{p}_i} = E_0 + \sum_{j=1}^{np} p_{ij}E_{ij}$ and $A|_{\vec{p}_i} = A_0 + \sum_{j=1}^{np} p_{ij}A_{ij}$.

Krylov subspace from each sample set $\vec{p}_i$, Q_i, will be as follows,

$$Q_i = \mathbb{K}_q\left(A^{-1}|_{\vec{p}_i}E|_{\vec{p}_i}, A^{-1}|_{\vec{p}_i}b\right) \tag{3.23}$$

The collected subspace becomes,

$$Q_{all} = [Q_1 \quad Q_2 \quad \cdots \quad Q_k] \tag{3.24}$$

The redundant information in Q_{all} will be filtered out based on singular value decomposition method as same as in TBR. Finally the orthonormal projection matrix $V \in \mathbb{R}^{n\times r}$ $(r \ll n)$ which has high singular values only is obtained. Despite of good result from a simple example, the same problems from random sampling of moment graph remain also here because both of them are based on sample sets of parameter values.

$$Q_{all} = USV^T \tag{3.25}$$

$$\text{where } S = diag\,(s_{ii}) \quad (s_{11} \geq s_{22} \geq \cdots)$$

$$U = [\vec{u_1} \quad \vec{u_2} \quad \cdots \quad \vec{u_r}]$$

$$V = [\vec{v_1} \quad \vec{v_2} \quad \cdots \quad \vec{v_r}]$$

3.4. Interpolation based method

Two main streams of PMOR are multiparameter moment maching method introduced in 3.3 and interpolation based method. The former is finding a common projector which can preserves the information about both system and parameters; the latter is reducing each system with different parameter set individually using their own projector and approximating via interpolation as shown in Fig. 3.2.
Common projector approach starts from the Talyor series approximation of parametric effects. Therefore as far the parameter value goes from its initial value, error will be increased. If the system with very distinctive parameter sets is interested, or if the system is nonlinearly dependent on parameters, the accuracy of reduced order model will be low. Consequently the required order of projector to maintain certain level of accuracy will be high; interpolation method starts from here. It is a combination of two different fields of study: model reduction and interpolation method. Therefore many variations are possible; however, the most actively investigated two methods are presented here.

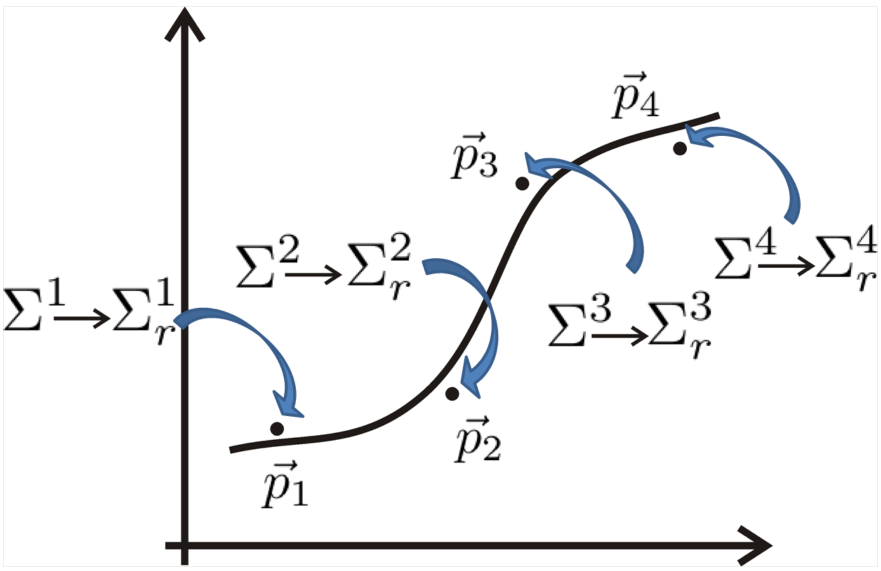

Figure 3.2.: Interpolation based Parametric Model Order Reduction

3.4.1. Linear superposition of locally reduced model

The simplest approximation between two points is a linear approximation. Lohmann and Eid[LE09] suggested to approximate a system with new parameter set $\vec{p}$ which lies between $\vec{p}_1$ and $\vec{p}_2$ by linear approximation of a reduced system at $\vec{p}_1$ and a reduced system at $\vec{p}_2$ based on weighting function.
First, the system equation is represented as a superposition of system matrices, A_i and b_i, from local points i as shown in equation (3.26). Note that terms A_i are different from common projector approach.

$$\begin{aligned} \dot{x} &= Ax + bu \\ &= \left(\sum_{i=1}^{ns} w_i(p) A_i\right) x + \left(\sum_{i=1}^{ns} w_i(p) b_i\right) u \end{aligned} \tag{3.26}$$

Assigning weighting function $w_i(p)$ as in Fig. 3.3, local system matrices A_i and b_i can be directly used in equation (3.26).
The projectors to reduce the order are calculated individually at each local system. Let W_i and $V_i \in \mathbb{R}^{n \times r}$ are orthogonal projector of a local system $\dot{x} = A_i x + b_i u$. Then, the reduced system will be

$$\dot{x}_{r,i} = W_i^T A_i V_i x_{r,i} + W_i^T b_i u \qquad \text{where } x = V_i x_r \tag{3.27}$$

Integrating them into overall system equation (3.26) is not simple. Since each projector transforms a original physical system into a mathematical space, each of locally reduced model has completely different interpretation of physical states. Therefore simply summing them up with weighting function does not make sense. In [LE09], transformation T_i is designed to bring each locally reduced state back to physical (but reduced) state. Some technically important q state variable, x^*, are selected, and using $R \in \mathbb{R}^{q \times n}$ such that $x^* = Rx$ transformation matrix T_is are derived as in equation (3.28).

$$x_i^* = R V_i x_{r,i} = T_i x_{r,i} \tag{3.28}$$

After then integration of locally reduced models is done as shown in equation (3.29).

$$\dot{x}_r^* = \sum_{i=1}^{ns} w_i(p) \left[T_i V_i^T A(p_i) V_i T_i^T x_r^* + T_i V_i^T B(p_i) u \right] \tag{3.29}$$

Locally reduced model provides high accuracy on sampled points or nearby. But the accuracy on interpolated point is still problematic. There are still open questions such as how to define technically important q state variables and how to secure moment matching property or stability on a interpolated model.

3.4.2. Spline interpolation after POD

Another interpolation based PMOR is investigated in [ACCF09, DVW09] more focusing on nonlinear systems. Because in nonlinear systems parametric effects or system

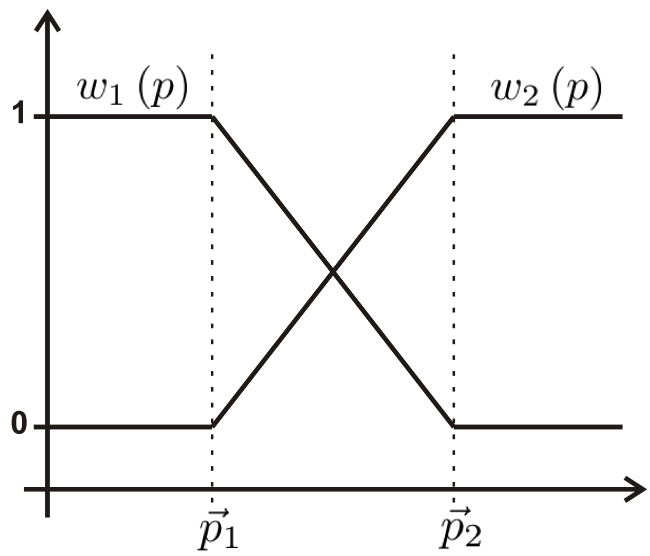

Figure 3.3.: Weighting function between two parameter sets

itself are hard to be formulated, proper orthogonal decomposition (POD) method introduced in section 2.4 is used for local reduction. Spline interpolation is used instead of linear interpolation. However, find a proper space to interpolate is still remained as a main problem. In [DVW09], both direct interpolation in the reduced space and interpolation in the space tangent to Riemann manifold are investigated. In former case spline interpolation is applied to locally reduced model A_r^i $(i = 1, \cdots, ns)$, which is corresponding to parameter set $\vec{p}^i$. Let the element in the gth row and hth column of A_r^i as $A_{r,gh}^i$. If samples x_j^i are ordered in monotonically increasing order, then spline interpolant f^i for $A_{r,gh}(x_j^i)$ in the interval $x_j^i \leq x_j \leq x_j^{i+1}$ is given as in equation (3.30). The coefficients α_k^i are calculated by boundary conditions.

$$f^i(x_j) = \sum_{k=0}^{3} \alpha_k^j \left(\frac{x_j - x_j^i}{x_j^{i+1} - x_j^i} \right)^k \tag{3.30}$$

As long as the variation of matrix elements according to parameter changes is well captured by the interpolants, this approach shows good results. For the other cases, mapping reduced system into another space where the change in matrix elements are well detected is recommendable. This second approach uses Riemann manifold as defined in Definition 3.1 and logarithmic mapping from it.

Definition 3.1 *A differentiable manifold where the tangent vectors about each point have an inner product so defined as to allow a generalized study of distance and orthogonality is called Riemann manifold.*

□

After defining a reference reduced model A_r^0, a tangential space from that point $\Gamma_{A_r^0}$ is used for interpolation. Θ^i is the image of A_r^i in $\Gamma_{A_r^0}$. Using the logarithmic mapping and exponential mapping A_r^i is transformed into Θ^i as shown in Fig. 3.4 and back to Riemann manifold M by equations (3.31)-(3.32).

$$\Theta^i = Log_{A_r^0}(A_r^i) = log\left[A_r^i (A_r^0)^{-1}\right] \tag{3.31}$$

$$A_r^i = Exp_{A_r^0}(\Theta^i) = exp\left[\Theta^i (A_r^0)^{-1}\right] \tag{3.32}$$

Spline interpolation is applied to the elements of matrix Θ with the same manner.
So far it is not clear whether the interpolation on tangential space is dominant or not. Depending on the model and parameter the results show different accuracy. The computational effort for interpolation is not negligible since it is interpolating every single element of the matrix. However, the combination of POD method and spline interpolation provide a possibility of PMOR on highly nonlinear models.

3.5. Note on rational reduction

Methods developed for the rational reduction are also often called as a parametric model order reduction treating the Laplace variable s as a parameter. Clearly rational reduction is valuable in dynamic system because interested frequency range is important. However, it is a totally different direction from this thesis; interested parameters are physical or geometrical parameters of structures not a frequency range. Hence, among discussions on rational reduction methods which are not applicable to general parametric model order reduction are left out. Rational reduction is dealing with changing expansion point in Pade approximation from the same physical model. In this thesis parameters which actually change the physical model are interested.

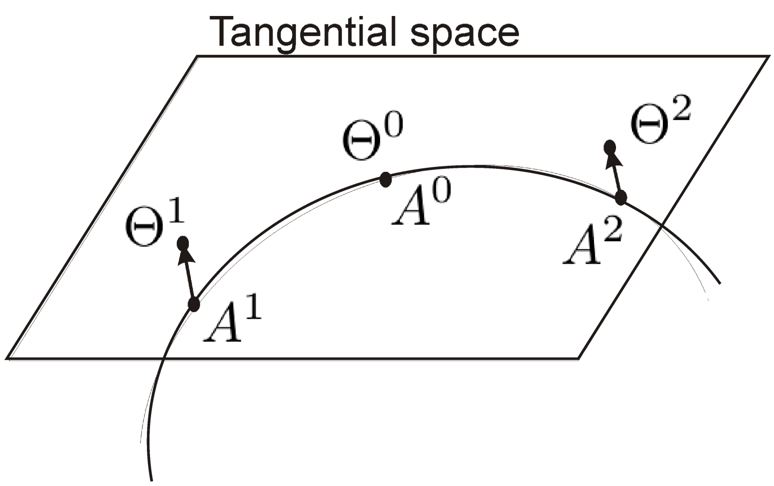

Figure 3.4.: Transformation from Rieman Manifold to its tangential space

4. PMOR method for FE model application

As introduced in chapter 3 most of the studies on PMOR are initiated for circuit design or controller design from state space dynamic system. Therefore they aim for including more frequency points to expand moments of transfer function as parameters (rational reduction), or including some system parameters from state space model. Contrastively PMOR for structural analysis is seldom because physical or geometrical parameters of structure influence entire finite element (FE) model, which is in most cases very large. The effects from each physical or geometrical parameters in a complicated finite element model are not seen straightforward as in analytical model or state space model. Therefore when parameters of structure are changed, it is simply considered as a new structure and analyzed anew. Another difficulty is transforming a parameterized second order dynamic model into a parameterized first order state space system. In many cases of previously studied methods, the parameterized system equation is already defined as a special form such as

$$\dot{x} = A(p)x + bu \tag{4.1}$$

But in reality the effects of parameters are hardly well organized like this. Starting with material and geometrical parameters of a structure, the connection to the system equation is complicated, especially through inversion.

$$M(p)\ddot{x} + D(p)\dot{x} + K(p)x = f \tag{4.2}$$

Therefore in this thesis parametric model order reduction method starting from real physical or geomentrical parameter, dealing with huge finite element model not just equation is investigated and tested with various examplary structures. Naturally there are some difficulties and errors occured while applying theory to a very large FE model. In this chapter, using the approach of common projector method, PMOR method for large FE model is induced both for static analysis and dynamic analysis. To have better accuracy some modification of algorithms are investigated and shown in this chapter. Using this method a model from commertial finite element software such as ANSYS and Nastran is reduced keeping the access to the parameters for instance material properties. In the next chapter, computational tools for real applications and numerical examples are shown.

4.1. Introduction of overall procedure

The overall procedure is as shown in Fig. 4.1. The parameterized system we have until the second step is the mass and stiffness matrices. The critical part is the third step, finding a proper projection matrix V keeping both the parametric effects and the important properties of the overall system, for example the moments of the transfer function in dynamic system. The method how will be explained in static model (section 4.2) and in dynamic model (section 4.3). Skills for parameterization in step 2 will be covered in section 4.4.

4.2. Static model

The governing equation of a static system is

$$Kx = f \tag{4.3}$$

$$\begin{gathered} K : \text{stiffness matrix} \in \mathbb{R}^{n\times n} \\ x : \text{displacement vector} \in \mathbb{R}^{n\times 1} \\ f : \text{load vector} \in \mathbb{R}^{n\times 1} \end{gathered}$$

From the finite element model, the order of system is (the number of nodes) $\times$ (the number of degrees of freedoms (d.o.fs) at each node). When the stiffness matrix K contains parameters, $p_1, p_2, \cdots, p_{np}$, as in equation (4.4) it can be represented by Talor series expansion as in equation (4.5).

$$K(p_1, p_2, \cdots, p_{np})x = f \quad \text{where } p_i(i = 1, \cdots, np) \text{ are parameters} \tag{4.4}$$

$$\begin{aligned} K(p_1, p_2, \cdots, p_{np}) = & \tilde{K}_0 + \sum_i \Delta\tilde{p}_i\, \tilde{K}_i + \sum_{j,k} \Delta\tilde{p}_j\, \Delta\tilde{p}_k\, \tilde{K}_{jk} \\ & + \sum_{l,m,n} \Delta\tilde{p}_l\, \Delta\tilde{p}_m\, \Delta\tilde{p}_n\, \tilde{K}_{lmn} + \cdots \end{aligned} \tag{4.5}$$

$$\begin{gathered} \text{where} \qquad \tilde{K}_0 = K(\bar{p}_1, \bar{p}_2, \cdots, \bar{p}_{np}) = K(\bar{p}) \\ \tilde{K}_i = \tfrac{\partial K}{\partial p_i}|_{\bar{p}}, \quad \tilde{K}_{ij} = \tfrac{\partial^2 K}{\partial p_i \partial p_j}|_{\bar{p}}, \quad \tilde{K}_{ijk} = \tfrac{\partial^3 K}{\partial p_i \partial p_j \partial p_k}|_{\bar{p}}, \\ \Delta\tilde{p}_i = p_i - \bar{p}_i \end{gathered}$$

Because the actual differenciation is almost impossible to find with this huge matrix, the first order approximation is applied.

$$\frac{\partial K}{\partial p_i}|_{\bar{p}} \approx \frac{\Delta K}{\Delta p_i} = \frac{K(\bar{p}_{j,j\neq i}, \bar{p}_i + \Delta p_i) - K(\bar{p})}{(\bar{p}_i + \Delta p_i) - \bar{p}_i} \tag{4.6}$$

To simplify the formula, the notations are reorganized with the same way in 3.3.

$$K_i = \begin{cases} \tilde{K}_i & i = 0, 1, \cdots, np \\ \tilde{K}_{ij} & i = 1, \cdots, np \quad j = 1, \cdots, np \\ \tilde{K}_{ijk} & i = 1, \cdots, np \quad j = 1, \cdots, np \quad k = 1, \cdots, np \\ \vdots & \end{cases}$$

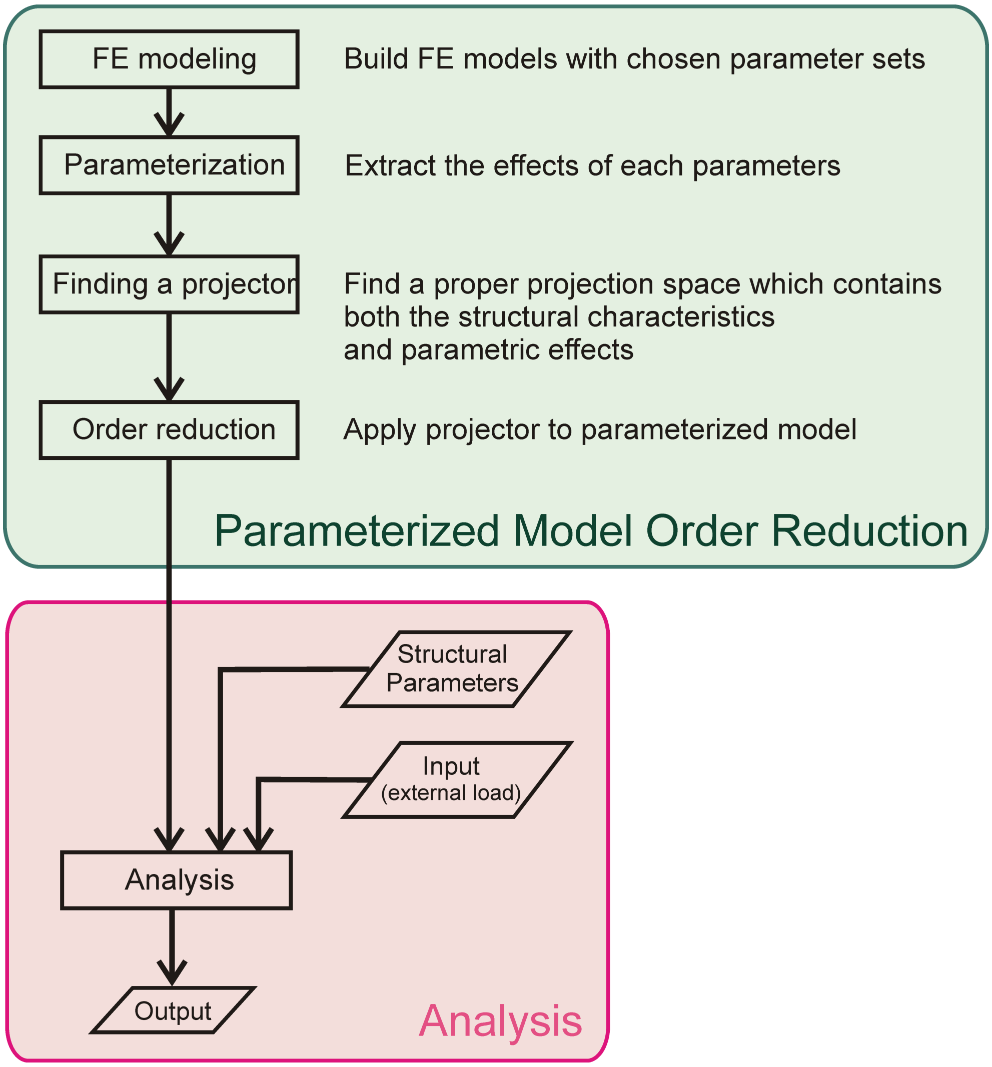

Figure 4.1.: Parametric Model Order Reduction Procedure

$$\Delta p_i = \begin{cases} \Delta\tilde{p}_i & i = 1, \cdots, np \\ \Delta\tilde{p}_i\, \Delta\tilde{p}_j & i = 1, \cdots, np \quad j = 1, \cdots, np \\ \Delta\tilde{p}_i\, \Delta\tilde{p}_j\, \Delta\tilde{p}_k & i = 1, \cdots, np \quad j = 1, \cdots, np \quad k = 1, \cdots, np \\ \vdots \end{cases}$$

Finally the static equation including parameters can be expressed as in equation (4.7)

$$K(p)x = \left(K_0 + \sum_{i=1}^{q} \Delta p_i K_i \right) x = f \tag{4.7}$$

The solution x can be represented as in equation (4.8)

$$\begin{aligned} x = K^{-1} f &= \left(K_0 + \sum_{i=1}^{q} \Delta p_i K_i \right)^{-1} f \\ &= \left(I + \sum_{i=1}^{q} \Delta p_i K_0^{-1} K_i \right)^{-1} K_0^{-1} f \\ &= \left(I - \sum_{i=1}^{q} \Delta p_i K_i' \right)^{-1} f_M \end{aligned} \tag{4.8}$$

where $K_i' = -K_0^{-1} K_i$ and $f_M = K_0^{-1} f$

By changing inversion term into infinite summation, following equation is derived.

$$x = \sum_{i=0}^{\infty} \left(\Delta p_1 K_1' + \Delta p_2 K_2' + \cdots + \Delta p_q K_q' \right)^i f_M \tag{4.9}$$

Since parameter changes Δp_is are scalar values, the space where solution x lies on can be expressed as in equation (4.10).

$$\begin{aligned} x &\in colspan \left\{ \sum_{i=0}^{\infty} \left(K_1' + K_2' + \cdots + K_q' \right)^i f_M \right\} \\ &\in \mathbb{K} \left(K_1' + K_2' + \cdots + K_q', f_M \right) \end{aligned} \tag{4.10}$$

Therefore, projector $V \in \mathbb{R}^{n \times r}$ is chosen as a matrix composed of Krylov subspace vectors from equation (4.11), and resultant reduced order model will be as in equation (4.12).

$$V = \mathbb{K} \left(K_1' + K_2' + \cdots + K_q', f_M \right) \tag{4.11}$$

$$
\begin{aligned}
K_r(p)x_r &= f_r \\
\left(V^T K_0 V + \sum_{i=1}^{q} \Delta p_i \left(V^T K_i V \right) \right) x_r &= f_r \\
\left(K_{0,r} + \sum_{i=1}^{q} \Delta p_i K_{i,r} \right) x_r &= f_r
\end{aligned} \tag{4.12}
$$

where $K_{i,r} = V^T K_i V$ $(i = 0, 1, \cdots, q)$, $Vx_r = x$, and $V^T f = f_r$

The application of this theory on a finite element model shows two main problems. First, the accuracy of the reduced model is remarkably dependent on initial loading vector. If a given loading is close to the initial load vector used in reduction process, the result shows very good agreement to original (unreduced) model. But if loads are quite different from initial loading accuracy is very low. Second, because of high sparsity of the stiffness matrix from finite element model projector matrix often ends up with singular matrix. To solve these problem following two modifications are suggested.

4.2.1. Two-step Arnoldi method

What Arnoldi or Lanczos algorithms are doing is basically collecting the column space of matrix A in $\mathbb{K}_r(A, b)$. The influence of initial vector b is high while Krylov subspace vectors are collected. Because new generated column vectors are chosen as a component orthogonal to the previously selected bases, the initial vector determines entire set of bases. Some suggested Block Krylov method for multi-input system; however it increases the resultant reduced space as many times as the increased number of input vectors. Unlike the control system, where the actuating points are already defined, in structural analysis we want to cope with various loading conditions at different locations. Consequently, block Krylov method cannot be a solution.

From numerical experiments it is observed that when PMOR is executed with a particular initial load, the reduced model is valid near that loading condition. Consequently the idea of collecting various possible loads and compressing them via Gram-Schmidt method is suggested. After that, block Krylov subspace method can be applied with compressed input matrix. Each of those steps are illustrated in Fig. 4.2. Sampled loading vectors and their second order Krylov subspaces are collected in the first step. The process is the Arnoldi algorithm using modified Gram-Schmidt method as described in Algorithm 2.3. For the second Krylov iteration, the block Arnoldi algorithm explained in Algorithm 4.1 is used. With this treatment, the reduced model can be used for various loading conditions and the accuracy increases remarkably. The result of this improvement is provided in chapter 5.

4.2.2. Deflation

Another problem observed is the loss of orthogonality. With a classical Gram-Schmidt process, the loss of orthogonality is occurred because of the round-off error. It is often

$$\begin{aligned}
\text{Step 1 :}\quad & W = \mathbb{K}_2\left(A, B\right) \text{ + deflation} \\
& \text{where, } B = \{b_1,\ b_2,\ \cdots\ ,\ b_p\} \\
\text{Step 2 :}\quad & V = \mathbb{K}_r\left(A, W\right) \text{ + deflation} \\
& \text{where, } W = \{w_1,\ w_2,\ \cdots\}
\end{aligned}$$

Figure 4.2.: Two-step Arnoldi method

reported as a main disadvantage of the classical Gram-Schmidt process and it leads to the modified Gram-Schmidt method, which is generally used in Arnoldi algorithm in thesedays. However, even with the modified Gram-Schmidt method orthogonality among the columns of projector V from Arnoldi algorithm is often lost. The reason comes from the sparsity of structural matrices from finite element model. When newly generated vector does not contain any element which is orthogonal to the previously selected bases, after modified Gram-Schmidt process it returns to one of the previously selected bases. This phenomenon ends up with singular matrix V; it makes the reduced system singular as well. To prevent the loss of orthogonality only the bases orthogonal to each other are selected after the Arnoldi iteration. The selection is based on the value of inner product. From the initial projector $V^\circ = \left[v_1^\circ\, v_2^\circ\, \cdots\, v_q^\circ\right]$, the columns which have one or nearly one value from $v_i^{\circ T} v_j^\circ$ $(i \neq j)$ remain and columns which have near zero value are removed.

Algorithm 4.1 *For matrix $A \in \mathbb{R}^{n\times n}$ and vector set $B = \{b_1\,,\,\cdots\,,b_p\} \in \mathbb{R}^{n\times 1}$*

Step 1. Initiation

$w_1^\circ = b_1/\|b_1\|$
for $i = 1, \cdots, p-1$
  $z = Aw_{2i-1}^\circ$
  for $j = 1, \cdots, 2i-1$
    $h'_{j,2i-1} = w_j^{\circ T} z$
    $z = z - h'_{j,2i-1} w_j^\circ$
  end
  $h'_{2i,2i-1} = \|z\|$
  $w_{2i}^\circ = z/h'_{2i,2i-1}$
  $z = b_{i+1}/\|b_{i+1}\|$
  for $j = 1, \cdots, 2i$
    $h'_{j,2i} = w_j^{\circ T} z$
    $z = z - h'_{j,2i-1} w_j^\circ$
  end
  $h'_{2i+1,2i} = \|z\|$
  $w_{2i+1}^\circ = z/h'_{2i+1,2i}$
end

Step2. Deflation

$j = 1$
$W^\circ = \left[w_1^\circ\, w_2^\circ\, \cdots\, w_{2p}^\circ\right]$
$ch = W^{\circ T} W^\circ$
for $i = 2, \cdots, 2p$
  if $|ch_{i,1:i-1}|$ *small enough*
    $w_j = w_i^\circ$
    $j = j + 1$
  end
end
$sz = j - 1$

Step 3. Block Arnoldi

$$
\begin{array}{l}
\textit{for} \quad i = sz, sz+1, \cdots \\
\qquad z = Aw_i \\
\qquad \textit{for} \quad j = 1, \cdots, i \\
\qquad\quad h_{j,i} = w_j^T z \\
\qquad\quad z = z - h_{j,i} w_j \\
\qquad \textit{end} \\
h_{i+1,i} = \|z\| \\
w_{i+1} = z / h_{i+1,i} \\
\textit{end}
\end{array}
$$

Step 4. Deflation

$$
\begin{array}{l}
j = 1 \\
W = [w_1 \, w_2 \; \cdots] \\
ch = W^T W \\
\textit{for} \quad i = 2, \cdots \\
\qquad \textit{if} \quad |ch_{i,1:i-1}| \quad \textit{small enough} \\
\qquad\qquad v_j = w_i \\
\qquad\qquad j = j + 1 \\
\qquad \textit{end} \\
\textit{end}
\end{array}
$$

4.3. Dynamic model

The general second order dynamic system as in equation (4.13) can be rewritten as the first order formula as in equation (4.14), and its transfer function $H(s)$ is derived as in equation (4.15) by transforming inversion into infinite summation term as in static case.

$$M\ddot{x} + D\dot{x} + Kx = f \tag{4.13}$$

$$\begin{aligned}
M &: \quad \text{mass matrix} \quad \in \mathbb{R}^{n\times n}\\
D &: \quad \text{damping matrix} \quad \in \mathbb{R}^{n\times n}\\
K &: \quad \text{stiffness matrix} \quad \in \mathbb{R}^{n\times n}\\
x &: \quad \text{displacement vector} \quad \in \mathbb{R}^{n\times 1}\\
f &: \quad \text{force vector} \quad \in \mathbb{R}^{n\times 1}
\end{aligned}$$

$$\begin{aligned}
\dot{z} &= \begin{bmatrix} 0 & I \\ -M^{-1}K & -M^{-1}D \end{bmatrix} z + \begin{Bmatrix} 0 \\ M^{-1}f \end{Bmatrix}\\
&= Az + b \qquad (4.14)\\
y &= Cz
\end{aligned}$$

$$\text{where } z = \begin{Bmatrix} x \\ \dot{x} \end{Bmatrix},\ A = \begin{bmatrix} 0 & I \\ -M^{-1}K & -M^{-1}D \end{bmatrix},\ b = \begin{Bmatrix} 0 \\ M^{-1}f \end{Bmatrix}$$

$$\begin{aligned}
H(s) &= C\,(sI - A)^{-1}b = C\,\left(sA^{-1} - I\right)^{-1}A^{-1}b\\
&= -C\sum_{i=0}^{\infty}\left(A^{-1}s\right)^{i}A^{-1}b = -C\sum_{i=0}^{\infty} m_i s^i \qquad (4.15)
\end{aligned}$$

The moments of system m_i is written as in equation (4.16) in the form of Krylov subspace.

$$\begin{aligned}
m_i &= \left(A^{-1}\right)^{i+1}b = \begin{bmatrix} -K^{-1}D & -K^{-1}M \\ I & 0 \end{bmatrix}^{i} \begin{Bmatrix} -K^{-1}f \\ 0 \end{Bmatrix} \qquad (4.16)\\
&= \mathbb{K}_i\left(A^{-1}, A^{-1}b\right) = \mathbb{K}_i\left(\begin{bmatrix} -K^{-1}D & -K^{-1}M \\ I & 0 \end{bmatrix}, \begin{Bmatrix} -K^{-1}f \\ 0 \end{Bmatrix}\right)
\end{aligned}$$

Because the lower parts of A are identity and zero matrices, the lower half of the vector $(A^{-1})^i b$ is the same with the upper half of the vector from former iteration $(A^{-1})^{i-1}b$. Hence, the vector space of moments can be simplified with the size of n instead of $2n$ concerning the upper half part only. Tracking the Krylov iterations, it is found that the terms in moments can be represented by second order Krylov form as in equation (4.18)[ESL+06].

Definition 4.1 *For the matrices A_1, $A_2 \in \mathbb{R}^{n\times n}$ and vector $b \in \mathbb{R}^{n\times 1}$, the second order Krylove subspace is defined as,*

$$\mathbb{K}_r(A_1, A_2, b) = colspan\left\{P_0, P_1, \cdots, P_{r-1}\right\} \tag{4.17}$$

$$\begin{aligned} \text{,where } P_0 &= G_1, \qquad P_1 = A_1 P_0 \\ P_i &= A_1 P_{i-1} + A_2 P_{i-2}, \qquad i = 2, 3, \cdots \end{aligned}$$

□

$$\begin{aligned} &\mathbb{K}_i\left(\begin{bmatrix} -K^{-1}D & -K^{-1}M \\ I & 0 \end{bmatrix}, \begin{Bmatrix} -K^{-1}f \\ 0 \end{Bmatrix}\right) \\ &= \begin{bmatrix} \mathbb{K}_i(-K^{-1}D, -K^{-1}M, -K^{-1}f) \\ \mathbb{K}_{i-1}(-K^{-1}D, -K^{-1}M, -K^{-1}f) \end{bmatrix} \end{aligned} \tag{4.18}$$

Moreover, if a proportional damping, $D = \alpha M + \beta K$ (α, β are scalars), is assumed, forementioned second order Krylov subspace can be reduced to the classical Krylov subspace form as in equation (4.19) because scalar multiplication to vector and summation of vectors do not change their column space.

$$\mathbb{K}_i(-K^{-1}D, -K^{-1}M, -K^{-1}f) = \mathbb{K}_i(-K^{-1}M, -K^{-1}f) \tag{4.19}$$

Based on the above theory, parameterization will be applied. Using Taylor series expansion, both the stiffness matrix K and the mass matrix M with parameters are formulated as in static case. The simplified formulas after parameterization are as follows.

$$M = M_0 + \sum_i \Delta p_i \; M_i \tag{4.20}$$

$$K = K_0 + \sum_i \Delta p_i \; K_i \tag{4.21}$$

Two parts in Krylov subspace of $\mathbb{K}_i(-K^{-1}M, -K^{-1}f)$ are also turned into parameterized form.

$$K^{-1}M = \left(I + \sum_i \Delta p_i \; K_0^{-1}K_i\right) K_0^{-1} \left(M_0 + \sum_i \Delta p_i \; M_i\right) \tag{4.22}$$

$$K^{-1}f = \left(K_0 + \sum_i \Delta p_i \; K_i\right)^{-1} f = \left(I + \sum_i \Delta p_i \; K_0^{-1}K_i\right) K_0^{-1}f \tag{4.23}$$

By putting equation (4.22) and (4.23) together into Krylov subspace form, equation (4.24) is derived.

$$\begin{aligned}
&\mathbb{K}_r(-K^{-1}M, -K^{-1}f) \\
&= \mathbb{K}_r\left(\left(\sum_{j=0}^{\infty}\left(\sum_i \Delta p_i\ K_i'\right)^j\right)\left(M_0' + \sum_i \Delta p_i\ M_i'\right), \left(\sum_{j=0}^{\infty}\left(\sum_i \Delta p_i\ K_i'\right)^j\right) f_M\right)
\end{aligned} \tag{4.24}$$

where $K_i' = -K_0^{-1}K_i$, $M_i' = -K_0^{-1}M_i$, and $f_M = K_0^{-1}f$

Since the parameter changes Δp_is are scalar values, following Krylov subspace will be taken as a projector.

$$\begin{aligned}
V &= \mathbb{K}_r(-K^{-1}M, -K^{-1}f) \\
&= \mathbb{K}_r\left(\left(\sum_{j=0}^{\infty}\left(\sum_i K_i'\right)^j\right)\left(M_0' + \sum_i M_i'\right), \left(\sum_{j=0}^{\infty}\left(\sum_i K_i'\right)^j\right) f_M\right)
\end{aligned} \tag{4.25}$$

Remark: Unlike in static case, the initial loading vector is no longer significant in dynamic PMOR, because eigen-values/-vectors are properties of the system itself, not a response from certain input force. Therefore two-step Arnoldi is not necessary here.

4.3.1. Reordering process

Because of the inversion term, both parts of Krylov subspace in equation (4.25) have a infinite summation term. It makes Krylov subspace imperfect with finite number of j. However even when any large number j is taken, still some error remains and sometimes the error increases with larger j. The reason of this problem is that while a sum of K_i' are multiplied j times, the order of parameter change Δp_i is also increased j times. Therefore the effects of parameter changes are not fairly reflected into Krylov subspace. As a solution, instead of taking large number j, reordering process is suggested. The coefficients according to the order of Δp_i are as shown in Table 4.1.

order	coefficients
0	$f_M,\ M_0'f_M\ ,\ (M_0')^2\ f_M\ ,\ \cdots\ ,\ (M_0')^j\ f_M$
1	$M_i'f_M,\ K_i'M_0'f_M,\ M_0'K_i'f_M,\ (M_0')^2\ K_i'f_M\ ,\ \cdots\ ,$ $(M_0')^jK_i'f_M\ (i = 1, 2, \cdots)$
2	$K_i'K_j'f_M,\ K_i'\,(M_0')^k\ K_j'f_M,\ (M_0')^k\ K_i'K_j'f_M,\ K_i'M_l'f_M,$ $(M_0')^m\ K_i'\,(M_0')^n\ M_l'f_M,\ \cdots\ (\ i, j, l = 1, 2, \cdots, np\ )\ (k, m, n = 1, 2, \cdots)$

Table 4.1.: The coefficients of Krylov space according to the order of Δp_i

In order to preserve above coefficients from the lower order to the higher order, projection matrix shown in equation (4.26) is suggested.

$$V = \mathbb{K}_r \left(\left(I + \sum_{i=1} K_i' \right) \sum_{i=0} M_i', \left(I + \sum_{i=1} K_i' \right) f_M \right) \in \mathbb{R}^{n \times r} \quad (r \ll n) \tag{4.26}$$

The resulting second order reduced system is in the following formular.

$$M_r \ddot{x}_r + D_r \dot{x}_r + K_r x_r = f_r \tag{4.27}$$

$$\begin{aligned}
\text{,where } M_r(p) &= M_{0,r} + \sum_{i=1} \Delta p_i \, M_{i,r} \\
D_r(p) &= D_{0,r} + \sum_{i=1} \Delta p_i \, D_{i,r} \\
K_r(p) &= K_{0,r} + \sum_{i=1} \Delta p_i \, K_{i,r} \\
x &= V x_r, \qquad f_r = V^T f \\
M_{i,r} &= V^T M_i V \quad \in \mathbb{R}^{r \times r} \qquad i = 0, 1, \cdots \\
D_{i,r} &= V^T D_i V \quad \in \mathbb{R}^{r \times r} \qquad i = 0, 1, \cdots \\
K_{i,r} &= V^T K_i V \quad \in \mathbb{R}^{r \times r} \qquad i = 0, 1, \cdots
\end{aligned}$$

As demanded, once reduced parametric model $M_{i,r}$, $D_{i,r}$, and $K_{i,r}$ are generated, parameter changes are applied to them regardless of original large model.

4.4. Parameter handling

To apply this theory in real applications, how to obtain parametric effective marices, K_is and M_is, will be an important issue. During the theoretical developement they are simplfied by renotation, however, their actual forms are (first or several order of) derivative forms. In this section how to handle parametric effects from finite element (FE) model will be explained.

The benefit from FE model in PMOR is that the fundamental characteristics of its components are already known. Because the FE model is a superposition of numerous elements, which are defined by FE theory, how each parameter will affect the entire structure can be analogized. The exact stiffness and mass matrices are surely in a complex form; however with considering the tendency of parametric effects, for instance whether they change the property of a structure linearly or quadratically, parametrization can be performed easily. And this tendency can be revealed from the matrix of single element. Starting from simple element like beam element, shell element and layered shell element will be shown as well.

4.4.1. Beam element

First by comparing the results from analytic formula and FE model, how the parameter affects to the solution is observed. A clamped beam in Fig. 4.3 is $3m$ long with square cross section of $10cm^2$. Its elastic modulus is $90GPa$. When the force F in $+y$ direction is applied to the tip, the deflection δ is represented analytically as in equation (4.28).From this equation we can easily see the effects of parameter b, h, and E.

$$\delta = \frac{FL^3}{3EI} \tag{4.28}$$

$$\text{where } I = \frac{1}{12}bh^3, \quad b = 10cm, \quad h = 10cm, \quad L = 3m$$

The same model can be solve with FE method as drawin in Fig. 4.4. A single element shown in Fig. 4.5 has a stiffness matrix as in equation (4.29).

$$[K]_{elem} = \frac{EI}{l^3}\left[\begin{array}{ccc|ccc} \frac{Al^2}{I} & 0 & 0 & -\frac{Al^2}{I} & 0 & 0 \\ 0 & 12 & 6l & 0 & -12 & 6l \\ 0 & 6l & 4l^2 & 0 & -6l & 2l^2 \\ \hline -\frac{Al^2}{I} & 0 & 0 & \frac{Al^2}{I} & 0 & 0 \\ 0 & -12 & -6l & 0 & 12 & -6l \\ 0 & 6l & 2l^2 & 0 & -6l & 4l^2 \end{array}\right] = \left[\begin{array}{c|c} M_1 & M_2^T \\ \hline M_2 & M_3 \end{array}\right] \tag{4.29}$$

The stiffness of the entire model is superposed as shown in Fig. 4.6, and the deflection is solved from a static equation $[K]\{x\} = \{f\}$. By plotting the deflection at the tip with various modulus E values, the effect of E on stiffness K can be approximated. From Fig. 4.7, we can see the linear dependency, which is expeceted from both analytical formula and individual element of FE model. To make this clear, the solution $\check{x}_2$ from a linearly approximated stiffness $\check{K}_{E_2}$(approximated stiffness with modulus E_2) will be compared to the solution x_2 from an actual stiffness K_{E_2}. The finite difference between stiffnesses at two reference values E_0 and E_1 is taken as a gradient. Then, approximated stiffness $\check{K}_{E_2}$ about modulus E_2 , E_1 , E_0 can be expressed as in equation (4.30).

$$\check{K}|_{E_2} = (E_2 - E_0) \cdot \frac{K|_{E_1} - K|_{E_0}}{E_1 - E_0} \tag{4.30}$$

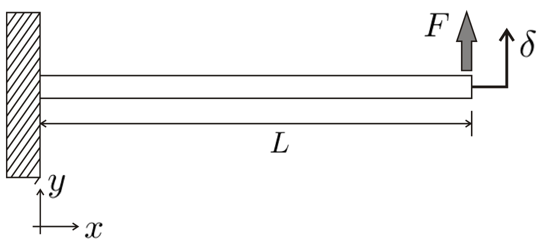

Figure 4.3.: Cantilever beam model

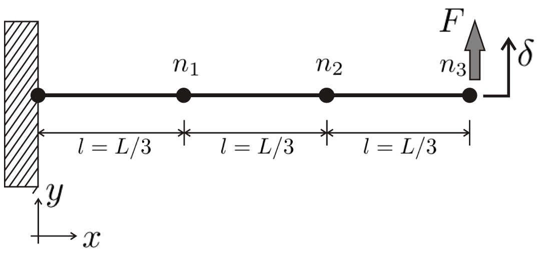

Figure 4.4.: Cantilever beam model in finite element form

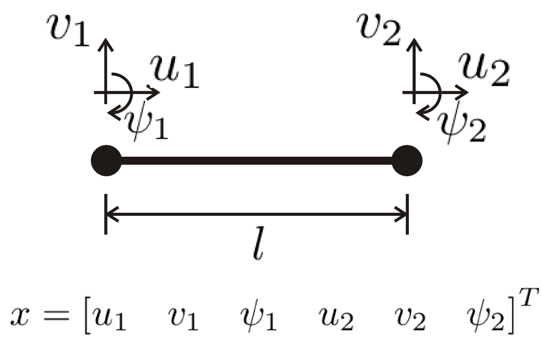

Figure 4.5.: Single beam element

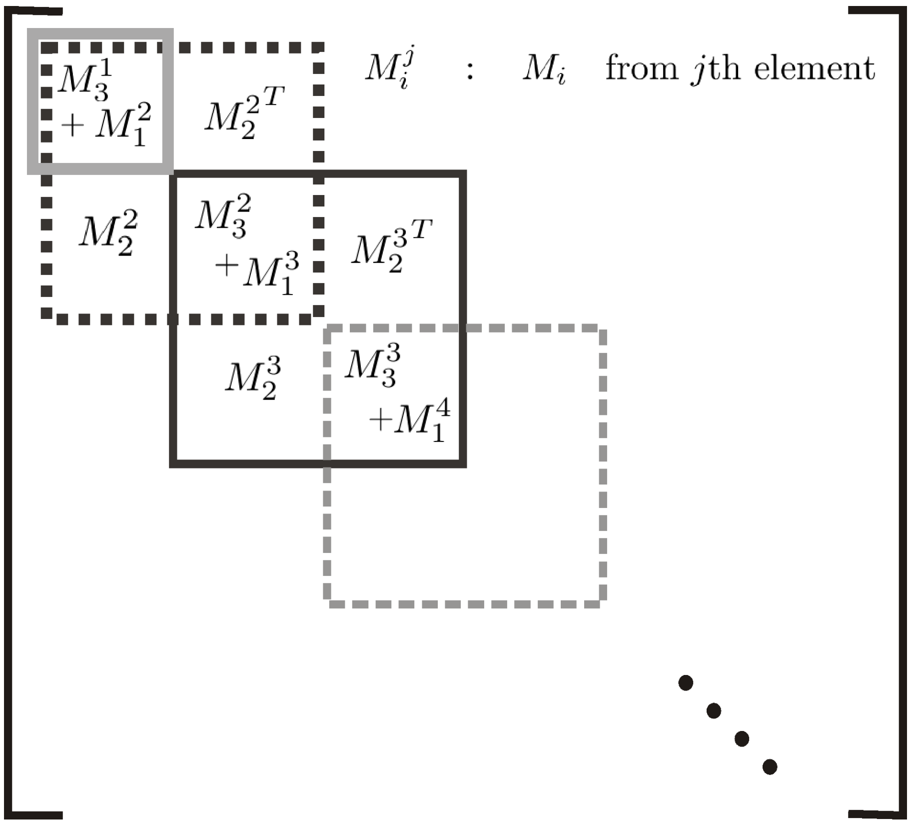

Figure 4.6.: Stiffness matrix superposed by single elements'

The graph comparing approximated solution $\check{x}_2 = \check{K}_{E_2}^{-1}\{f\}$ and exact solution $x_2 = K_{E_2}^{-1}\{f\}$ is shown in Fig. 4.8. The linear assumption to the effect of modulus on stiffness matrix seems correct. The same methodology can be applied to other physical or geometrical parameters in FE model with different element types.

4.4.2. Shell element

As an advanced example shell element is considered. Not only linearly affecting parameters such as modulus and density but also more complicated cases such as thickness are studied. The material property matrix $[D]$ of shell element is in the form of equation (4.31)[ANS07].

$$[D] = \begin{bmatrix} B\,E_x & B\,\nu_{xy}\,E_x & 0 & 0 & 0 & 0 \\ B\,\nu_{xy}\,E_x & B\,E_y & 0 & 0 & 0 & 0 \\ 0 & 0 & 0 & 0 & 0 & 0 \\ 0 & 0 & 0 & G_{xy} & 0 & 0 \\ 0 & 0 & 0 & 0 & G_{yz}/f & 0 \\ 0 & 0 & 0 & 0 & 0 & G_{xz}/f \end{bmatrix} \tag{4.31}$$

$$B = \frac{E_y}{E_y - (\nu_{xy})^2\,E_x}$$

$$f = \left\{ \begin{matrix} 1.2 \\ 1 + 0.2\,\frac{A}{25t^2} \end{matrix} \right\}$$

E_x : Young's modulus in x direction
E_y : Young's modulus in y direction
G_{ij} : Shear modulus in ij plane (i,$j = x,\ y,\ z$)
ν_{xy} : Poisson's ratio in xy plane
A : element area
t : average total thickness

Actual stiffness matrix K can be derived from $[D]$ using following relations.

$$\sigma = [D]\,\varepsilon \tag{4.32}$$

$$\varepsilon = Nu \tag{4.33}$$

$$K = \int N^T\,[D]\,N \tag{4.34}$$

where σ : stress, ε : strain, N : strain-dispalcement matrix, and u : displacement

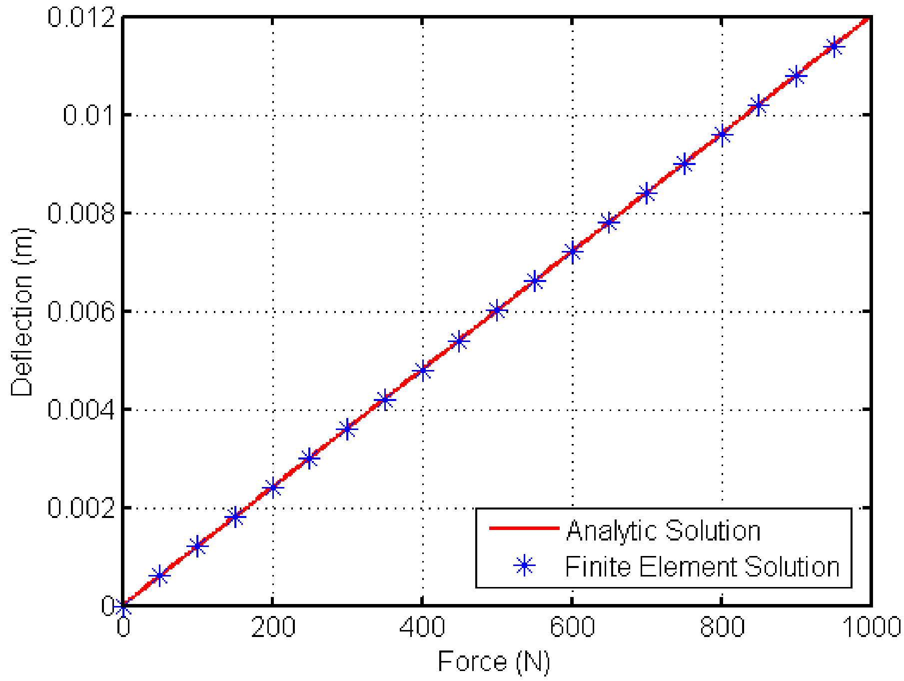

Figure 4.7.: Deflections of beam tip from analytical formula and finite element method according to elastic modulus

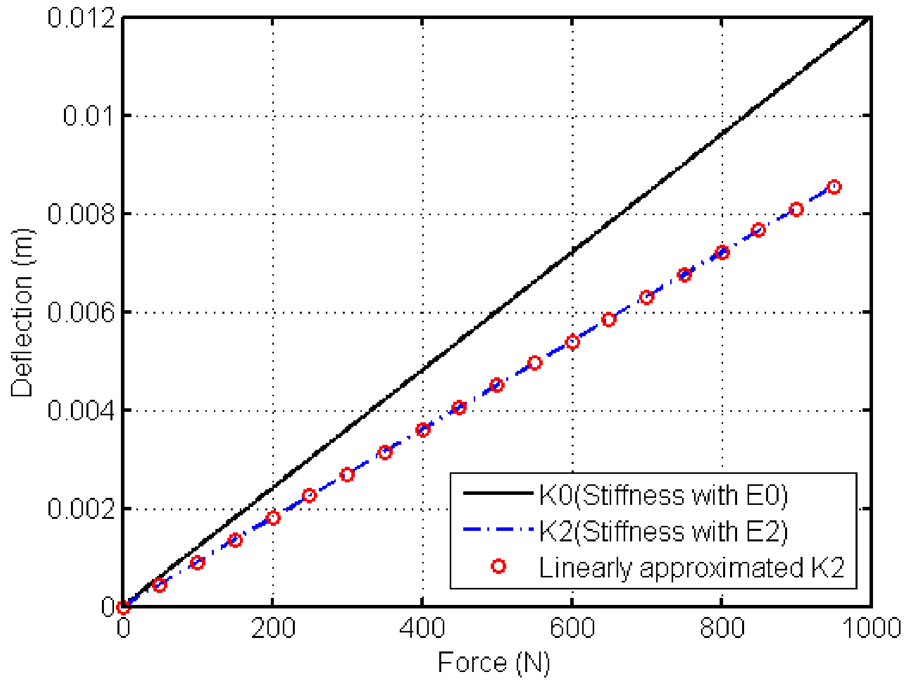

Figure 4.8.: Comparions of exact solution and linearly approximated solution

Because the strain-displacement matrix N is the function of shape function and nodal position, it is independent on the material properties or thickness of the shell. Therefore the stiffness matrix will be affected by those parameters in the same way the material property matrix is affected. By observing the role of each parameter in $[D]$ we can determine how to handle each parameter.

1) Shear modulus G_{xy}, G_{yz}, G_{xz}
From equation (4.31), shear moduluses are lineary affecting parameters. Their effects are approximated by equation (4.35)

$$K|_{G_2} = K|_{G_0} + \frac{K|_{G_1} - K|_{G_0}}{G_1 - G_0} \cdot (G_2 - G_0) \tag{4.35}$$

2) Elastic modulus E_x
By considering each element of K, the effects of E_x can be approximated as follows.

$$K_{(1,1)} = BE_x = \frac{E_x E_y}{E_y - \nu^2 E_x} \tag{4.36}$$

$$K_{(1,2)} = K_{(2,1)} = \nu_{xy} BE_x \tag{4.37}$$

$$K_{(2,2)} = BE_y = \frac{E_y^2}{E_y - \nu^2 E_x} \tag{4.38}$$

$$K_{(1,1)}|_{E_x+\Delta E_x} - K_{(1,1)}|_{E_x} = \frac{\Delta E_x \; E_y^2}{(E_y - \nu^2 E_x)(E_y - \nu^2 E_x - \nu^2 \Delta E_x)} \tag{4.39}$$

$$\approx k_1 \Delta E_x \quad (*) \tag{4.40}$$

$$K_{(2,2)}|_{E_x+\Delta E_x} - K_{(2,2)}|_{E_x} = \frac{\nu^2 \Delta E_x \; E_y^2}{(E_y - \nu^2 E_x)(E_y - \nu^2 E_x - \nu^2 \Delta E_x)} \tag{4.41}$$

$$\approx k_2 \Delta E_x \quad (*) \tag{4.42}$$

where k_1, k_2 : scalar

$(*) \because \nu 1, \quad E_y - \nu^2 E_x \gg \nu^2 \Delta E_x$ with small ΔE_x

3) Elastic modulus E_y
With the same manner in E_x case, the effect of E_y can be approximated as follows.

$$K_{(1,1)}|_{E_y+\Delta E_y} - K_{(1,1)}|_{E_y} = \frac{-\nu^2 \; E_x^2 \; \Delta E_y}{(E_y - \nu^2 E_x)(E_y + \Delta E_y - \nu^2 E_x)} \tag{4.43}$$

$$\approx k_3 \Delta E_y \tag{4.44}$$

$$K_{(2,2)}|_{E_y+\Delta E_y} - K_{(2,2)}|_{E_y} = \frac{-\nu^2 \; E_x \; (\Delta E_y)^2 \; + \; 2E_y \; (E_y - \nu^2 E_x) \; \Delta E_y}{(E_y - \nu^2 E_x)(E_y + \Delta E_y - \nu^2 E_x)} \tag{4.45}$$

$$\approx k_4 \Delta E_y \tag{4.46}$$

where k_3, k_4 : scalar

(4.47)

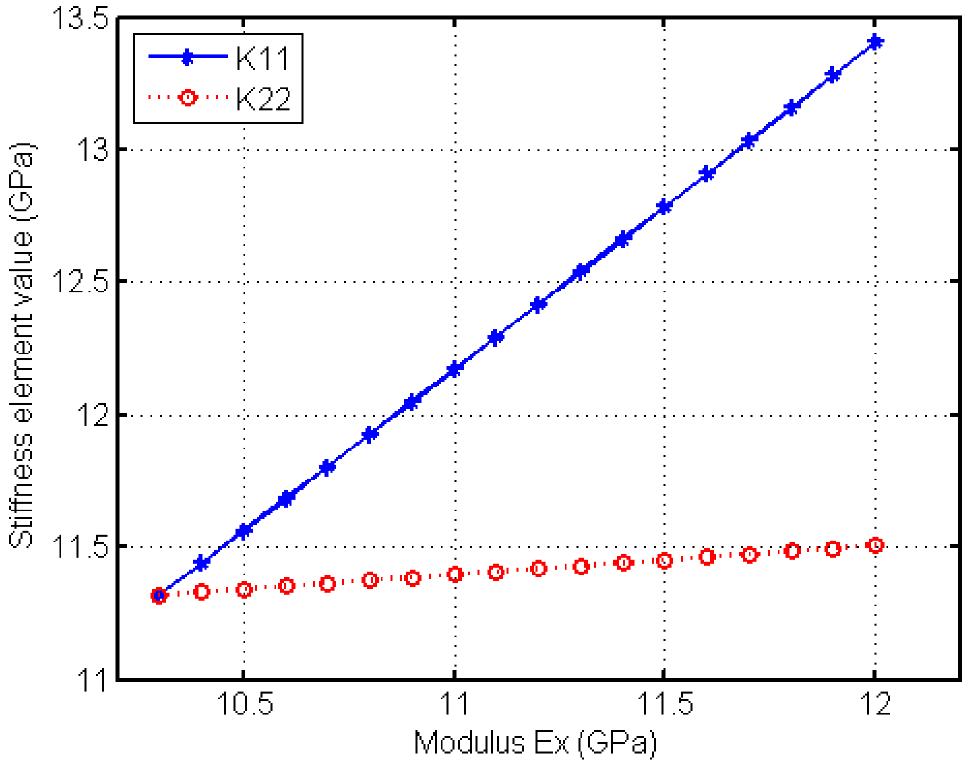

Figure 4.9.: Element in a stiffness matrix, $K_{(1,1)}$ plot depending on E_y

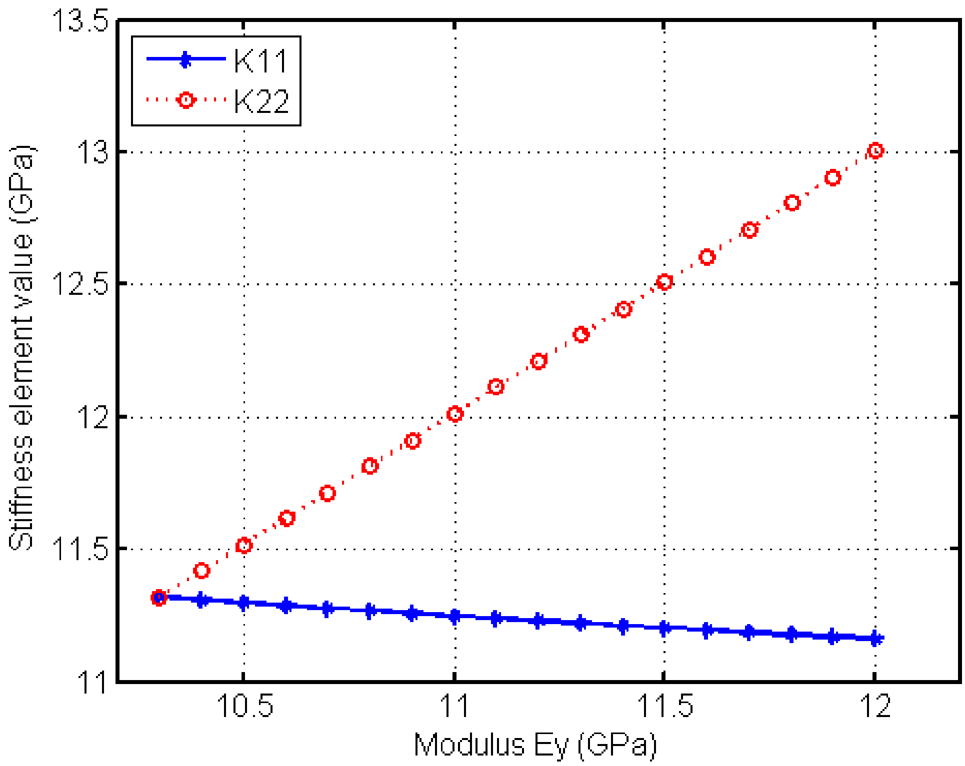

Figure 4.10.: Element in a stiffness matrix, $K_{(2,2)}$ plot depending on E_y

This linear tendency is also graphcally checked in Fig. 4.9 and Fig. 4.10.

4) Thickness t
In a single element, if its area is bigger than $25t^2$, shear modulus G_{yz} and G_{xz} in matrix $[D]$ are devided by $f = 1 + 0.2A/(25t^2)$ instead of 1. The effect of thickness t is shown analytically and graphically in equation (4.48) and Fig. 4.11.

$$\frac{G}{1 + k/t^2} = \frac{G\,t^2}{t^2 + k} = G - \frac{Gk}{t^2 + k} \tag{4.48}$$

From those observations it makes more sense treating t^2 as a parameter instead of t. For such a case, chain rule is used to obtain a parametric effectiveness matrix.

$$\frac{dK}{d(t^2)} = \frac{\partial K}{\partial t}\frac{\partial t}{\partial t^2} = \frac{\partial K}{\partial t}\frac{1}{2t} \tag{4.49}$$

Thickness alters not only a stiffness matrix but also a mass matrix; however, the increment or decrement in mass caused by thickness change is linear. Therefore the effect of thickness change on a mass matrix will be linear.

5) Density ρ
Density does not change stiffness matrix but mass matrix linearly. Hence, density doesn't need to be treated as a parameter in static case, but it does in dynamic case.

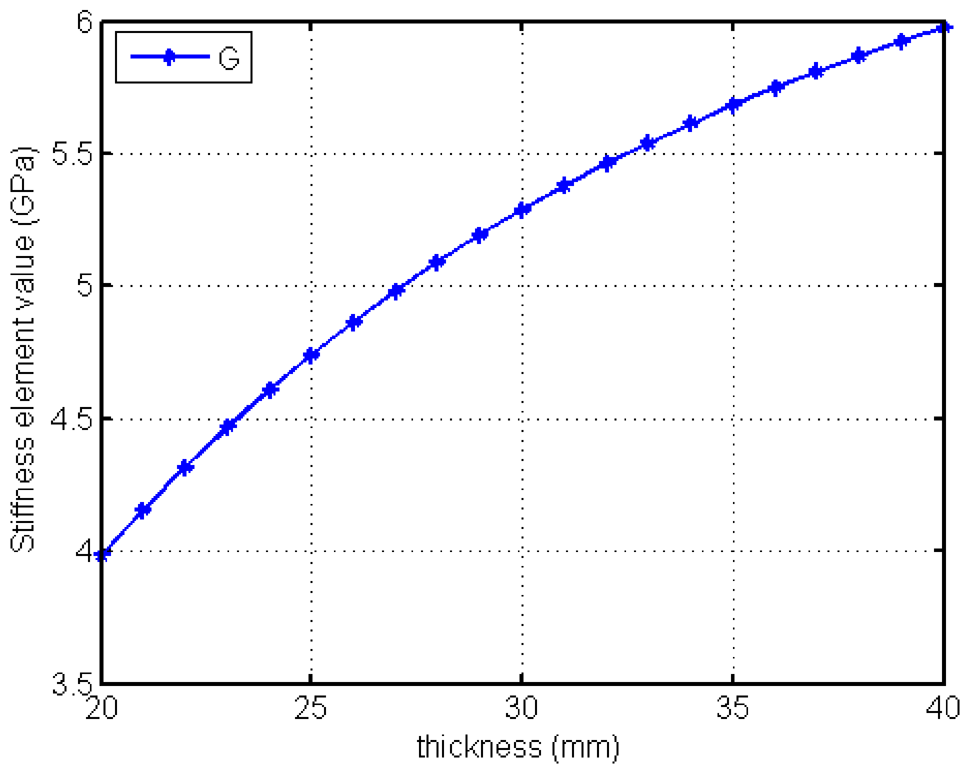

Figure 4.11.: Shear modulus depending on thickness t

4.4.3. Layered shell element

A layered shell element is commonly used for composite structures. Its basic formulation is very similar to the normal shell element we looked in previous section 4.4.2. The only difference is that the material property matrix from each layer is summed up to construct the material property matrix for the entire layered element as shown in equation (4.50). Note that the thickness which divides the shear modulus in equation (4.31) is not a thickness of each layer but a total averatge thickness.

$$[D] = \sum_{j=1}^{nl} [D]_j \tag{4.50}$$

where $[D]_j$ is constructed as same as in equation (4.31)
and nl is the number of layers

Consequently the effect of the parameters from each layer follows the same way as shown in section 4.4.2. If a sandwich structure is modeled, the term f in equation (4.31) is set to 1 and G_{yz} and G_{xz} of facesheets are set to 0. Therefore the thickness of the core is treated as a linear parameter, and G_{yz} and G_{xz} of facesheets are not considered as parameters.

4.5. Application of LU decomposition method

The methodology shown in previous sections, 4.2 and 4.3, is designed to find the common projector matrix V, which contains the essential information about the structure and parameters' effects on it. From the equation (4.11) and the equation (4.25), which are finally used to calculate V, we can see that an inversion of stiffness matrix K_0 is included. Since a stiffness matrix from finite element (FE) momdel is very sparse, inverting it is computationally expensive, and the resultant inversion is very densed. It causes high computation on further processes in model order reduction, because the matrices used for Krylov subspace calculation are no longer sparse after dense inversion matrix is multiplied to them. Furthermore, the inversion requires large memory as well; for instance, an inversion from a 34380 by 34380 very sparse stiffness matrix from FE model consumes about 10 gigabyte(GB) memory. It means that reading and saving the matrix spend a lot of time inefficiently. This inversion included in parametric model order reduction (PMOR) algorithm has been a major weakness of this method as reported in [YB09]. However, we can avoid inversion using LU decomposition method as in general matrix equation solver. Applying LU decomposition method to the PMOR algorithm will be introduced in this section.

4.5.1. LU decomposition method

LU decomposition is a powerful method in solving large linear system equation, $Ax = b$, where $A \in \mathbb{R}^{n\times n}$, $b \in \mathbb{R}^{n\times 1}$, and solution $x \in \mathbb{R}^{n\times 1}$. One can solve this equation by Gaussian elimination and back substitution, but it requires a computation order of $n^3/3$; therefore when the system needs to be solved for many input b_is $\in \mathbb{R}^{n\times 1}$, computational effort could be a major problem. One way to solve a matrix equation easily is turning a matrix into a tridiagonal form, as in Gaussian method. But in Gaussian method specific vector b is used during the transformation process. The idea of LU decomposition method is to use triangular matrices which depend on the system matrix A only, not on the input vector b. It is possible and guaranteed for any invertible matrix A as shown in Theorem 4.1

Theorem 4.1 *If matrix $A \in \mathbb{R}^{n\times n}$ is nonsingular, there exist a lower triangular matrix L and an upper triangular matrix U such that $A = LU$, and they are unique.*

□

Once the system matrix A is decomposed into two triangular matrices L and U, the solution x can be much efficiently calculated through two times of forward- or backward-substition as shown in Fig. 4.12.

4.5.2. Application to the PMOR algorithm

The equation (4.11) can be simplified as in equation (4.51).

$$V = \mathbb{K}_r\left(K_0^{-1}K_s^*, K_0^{-1}f\right) \text{ where } K_s^* = \sum_{i=1} -K_i$$

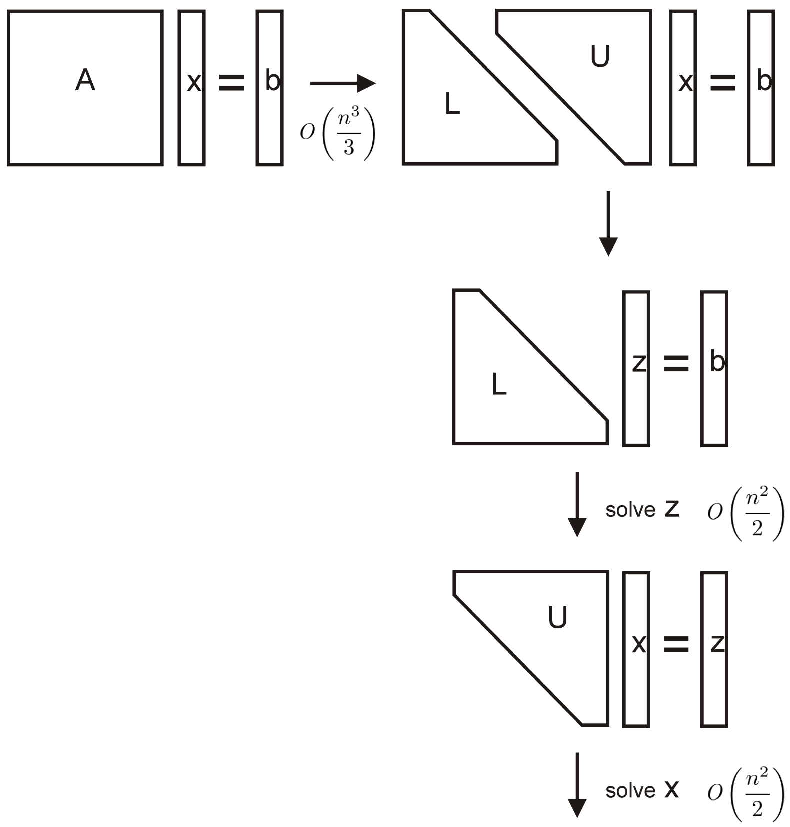

Figure 4.12.: LU decomposition method to solve matrix equation

In the reduction of dynamic system, the equation (4.25) can be expressed as in equation (4.51).

$$V = \mathbb{K}_r \left(K_0^{-1} K_d^* K_0^{-1} M_d^*, \quad K_0^{-1} K_d^* K_0^{-1} f \right) \tag{4.51}$$
$$\text{where} \quad K_d^* = K_0 + \sum_{i=1} -K_i, \quad M_d^* = \sum_{i=0} M_i$$

As explained in the beginning of this subchapter, the most controversial part here is the calculation and multiplication of K_0^{-1} before the Arnoldi iteration. However, as the Krylov subspace method has a great benefit that it runs only with matrix-vector multiplication, we can apply LU decomposition method inside of the Arnoldi algorithm which used in PMOR so that matrix L and U play the same roles as in solving $Ax = b$.
Let us take a closer look; the first Krylov vector $x_1 = K_0^{-1} f$ can be calculated by solving $K_0 x_1 = f$ using L and U. The next Krylov vector, $x_2 = K_0^{-1} K_s^* x_1$ can be calculated by solving $K_0\, x_2 = K_s^*\, x_1 \in \mathbb{R}^{n\times 1}$. The further process will be continued in the same manners. Extracting orthogonal basis vectors is the same as in general Arnoldi algorithm.
In dynamic case solving matrix-vector equation with L and U should be used twice in each iteration, because K_0^{-1} is used twice in each iteration. The first Krylov vector $x_1 = K_0^{-1}\, K_d^*\, K_0^{-1} f$ will be calculated by following two steps:

1) calculate $z_1 = K_0^{-1} f$ by solving $K_0\, z_1 = f$.

2) calculate $x_1 = K_0^{-1}\,(K_d^*\,z_1)\,f$ by solving $K_0\,x_1 = K_d^*\,z_1$.

The next Krylov vector $x_2 = K_0^{-1}\,K_d^*\,K_0^{-1}\,M_d^*\,x_1$ can be obtained by following two steps:

1) calculate $z_2 = K_0^{-1}\,(M_d^*\,x_1)$ by solving $K_0\,z_2 = M_d^*\,x_1$.

2) calculate $x_2 = K_0^{-1}\,(K_d^*\,z_2)$ by solving $K_0\,x_2 = K_d^*\,z_2$.

Further iterations are continued in the same way. The algorithms including the general Arnoldi iteration and two-step method with deflation in static case are summarized in Algorithm 4.2 and Algorithm 4.3.

Algorithm 4.2 *For lower and upper triangular matrices L and U such that $K_0 = LU \in \mathbb{R}^{n\times n}$, vector set $B = \{b_1\,, \cdots, b_p\} \in \mathbb{R}^{n\times 1}$, and matrix $K_s^* = \sum_{i=1} -K_i$ from equation (4.51), the following algorithm is applied.*

Step 1. Initiation

$$
\begin{aligned}
& x = U \setminus (L \setminus b_1) \\
& w_1^\circ = x/\|x\| \\
& \textit{for} \quad i = 1, \cdots, p-1 \\
& \qquad z = U \setminus \left(L \setminus \left(K_s^* \, w_{2i-1}^\circ\right)\right) \\
& \qquad \textit{for} \quad j = 1, \cdots, 2i-1 \\
& \qquad\qquad h'_{j,2i-1} = \left(w_j^\circ\right)^T z \\
& \qquad\qquad z = z - h'_{j,2i-1} w_j^\circ \\
& \qquad \textit{end} \\
& \qquad h'_{2i,2i-1} = \|z\| \\
& \qquad w_{2i}^\circ = z/h'_{2i,2i-1} \\
& \qquad x = U \setminus (L \setminus b_{i+1}) \\
& \qquad z = x/\|x\| \\
& \qquad \textit{for} \quad j = 1, \cdots, 2i \\
& \qquad\qquad h'_{j,2i} = \left(w_j^\circ\right)^T z \\
& \qquad\qquad z = z - h'_{j,2i-1} w_j^\circ \\
& \qquad \textit{end} \\
& \qquad h'_{2i+1,2i} = \|z\| \\
& \qquad w_{2i+1}^\circ = z/h'_{2i+1,2i} \\
& \textit{end}
\end{aligned}
$$

Step2. Deflation

$$
\begin{aligned}
& j = 1 \\
& W^\circ = \left[w_1^\circ \, w_2^\circ \, \cdots \, w_{2p}^\circ\right] \\
& ch = W^{\circ T} W^\circ \\
& \textit{for} \quad i = 2, \cdots, 2p \\
& \qquad \textit{if} \quad |ch_{i,1:i-1}| \quad \textit{small enough} \\
& \qquad\qquad w_j = w_i^\circ \\
& \qquad\qquad j = j+1 \\
& \qquad \textit{end} \\
& \textit{end} \\
& sz = j-1
\end{aligned}
$$

Step 3. Block Arnoldi

for $i = sz, sz+1, \cdots$
  $z = U \setminus (L \setminus (K_s^* \, w_i))$
  for $j = 1, \cdots, i$
    $h_{j,i} = w_j^T z$
    $z = z - h_{j,i} w_j$
  end
$h_{i+1,i} = \|z\|$
$w_{i+1} = z / h_{i+1,i}$
end

Step 4. Deflation

$j = 1$
$W = [w_1 \, w_2 \, \cdots]$
$ch = W^T W$
for $i = 2, \cdots$
  if $|ch_{i,1:i-1}|$ *small enough*
    $v_j = w_i$
    $j = j + 1$
  end
end

Algorithm 4.3 *For lower and upper triangular matrices L and U such that $K_0 = LU \in \mathbb{R}^{n\times n}$, a vector $f \in \mathbb{R}^{n\times 1}$, and matrix $K_d^* = K_0 + \sum_{i=1} -K_i$ and $M_d^* = \sum i = 0M_i$ from equation (4.51), the following algorithm is applied.*

Step 1. Arnoldi iteration for PMOR

$$
\begin{aligned}
& x = U \setminus (L \setminus f) \\
& z = U \setminus (L \setminus (K_d^* \, x)) \\
& w_1 = z/\|z\| \\
& \textit{for} \quad i = 1, \cdots, r \\
& \qquad x = U \setminus (L \setminus (M_d^* \, w_i)) \\
& \qquad z = U \setminus (L \setminus (K_d^* \, x)) \\
& \qquad \textit{for} \quad j = 1, \cdots, i \\
& \qquad\qquad h'_{j,i} = w_j^T z \\
& \qquad\qquad z = z - h'_{j,i} w_j \\
& \qquad \textit{end} \\
& \qquad h'_{i+1,i} = \|z\| \\
& \qquad w_{i+1} = z/h'_{i+1,i} \\
& \textit{end}
\end{aligned}
$$

Step 2. Deflation

$$
\begin{aligned}
& j = 1 \\
& W = [w_1 \, w_2 \, \cdots] \\
& ch = W^T W \\
& \textit{for} \quad i = 2, \cdots \\
& \qquad \textit{if} \quad |ch_{i,1:i-1}| \quad \textit{small enough} \\
& \qquad\qquad v_j = w_i \\
& \qquad\qquad j = j + 1 \\
& \qquad \textit{end} \\
& \textit{end}
\end{aligned}
$$

With this method the computational time and required memory to calculate projector matrix V is reduced enormously. Although in the beginning quite amount of computation $(2n^3/3)$ is required to calculate L and U, it is still much less than inverting a matrix. Considering further usauages of inversion in the Arnoldi algorithm and the memory problem, using LU decomposition instead of inversion provides much more effective. Moreover, the reduced model from LU method shows as accurate result as the model from inversion, which will be shown with numerical examples in chapter 5.

5. Numerical Examples

The parametric model order reduction (PMOR) method developed in chapter 4 is applied to a large finite element (FE) model. The main point here is 1) how much order can be reduced 2) without losing its accuracy in a certain level 3) and the amount of saving in computational effort. The two main types of structural analysis, static analysis and dynamic analysis are examined. Furthermore, PMOR is used for a design optimization problems. The target models are generated by commercial FE program, ANSYS. Its structural matrices, stiffness matrix and mass matrix, are read from the binary files generated by ANSYS. The modified codes from Structural Modeling Interface (SMI) Toolbox developed by Institute of Lightweight Structures (LLB) are used[MB]. After then PMOR procedure is taken place in MATLAB platform, a numerical matrix computation program. The flowchart in Fig. 5.1 shows the overall procedure of PMOR according to the software platform. The stiffness and mass matrices extracted from ANSYS directly correspond to the stiffness and mass matrices in the equations in chapter 4. Parametric effectiveness matrices concerning derivative terms in equation (4.5) are calculated based on linear approximation and chain rule as explained in section 4.4.

The results from static and dynamic analyses of reduced model are compared with those of original large model as well as optimization problems. Not only accurate result at the reduced point but also accurate result with many cases of parameter changes will be achieved. Furthermore, structural control will be attempted. The final goal is to design a controller with parameterized reduced model showing good performances under various parameter changes. A prospect of PMOR for the optimization will also be observed. Design variables in optimization problem can be treated as parameters; then, each functional evaluation can be done quickly with the reduced model.

For static case large scale reflector made of carbon fiber reinforced polymer(CFRP)-aluminum(Al) honeycomb sandwich is chosen. For dynamic case, truss structure with some active elements and solar array panel made of 5-layered CFRP-Al honeycomb-steel sandwich structure will be shown. Designing a composite plate under torsional load is the first optimization example. As a more complicated example, a model of a mirror panel of the overwhelming large (OWL) telescope developed by the European Southern Observatory (ESO) is taken.

5.1. PMOR for static analysis and control of FE model

Model order reduction for static analysis is often ignored because static analysis does not require high computational effort as in dynamic analysis. In spite of that, when

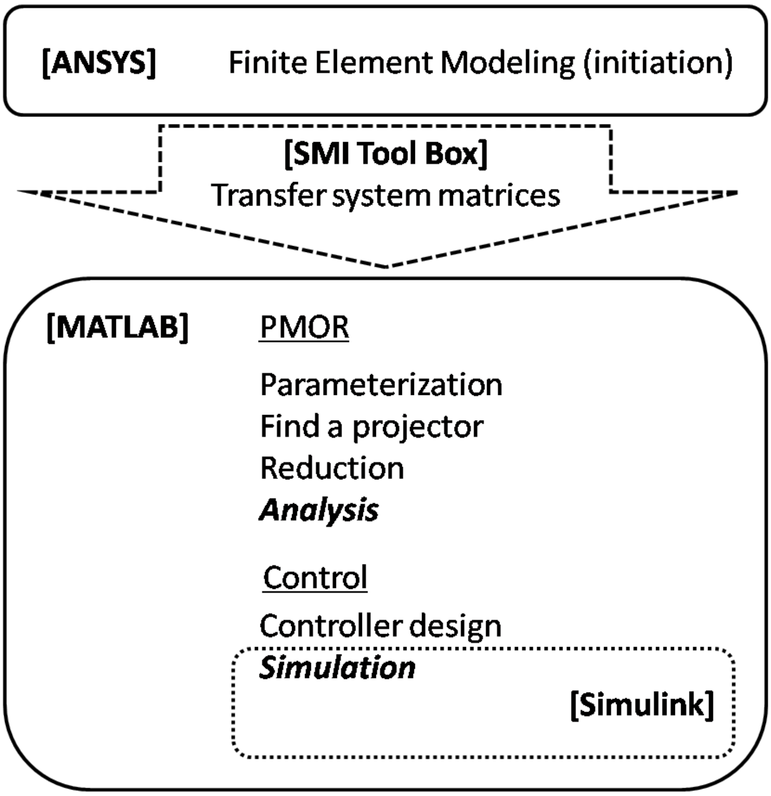

Figure 5.1.: Actual PMOR procedure in ANSYS-SMI-MATLAB platform

the model need to be evaluated many times as in optimization problems, a reduced model is much more beneficial. Here in this chapter, large reflector model is examined for PMOR. And the optimal control force for shape control is calculated based on the reduced model via optimization algorithm. As the number of actuators is high, which is common in such a large structure, the required functional evaluation is increased drastically both from the parameter changes and from the input changes. Therefore a reduced model can diminish a lot of computational load.

5.1.1. Large reflector

Model and parameter definition

A large scale reflector illustrated in Fig. 5.2 is modeled. Its diameter is 20m, and it is made of CFRP-Al honeycomb sandwich. As stiffners, beam supports are located on every 30 degrees. The center of the reflector is fixed. And the overall structure except beam supports are modeled by layered shell element. The model is meshed freely using smart meshing option in ANSYS except the nodes on the beam support, where the actuators are applied later. It indicates that the PMOR method can be applied to any types of FE model not only to manually designed FE matrices.

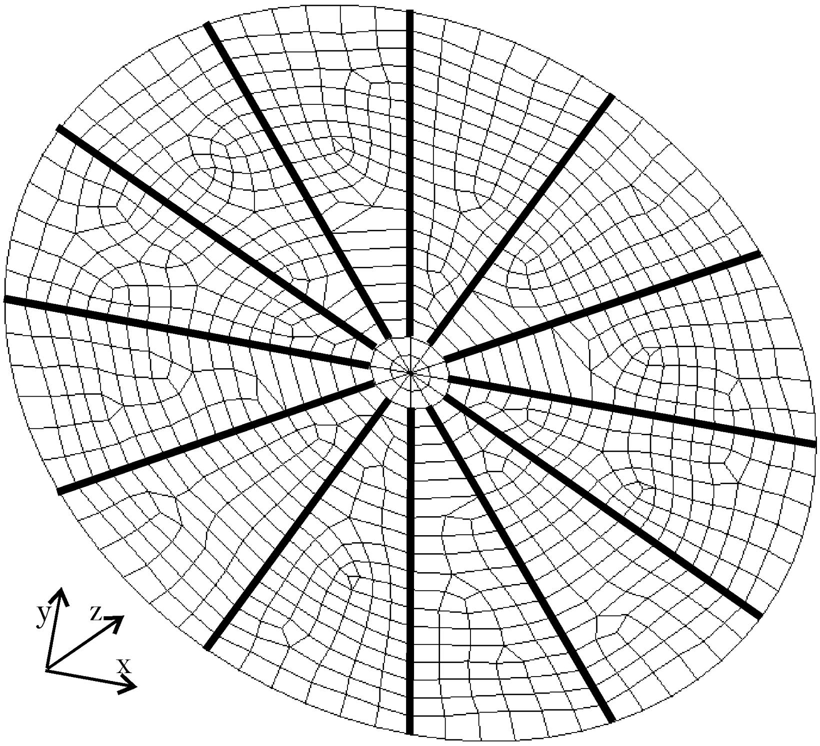

Figure 5.2.: Large reflector model

A composite sandwich plate is built as shown in Fig. 5.3. The modulus and thickness of facesheet and core are chosen as parameters. Since CFRP composite is artificially made, the variation of its property is quite wide by adjusting fiber angles and contents as well as selecting materials for fiber and matrix. Core has relatively limited property variation; but still there is a possibility to change its parameter by adjusting the shape and size of the cells in honeycomb. Therefore above parameters are reasonable choices for parametric study. Overall there are 6 parameters concerned: elastic modulus of facesheet E_x and E_y, shear modulus of facesheet G_{xy}, elastic modulus of core E_c, thickness of facesheet t_f, and thickness of core t_c. Initial values of these parameter are listed in Table 5.1. The facesheet is modeled as a carbonfiber-epoxy composite [Hexa] with 60% fiber contents, fiber angle layup of $[0/90/\pm 45]_S$. The material properties for honeycomb are taken from Hexweb Al 5052 honeycomb ($1/8$-5052-0.0001) product [Hexb].

Parametrization

To build parametric effectiveness matrices, six parameters are varied to $\pm 50\%$ of their initial values. To increase the accuracy of the reduced model, both of the region where each parameter is increasing or decreasing are considered as shown in Fig. 5.4. However, the same projection matrix V will be applied on both regions.

Parameterization proccedure is summarized in Fig. 5.5. As examined in section 4.4.2 and 4.4.3, the effect of elastic modulus E_x and E_y from facesheet will be assumed

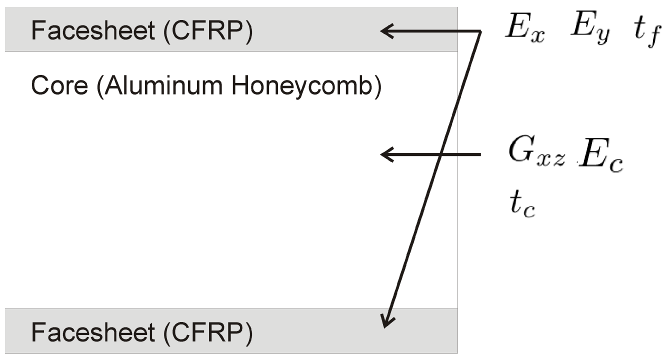

Figure 5.3.: A composite structure of reflector model

E_x	62.9 (GPa)
E_y	62.9 (GPa)
G_{xy}	23.0 (GPa)
E_c	1.03 (GPa)
t_f	1 (mm)
t_c	18 (mm)

Table 5.1.: Initial parameter values for a large reflector model

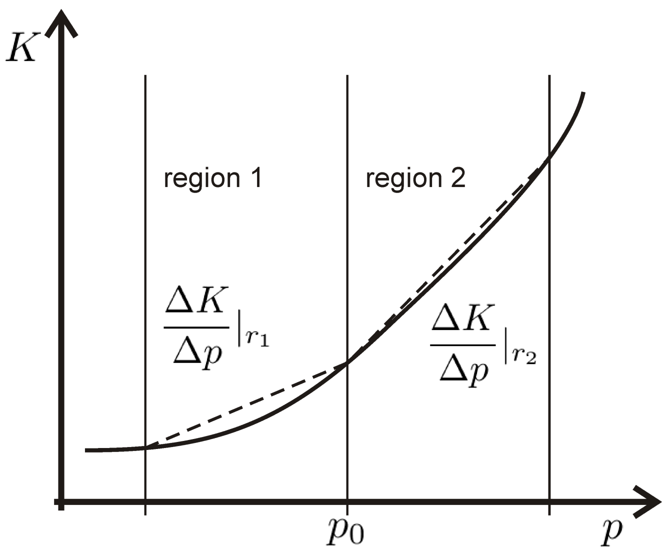

Figure 5.4.: Two sections used for parameterization

linearly. The moduluses from the core,G_{xz}, G_{yz}, and E_c changing all together proportionally, are linearly approximated as well. The thicknesses are treated differently. Within the initial variation, which is $\pm 50\%$ in this example, they are also assumed as linearly affecting parameters. Over the initial variation the effects are approximated quadratically. As shown in section 4.4.2, t^2 is treated as a parameter instead of t using chain rule. In equation (4.49) the only difference from linear approximation is that the term $\frac{1}{2t}$ is multiplied. Therefore, the reduction procedure itself can remain same as with t; but when new parameter t is applied from initial value t_0, the parameter change should applied by $\frac{1}{2t_0}(t^2 - t_0^2)$ instead of $(t - t_0)$. Additionally, since thickness t is an average thickness of whole shell element, the effect of $t_f t_c$ from $t^2 = (t_f + t_c)^2$ should be considered as well.

Parametric model reduction

Based on the theory in section 4.2, projection matrix V is calculated from equation (4.10). Both two-step Arnoldi algorithm and deflation process are applied. Finally parameterized reduced model $K_{i,r} \in \mathbb{R}^{r \times r}$ $(i = 0, 1, \cdots)$ is induced by projection. Parameter changes are applied as in equation (5.1) and the solution in the reduced space x_r can be quickly solved. Back projecting x_r into the original space through equation (5.2), we have approximated solution x in the original space.

$$\left(K_{0,r} + \sum_{i=1}^{q} \Delta p_i K_{i,r} \right) x_r = K_r(p) x_r = f_r \tag{5.1}$$

$$x = V x_r \tag{5.2}$$

Analysis results and computational order

The model is reduced from the order of 17,262 to the order of 150, which is only 0.87% of the original model. Displacement caused by various loading on z-direction, perpendicular to the surface of the reflector, is observed both from the ANSYS analysis and from the reduced model analysis. To show an exemplary case, arbitrarily

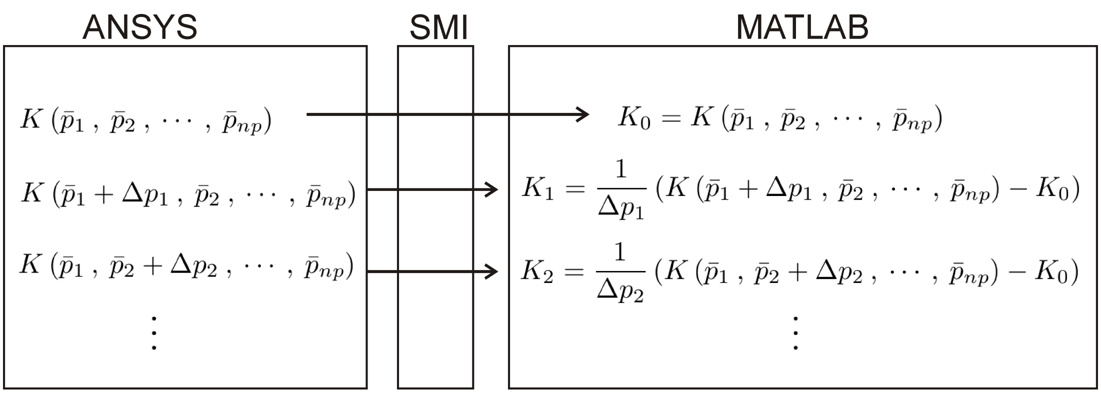

Figure 5.5.: Parameterization process

generated forces as shown in Fig. 5.6 are applied. The accuracy of parameterized reduced model is measured by root mean square (RMS) value of the shape deformation error between the reduced model and ANSYS analysis from all nodes. The reduced model and original model show good agreement, and parametric effects are also reflected on the reduced model very well.
As an example, the case with 40% change of each parameter ($\Delta p_i = +40\%, i = 1, \cdots, 6$), and the case with mixed parameter change are observed as well as no parameter change case. The parameter changes by cases are listed in Table 5.2. The deformation RMS error values are shown in Table 5.3. It shows that the reduced model gives acceptable results with only 150 order model, and it also reflects parameter changes to the model well. To present the effect of parameters' changes more clearly, the RMS error of shape deformation between the model without parameter change and with parameter changes are shown in 3th column. Graphical comparison between reduced model and original model with parameter change is also shown. Two pathes are taken as drawn in Fig. 5.7 to observe the deformation: the first path is along the x axis, and the second path is 60° apart from the first path. The deformed shapes from the cross-section area along the path are shown in Fig. 5.8 and Fig. 5.9 from case 7 and case 8. The results from other cases (from case 0 to case 6) are provided in Appendix B.1.

Note on the role of two-step Arnoldi method

As mentioned in 4.2.1, with single initial loading vector resultant reduced model shows inaccurate results even without any parameter change. The comparison between general PMOR method suggested in [DSC+04] and PMOR with two-step Arnoldi method is presented here. If the load near the initial loading is applied or the result near the initial loading point is interested only, the reduced model from general PMOR method gives fairly accurate result. For instance, when a single loading vector which gives force on $(1500, 0, 0)$ is used for PMOR, the deflection plot along the x axis shows acceptable result as shown in Fig. 5.10. However, the deflection along the path 2 in Fig. 5.11 shows that this reduced model gives completely wrong result. From here we can conclude that two-step Arnoldi is necessary to be used in static PMOR.

Optimal control input design and shape control results

The parameterized low-order model can be used for a shape control of the reflector; for exmaple, to find an optimal control input involving many actuators. For the flat and wide structure as a large reflector, large number of actuators are required, which means large number of design variables (actuation forces) should be considered. In such a case finding optimal solution requires enormous computational effort because the analysis should be repeated many times until the convergence. Therefore using a reduced model is computationally much more beneficial than using a full order model. The *fmincon* function in MATLAB is applied here. *fmincon* uses the Sequential Quadratic Programming (SQP) method, and can handle upper and lower bounds of

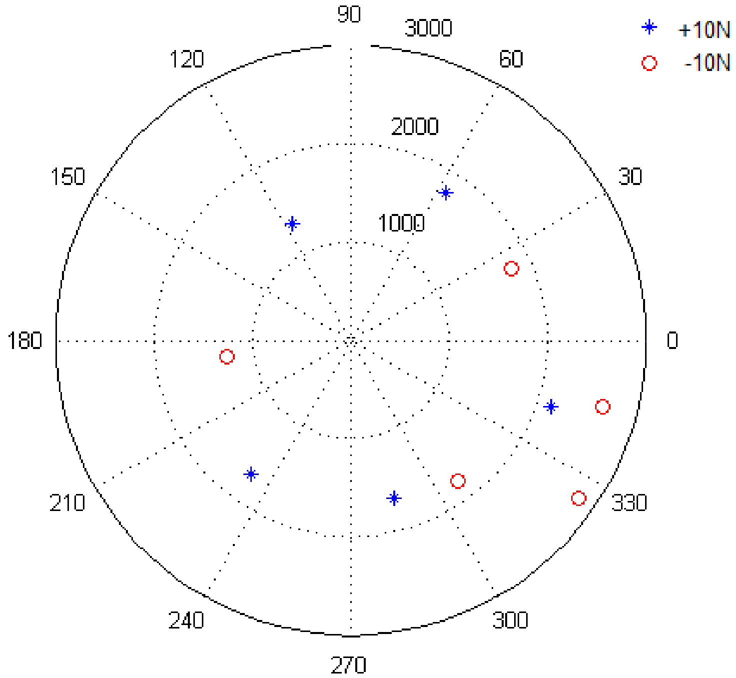

Figure 5.6.: Locations of the randomly chosen loading

case number	parameter changes
case 0	$\Delta p_i = 0 \ (i = 1, 2, \cdots, 6)$
case 1	$\Delta p_1 = +40\%$
case 2	$\Delta p_2 = +40\%$
case 3	$\Delta p_3 = +40\%$
case 4	$\Delta p_4 = +40\%$
case 5	$\Delta p_5 = +40\%$
case 6	$\Delta p_6 = +40\%$
case 7	$\Delta p_1 = +20\%$, $\Delta p_2 = +20\%$, $\Delta p_3 = +20\%$, $\Delta p_4 = +20\%$, $\Delta p_5 = +20\%$, $\Delta p_6 = +20\%$
case 8	$\Delta p_1 = -40\%$, $\Delta p_2 = +40\%$, $\Delta p_3 = +20\%$, $\Delta p_4 = -20\%$, $\Delta p_5 = -10\%$, $\Delta p_6 = +10\%$

Table 5.2.: Parameter changes from each cases

case number	RMS error between reduced and original model (mm)	RMS value caused by parameter changes (mm)
case 0	0.015	0
case 1	0.021	0.208
case 2	0.030	0.363
case 3	0.021	0.243
case 4	0.015	0.015
case 5	0.013	0.709
case 6	0.034	0.974
case 7	0.078	1.130
case 8	0.078	0.633

Table 5.3.: Deformation RMS error between reduced model and full model with various parameter sets

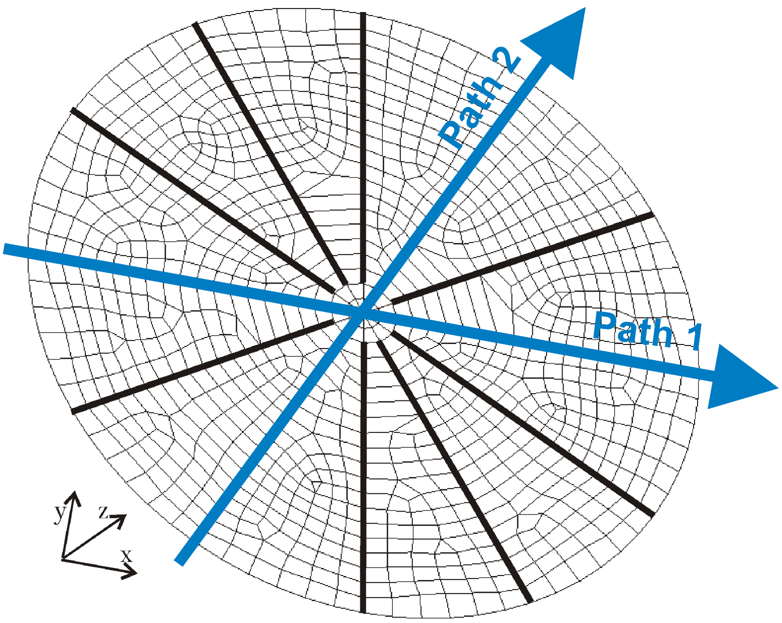

Figure 5.7.: Paths to observe the deformation on the cross section

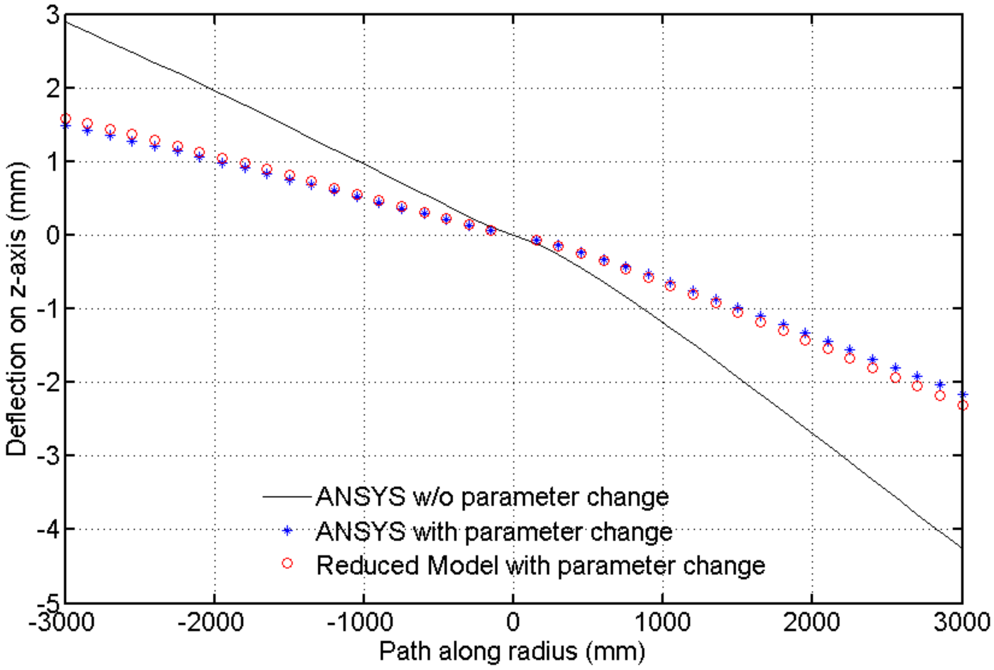

a) case 7

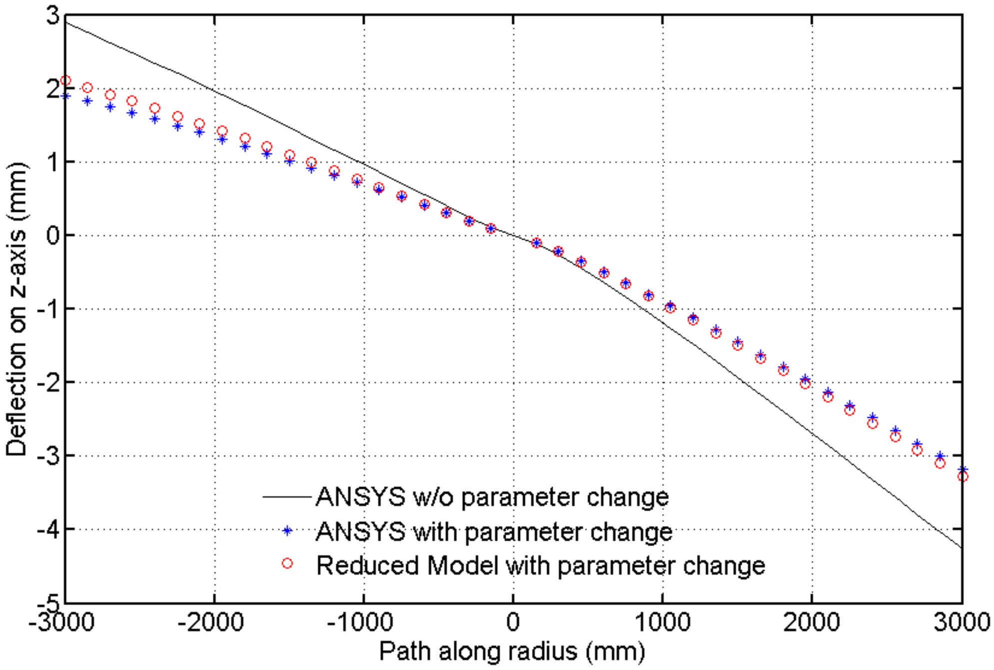

b) case 8

Figure 5.8.: Deflection plots on cross sectional area along the path 1

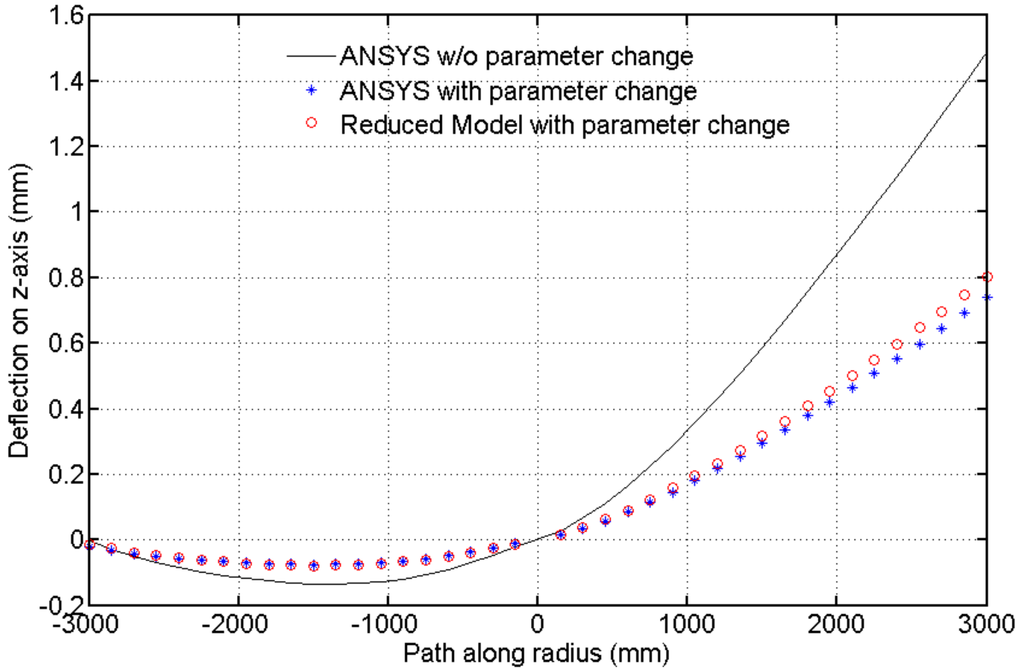

a) case 7

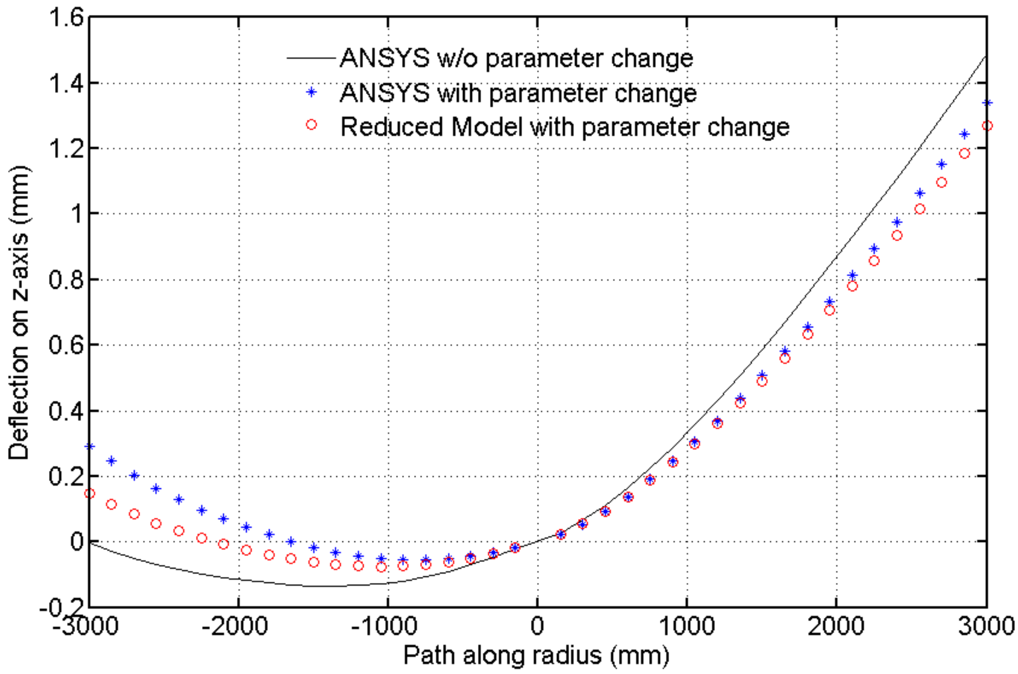

b) case 8

Figure 5.9.: Deflection plots on cross sectional area along the path 2

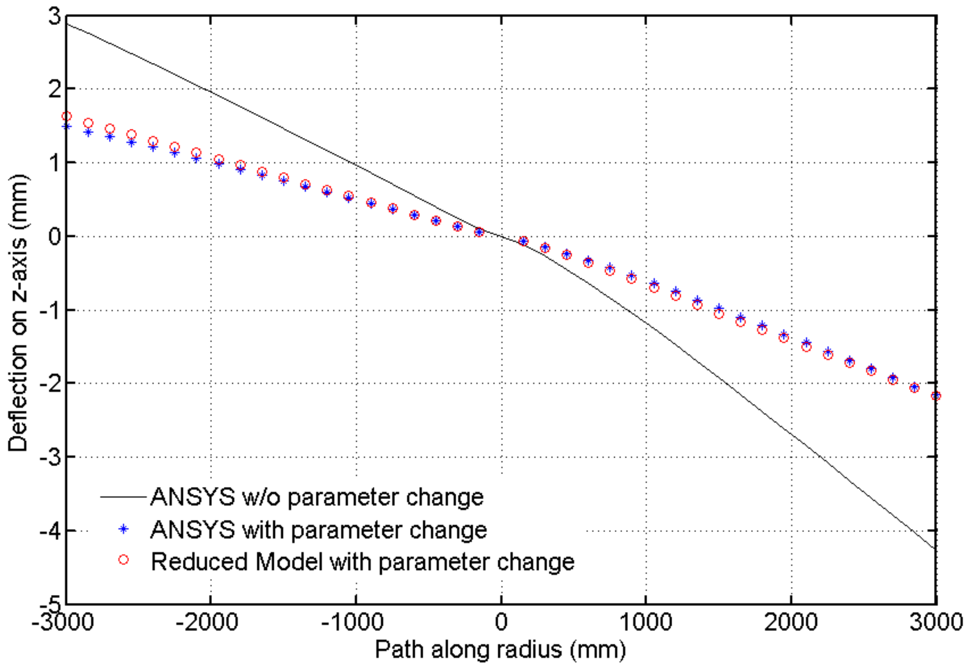

a) case 7

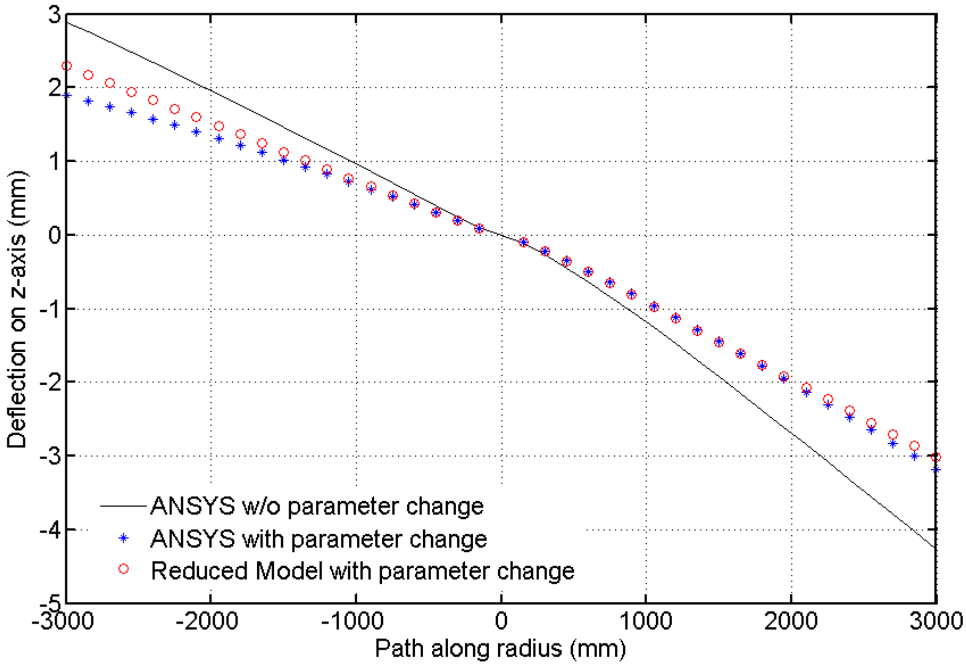

b) case 8

Figure 5.10.: Deflection plots on cross sectional area along the path 1 with a wrong reduction

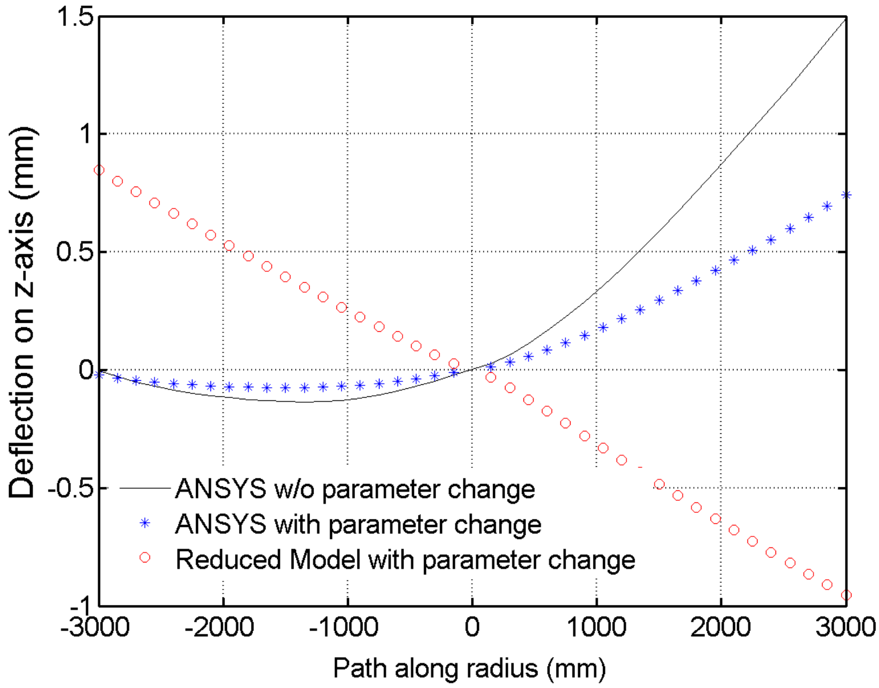

a) case 7

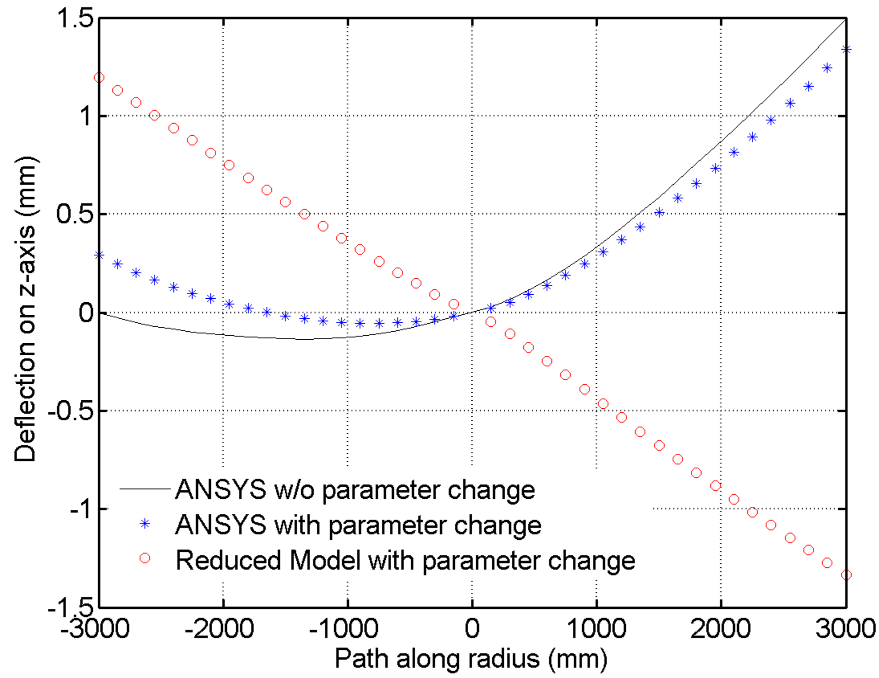

b) case 8

Figure 5.11.: Deflection plots on cross sectional area along the path 2 with a wrong reduction

the design variables as well as linear and nonlinear constraints. The objective function which will be minized is the RMS of shape deformation error between desired shape and current shape. The current shape will be calculated from a reduced model as described previously. The optimal input obtained will be applied to ANSYS model for the verification. In this example actuators are located along the beam supports as shown in Fig. 5.12; however, the location of actuators can be changed freely after the reduction by alternating input matrix P in equation (5.3).

$$K_r x_r = f_r = V^T f = V^T P\, u \tag{5.3}$$
$$P \in \mathbb{R}^{n \times na}, \quad u \in \mathbb{R}^{na \times 1} \quad na: \text{number of actuators}$$

As an example, parabolic shape $z = (x^2 + y^2)/9e^5$ (mm) is taken as a desired shape, and case 8 in Table 5.2 is used. 60 actuators are involved, and the upper and lower bound of control force are -500(N) and $+500$(N) accordingly. In each iteration, reduced model requires only 0.06s, while calling and running ANSYS consumes 1.48s. Considering that optimization process with 60 design parameters generally requires several hundred thousands functional evaluations, it is clear that reduced model is much more beneficial in optimization.
The ANSYS results after the actuation force are applied are shown in Table 5.4 and Fig. 5.13. The RMS error remains very small, and the cross-sectional deformation shape also shows that the control input works effectively. To observe the influence of parameter changes, the control input is calculated from the model without parameter change, and applied to the ANSYS model as well. The results from both cases are compared in Table 5.5 and Fig. 5.14.

deformation RMS error with controller	deformation RMS error without controller
0.80 (mm)	5.49 (mm)

Table 5.4.: Comparison of deformation RMS error without controller and with contoller based on parametric reduced model

deformation RMS error with controller including parameter changes	deformation RMS error with controller excluding parameter changes
0.80 (mm)	2.47 (mm)

Table 5.5.: Comparison of deformation RMS error after control with and without parameter changes

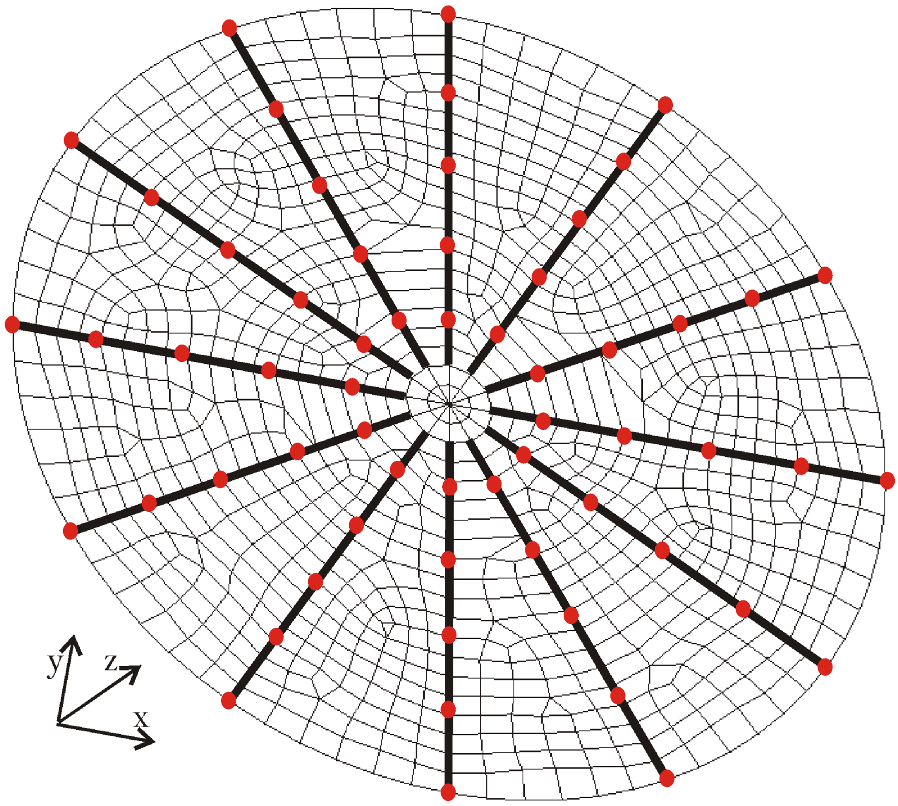

Figure 5.12.: Actuator locations on the reflector

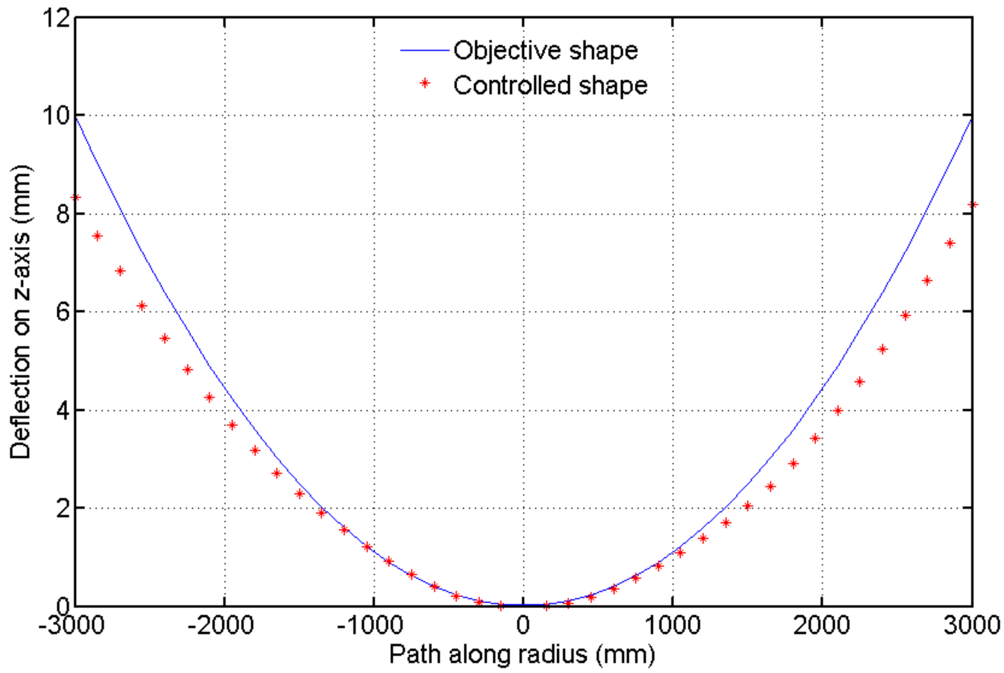

a) along the path 1

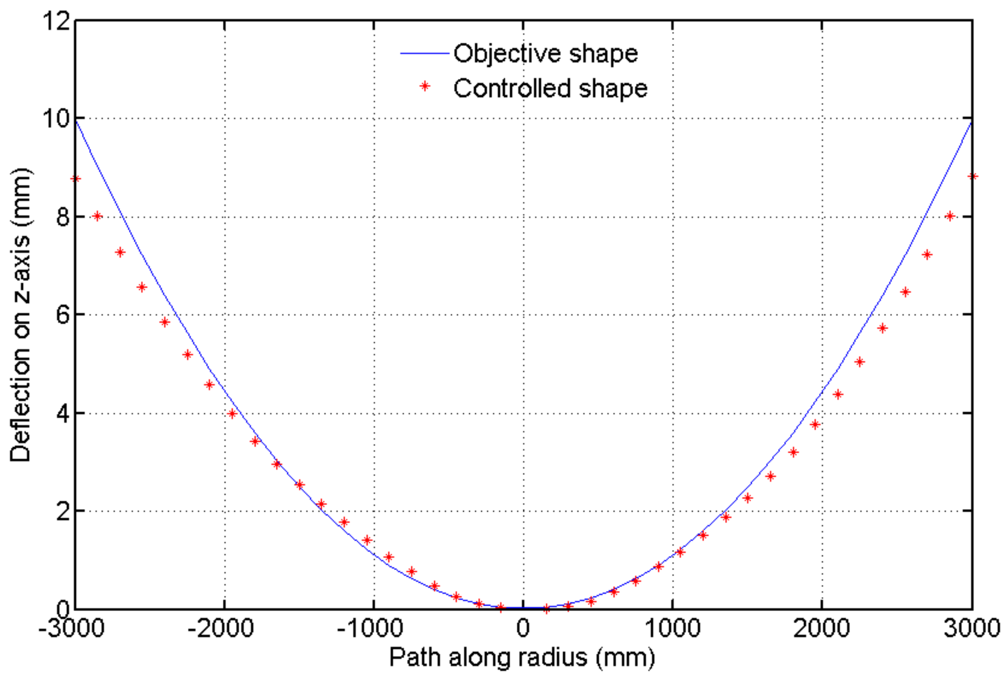

b) along the path 2

Figure 5.13.: Deflection on cross sectional area with shape control including parameter changes

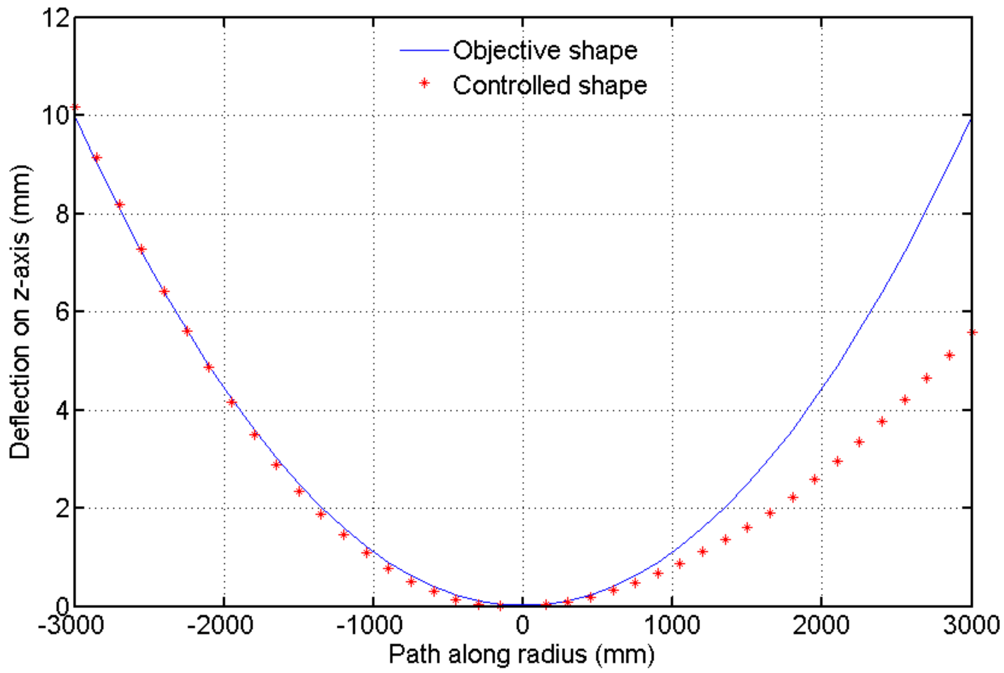

a) along the path 1

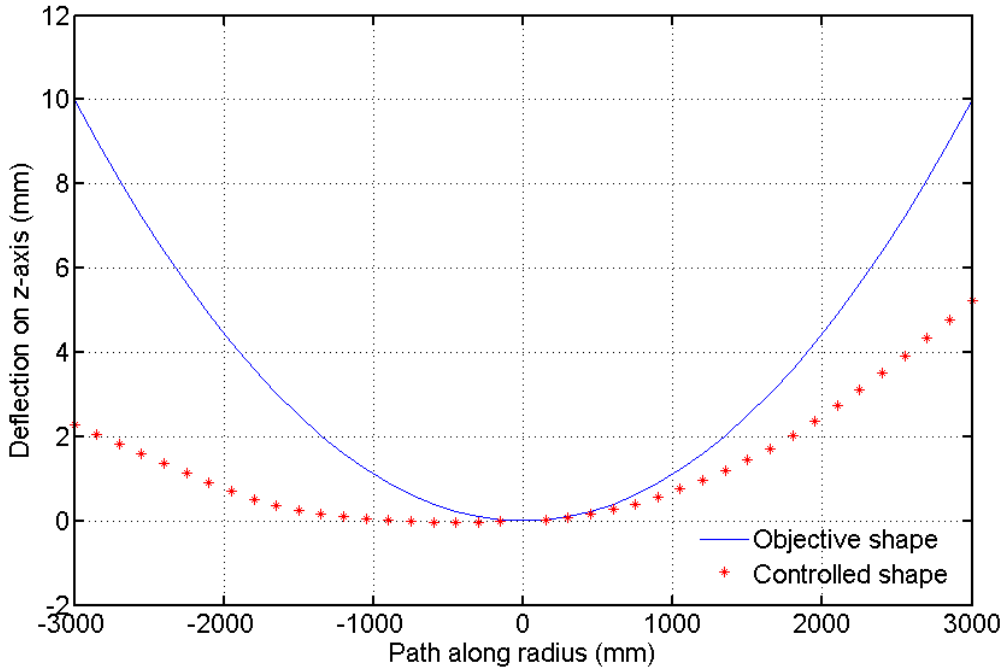

b) along the path 2

Figure 5.14.: Deflection on cross sectional area with shape control excluding parameter changes

5.2. PMOR for vibrational analysis and control of FE model

In structural dynamic analysis, modal information (eigen-values and eigen-forms) is the most important since the response of a structure is represented by them. Because of its direct connection to the physical state, modal space is still the most preferrable reduction space in structural engineering in these days; the loss of physical meaning in reduced space is the biggest weakness of modern reduction theories such as balanced truncation or Krylov subspace reduction. Therefore we will focus on obtaining accurate modal space after the reduction. Eigen-analysis, which requires a computation order of $O(n^3)$, will be performed in the reduced space with much less computational effort. And then it is reprojected into physical state composing eigen-vector. The correctness of reduced model is examined through eigen-values(natural frequencies) and eigen-forms(mode shapes). Model with and without parmater changes are compared to see whether parameter changes are well reflected into the reduced model. Based on the reduced model, a vibration controller will be designed and applied to the original model. Its simulation will be performed in SIMULINK from MATLAB.
Starting with a relatively simple and low order model, namely a truss structure, a more complex solar array panel model will be tested.

5.2.1. Actively damped truss structure

Model and parameter definition

A truss structure is taken as a preliminary test as shown in Fig. 5.15. Since it consists of simple beam elements, it does not need to be meshed densely; therefore the order of original model is not extremely high. However, it would be a good example to observe how reduced model works in dynamic analysis and to run the full order model simulation with controller easily. The higher order application will be followed as a next example.
The structure is 2m long, composed of trigonal pyramids. Each element is a hollow circular beam, and connectors are spheres with threaded holes in various directions where beams can be screwed in. Beam members are modeled as PIPE element, which is basically a type of beam element, and connectors are modeled as nonstructural mass in ANSYS. Following 5 parameters are considered: elastic modulus and shear modulus of beam, density of the material, outer diameter and wall thickness of the beam. The initial material properties are based on steel. Parameter variation of $\pm50\%$ are taken for derivative computation.

Parametric model reduction

Using parameterized mass and stiffness matrices equation, projection matrix V is computed based on equation (4.26). Once the parameterized reduced matrices, $K_{i,r}$

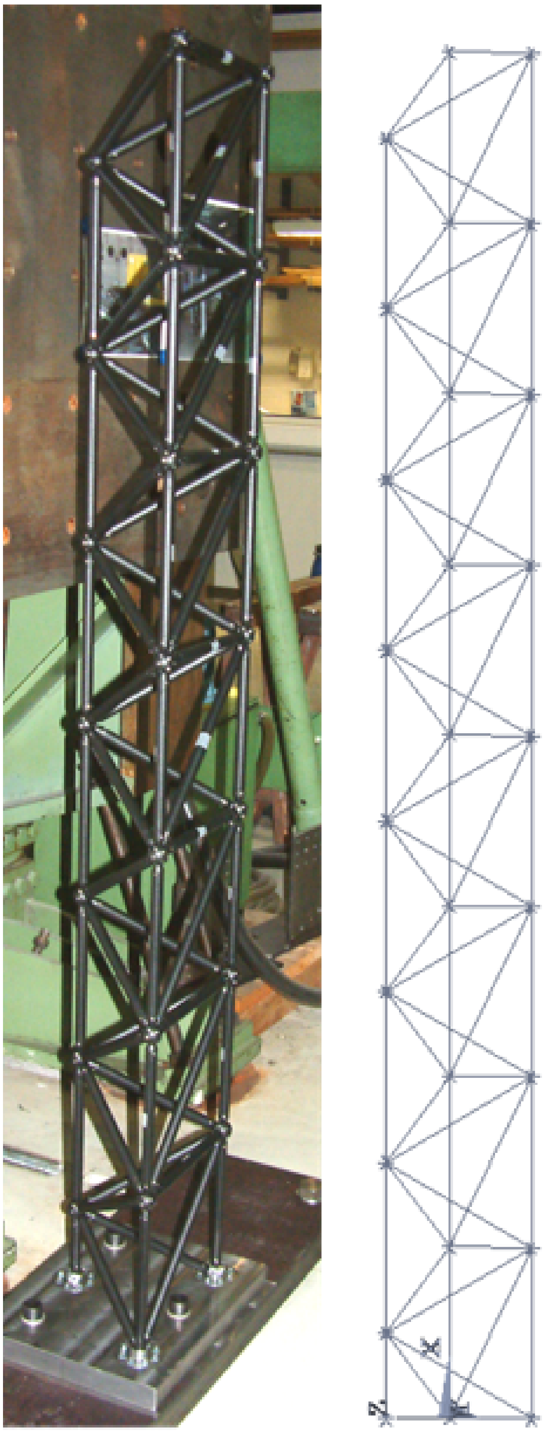

Figure 5.15.: Laboratory and FE model of active truss structure

and $M_{i,r} \in \mathbb{R}^{r\times r}$ $(i = 0, 1, \cdots)$, are obtained, parameter changes Δp_is are directly applied to them as in equation (5.4).

$$\begin{aligned} \left(M_{0,r} + \sum_{i=1} \Delta p_i \; M_{i,r}\right) \ddot{x}_r + \left(D_{0,r} + \sum_{i=1} \Delta p_i \; D_{i,r}\right) \dot{x}_r \\ + \left(K_{0,r} + \sum_{i=1} \Delta p_i \; K_{i,r}\right) x_r = f_r \end{aligned} \tag{5.4}$$

$$M_r \ddot{x}_r + D_r \dot{x}_r + K_r x_r = f_r \tag{5.5}$$

The eigen-values calculated from M_r and K_r after parameter changes are applied will remain same during back-projection as shown in equation (5.2.1). But the eigen-forms will be in a physical state $\mathbb{R}^{n\times 1}$ by back-projection as shown in equation (5.7).

$$\begin{aligned} \left[K_r - \lambda_{i,r} M_r\right] \phi_{i,r} = 0 \\ \left[V^T K V - \lambda_{i,r} V^T M V\right] \phi_{i,r} = 0 \\ V^T \left[K - \lambda_{i,r} M\right] V \phi_{i,r} = 0 \end{aligned} \tag{5.6}$$

where $\lambda_{i,r}$: ith eigen-value from reduced system

$\phi_{i,r}$: ith eigen-vector from reduced system

$$\phi_i \approx \tilde{\phi}_i = V \phi_{i,r} \tag{5.7}$$

Modal analysis results

The order is reduced from 144 to 36, and the natural frequencies (Hz) are calculated both from the reduced model and ANSYS with and without parameter changes. Parameter cases chosen as examples are shown in Table 5.6. For the mode shape comparison, Modal Assurance Criterion (MAC) defined in equation (5.8) is used.

$$\text{MAC}(\vec{u}, \vec{v}) = \frac{|\sum_{j=1}^{n} u_j v_j|^2}{\left(\sum_{j=1}^{n} u_j u_j\right)\left(\sum_{j=1}^{n} v_j v_j\right)} = \frac{\left(\vec{u}^T \cdot \vec{v}\right)^2}{\left(\vec{u}^T \cdot \vec{u}\right)\left(\vec{v}^T \cdot \vec{v}\right)} \tag{5.8}$$

,where u_j is jth element of vector $\vec{u}$

and v_j is jth element of vector $\vec{v}$

If two modes are same or parallel, MAC value is 1, and if two modes are orthogonal to each other, MAC value is 0. As shown in Table 5.7, the results from the reduced model show good agreement to the results from the full model. The frequency change caused by parameter change is also tracked well by the reduced model. Since eigen-analysis requires computation order of $O(n^3)$, the computational effort to obtain a proper modal space decreases a lot by reduced model.

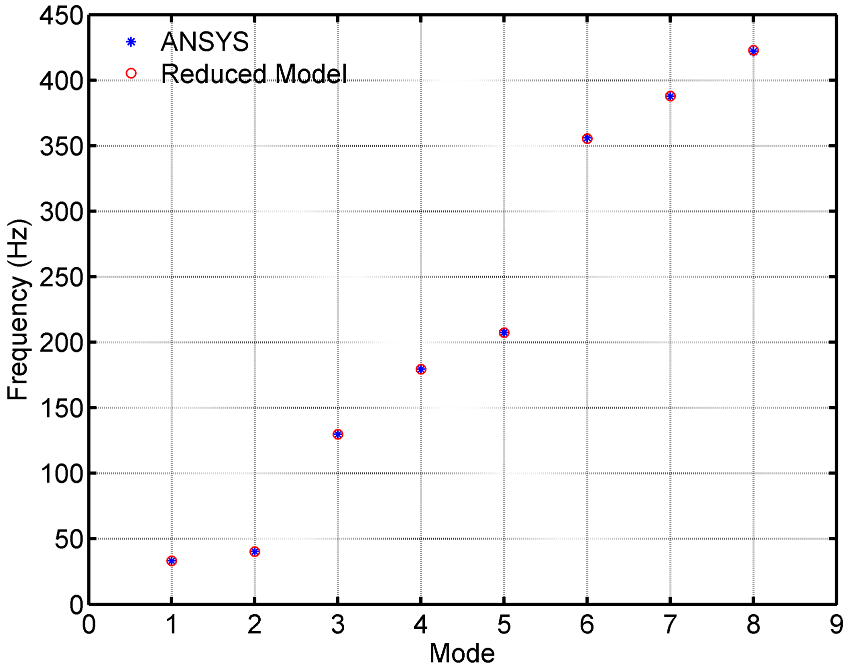

a) case 6

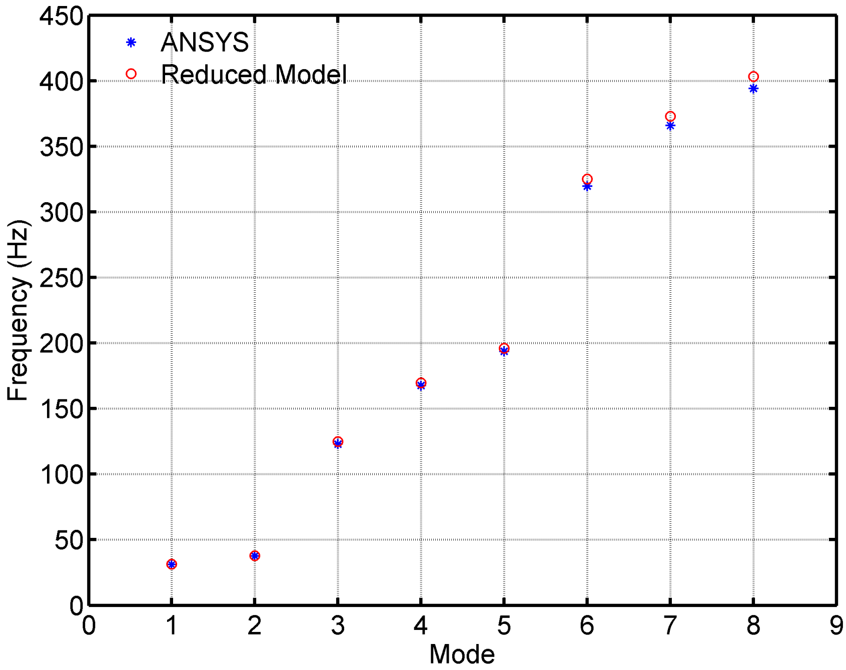

b) case 7

Figure 5.16.: Natural frequencies of active truss model according to parameter cases

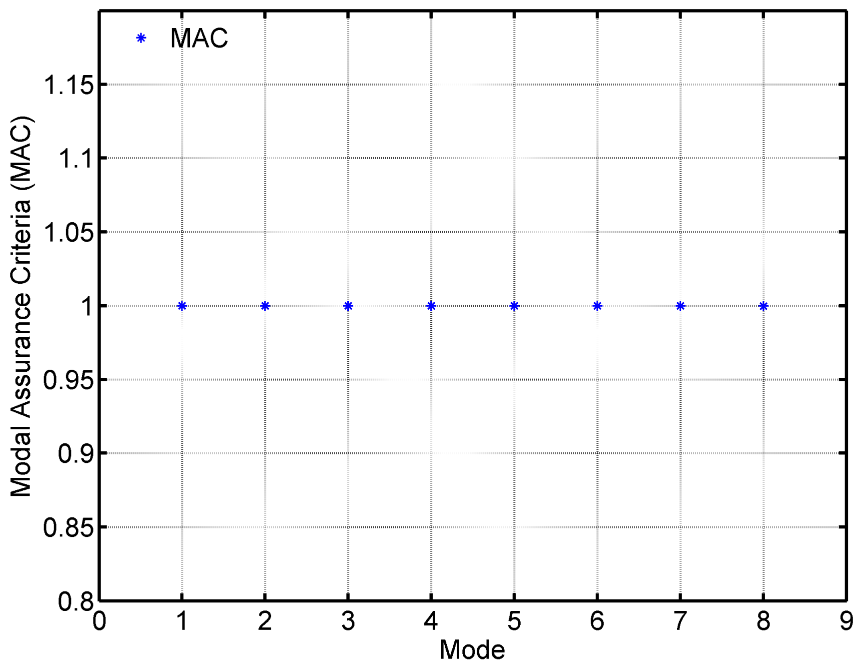

a) case 6

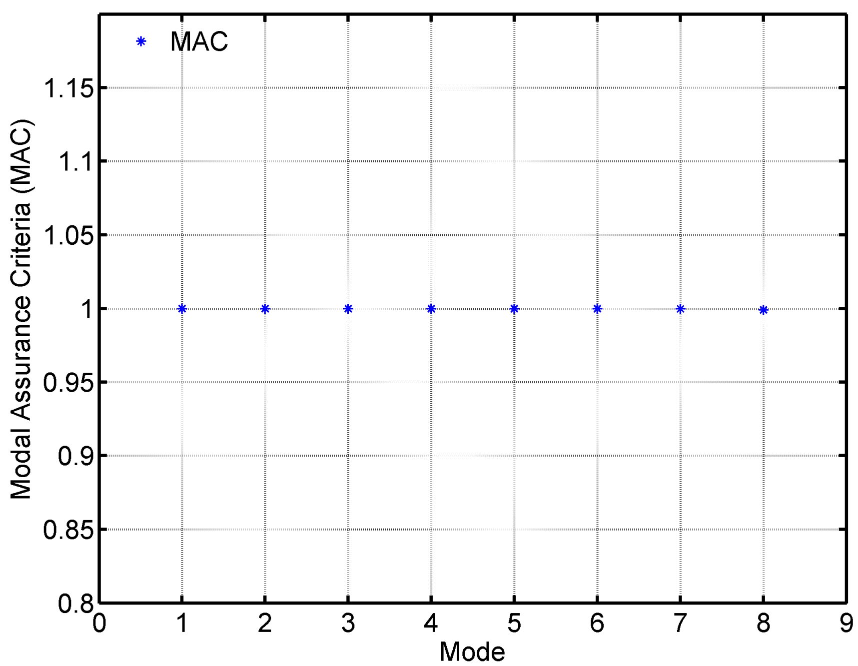

b) case 7

Figure 5.17.: MAC values between reduced and full model of active truss model according to parameter cases

case number	parameter changes
case 0	$\Delta p_i = 0\ (i = 1, 2, \cdots, 5)$
case 1	$\Delta p_1 = +30\%$
case 2	$\Delta p_2 = +30\%$
case 3	$\Delta p_3 = +30\%$
case 4	$\Delta p_4 = +30\%$
case 5	$\Delta p_5 = +30\%$
case 6	$\Delta p_1 = +20\%$, $\Delta p_2 = +20\%$, $\Delta p_3 = +20\%$, $\Delta p_4 = +20\%$, $\Delta p_5 = +20\%$
case 7	$\Delta p_1 = -30\%$, $\Delta p_2 = +30\%$, $\Delta p_3 = -20\%$, $\Delta p_4 = +20\%$, $\Delta p_5 = -10\%$

Table 5.6.: Parameter changes from each cases

Vibration control

A control system will be designed based on the reduced model under parameter changes. Active elements with piezo stack actuator are used; hence, forces will be applied in a longitudinal direction of each element. Displacement information from a laser sensor will be used for feedback. The location of actuators and sensors are determined by the performance index (PI) from controllability gramian and by the performance index (PI) from observability gramian accordingly. The theory behind will be found in Appendix A.1. PI values are calculated from each element location, and sorted by highest value as shown in Table 5.8 and Table 5.9. The element with higher PI value means that it has higher controllability or observability on that mode. As an example, parameter case 7 is taken. From the results it is clear that the reduced order model gives the same results as the full order model does.

Elements number 19,2, and 5 are selected for active members, and each of them will be used to control the first three modes accordingly. For sensors, z and y directional deflection are observed at node 25, as well as y directional deflection at node 27. The Fig. 5.18 represents actuator locations (red bars) and sensor locations (blue marks). The selected actuating location from PI value corresponds to the engineering point of view, because the elements near root experience high strain as can be seen from ANSYS results in Fig. 5.19. Sensor points are also logically understandable, because for the first three modes the end points show the largest displacement as you can see in Fig. 5.20.

The PI values calculated here are from a single mode because one pair of actuator and sensor will be applied for a single mode control using positive position feedback (PPF) controller. However, PI values can be also calculated regarding many numbers

case	mode		1	2	3	4	5	6	7	8
0	Freq.	FM	33.1	40.1	127.9	178.2	206.1	344.1	381.2	414.9
	(Hz)	RM	33.1	40.1	127.9	178.2	206.1	344.1	381.2	414.9
	MAC		1.00	1.00	1.00	1.00	1.00	1.00	1.00	1.00
1	Freq.	FM	37.7	45.7	145.4	203.1	234.9	392.3	433.5	472.7
	(Hz)	RM	37.7	45.7	145.4	203.1	234.9	392.3	433.5	472.6
	MAC		1.00	1.00	1.00	1.00	1.00	1.00	1.00	1.00
2	Freq.	FM	33.1	40.1	128.3	178.3	206.1	344.1	382.5	415.4
	(Hz)	RM	33.1	40.1	128.3	178.3	206.1	344.1	382.5	415.4
	MAC		1.00	1.00	1.00	1.00	1.00	1.00	1.00	1.00
3	Freq.	FM	29.0	35.2	112.2	156.4	180.9	306.5	334.5	364.3
	(Hz)	RM	29.0	35.2	112.2	156.4	180.9	306.5	334.5	364.3
	MAC		1.00	1.00	1.00	1.00	1.00	1.00	1.00	1.00
4	Freq.	FM	33.2	40.2	130.6	179.6	207.6	351.5	389.9	423.6
	(Hz)	RM	33.2	40.3	131.3	180.1	208.2	353.3	392.4	427.4
	MAC		1.00	1.00	1.00	1.00	1.00	1.00	1.00	1.00
5	Freq.	FM	33.1	40.1	128.1	178.4	206.4	345.0	382.0	416.0
	(Hz)	RM	33.1	40.1	128.1	178.4	206.4	350.1	382.1	416.2
	MAC		1.00	1.00	1.00	1.00	1.00	1.00	1.00	1.00
6	Freq.	FM	33.2	40.2	129.8	179.4	207.4	356.0	387.6	421.9
	(Hz)	RM	33.2	40.2	129.8	179.4	207.5	355.3	387.8	422.8
	MAC		1.00	1.00	1.00	1.00	1.00	1.00	1.00	1.00
7	Freq.	FM	31.0	37.6	122.9	167.6	193.7	319.7	365.9	394.2
	(Hz)	RM	31.3	37.9	124.9	169.6	196.0	325.1	372.8	403.3
	MAC		1.00	1.00	1.00	1.00	1.00	1.00	1.00	1.00

Table 5.7.: Comparison of natural frequencies and mode shapes between reduced model and full model

order		1		2		3		4	
		element number	PI value	element number	PI value	element number	PI value	element number	PI value
mode 1	FM	19	1.00	28	0.40	4	0.17	10	0.13
	RM	19	1.00	28	0.40	4	0.17	10	0.13
mode 2	FM	2	1.00	4	0.84	11	0.41	13	0.40
	RM	2	1.00	4	0.84	11	0.41	13	0.39
mode 3	FM	5	1.00	14	0.94	23	0.62	32	0.33
	RM	5	1.00	14	0.94	23	0.65	32	0.34

Table 5.8.: Highest performance index (PI) values from the controllability gramian and corresponding element numbers for actuator selection

order		1		2		3		4	
		node and dof	PI value	node and dof	PI value	node and dof	PI value	node and dof	PI value
mode 1	FM	25z	1.00	26z	0.80	27z	0.63	22z	0.49
	RM	25z	1.00	26z	0.80	27z	0.63	22z	0.49
mode 2	FM	25y	1.00	26y	0.99	27y	0.61	22y	0.49
	RM	25y	1.00	26y	0.99	27y	0.61	22y	0.49
mode 3	FM	27y	1.00	25z	0.75	24y	0.66	22z	0.62
	RM	27y	1.00	25z	0.76	24y	0.66	22z	0.63

Table 5.9.: Highest performance index (PI) values from the observability gramian and corresponding element numbers for sensor selection

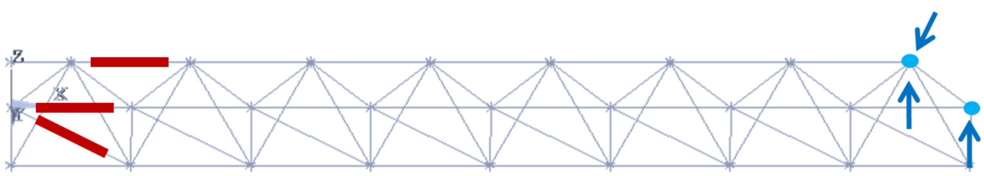

Figure 5.18.: Actuator and sensor locations on active truss structure

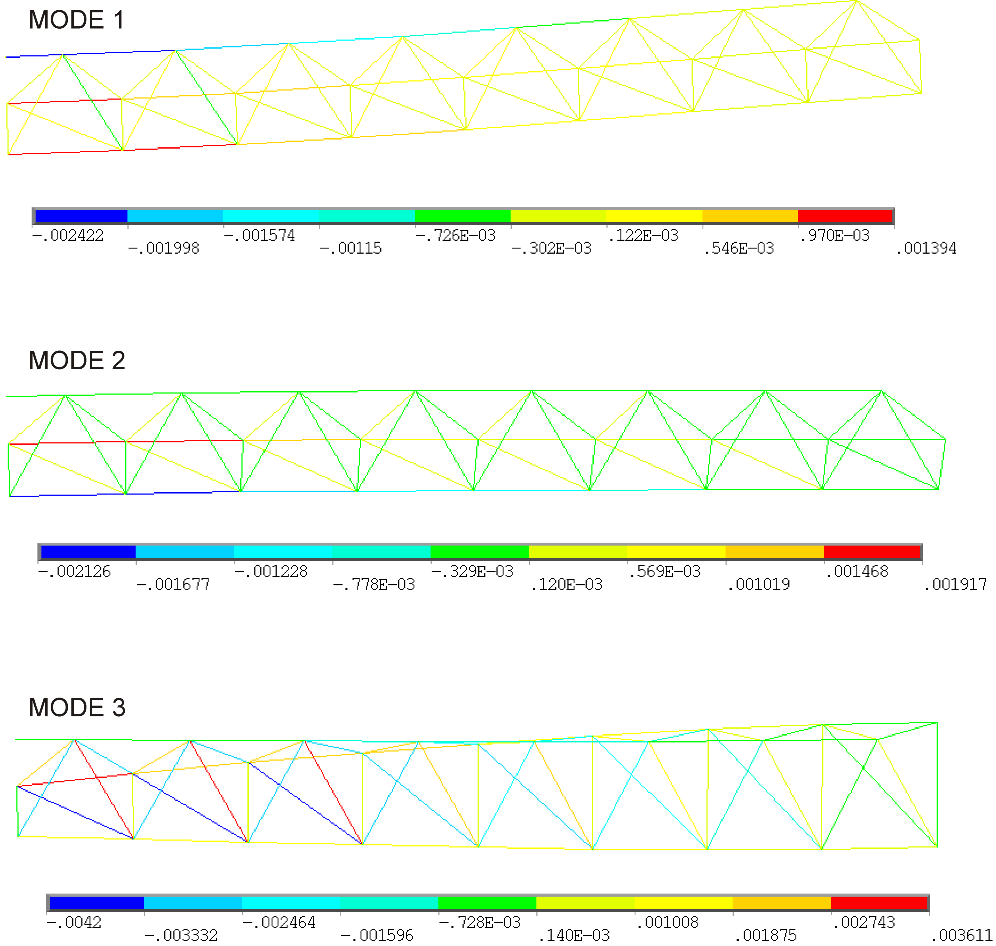

Figure 5.19.: Strain distribution of truss structure on the first three mode

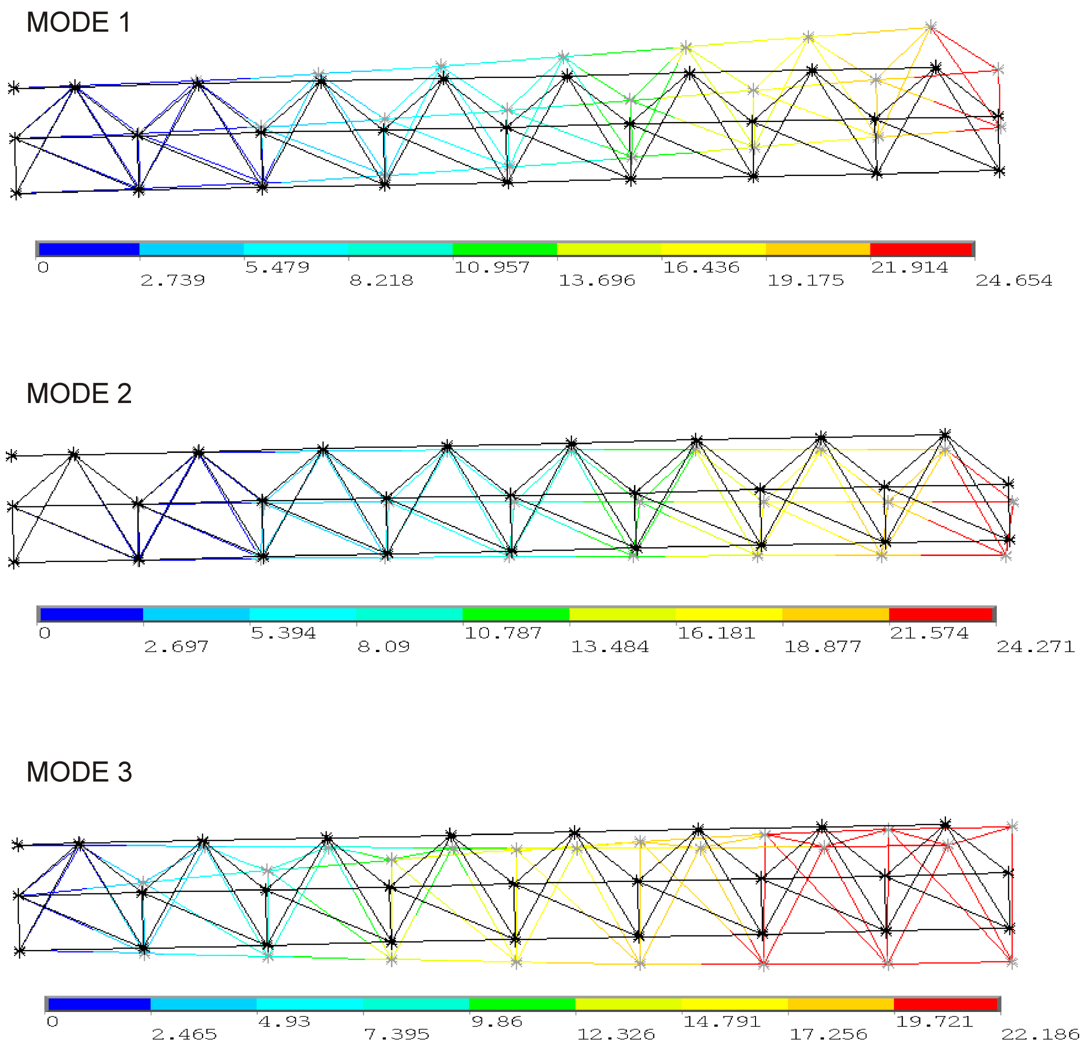

Figure 5.20.: Mode shapes of truss structure on the first three mode

of modes to design more advanced controller. Both controllability and observability gramians are obtained from solving Lyapunov equation. So far there is no mathematical proof about the accuracy of gramains from the reduced model; however, according to [Gaw98] the eigen-values of gramians can be approximated using eigen-values and eigen-vectors. Since the reduced model provides quite accurate eigen-information, it is also reasonable that reduced model provides performance index values close to the full model does.

Three PPF controllers tuned with the first three natural frequencies calculated from the reduced model are used for vibration control. Fig. 5.21 shows its SIMULINK model and Fig. 5.22 - 5.24 shows time response of displacement from each sensors. Three cases are shown: 1) without controller, 2) with controller tuned by parameterized reduced model, 3) with controller tuned by a model with no parameter influence (badly tuned controller). It is clear that the controller designed by parameterized reduced model declines vibration effectively while badly tuned controller shows bad performance.

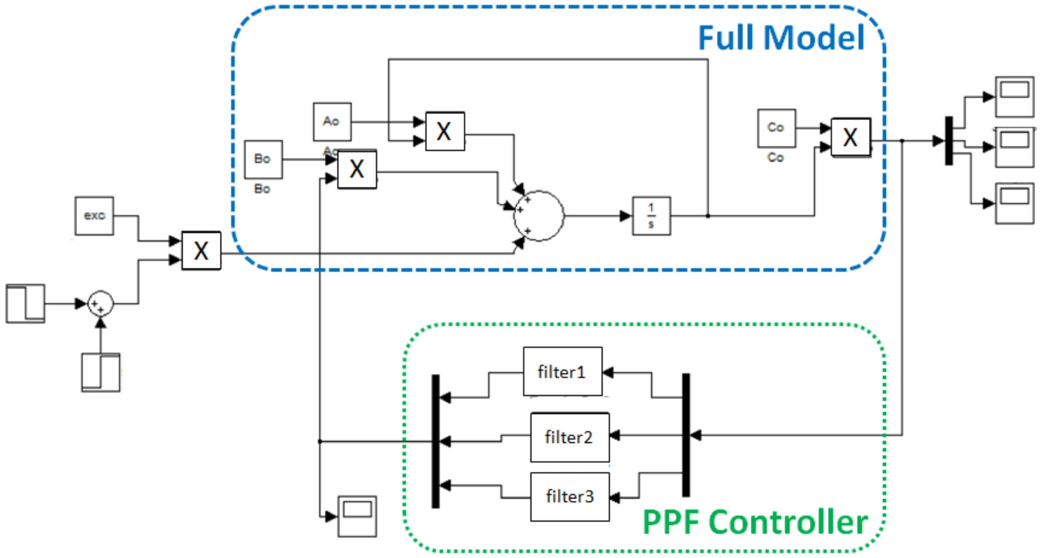

Figure 5.21.: Simulink model for vibration control of active truss structure

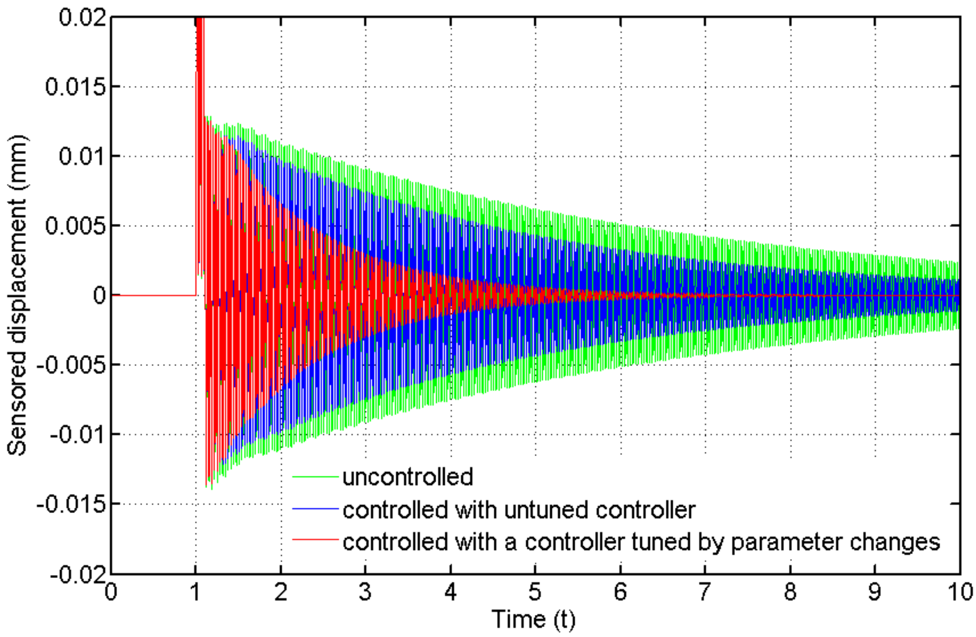

Figure 5.22.: Displacement plot from sensor 1 (case 7)

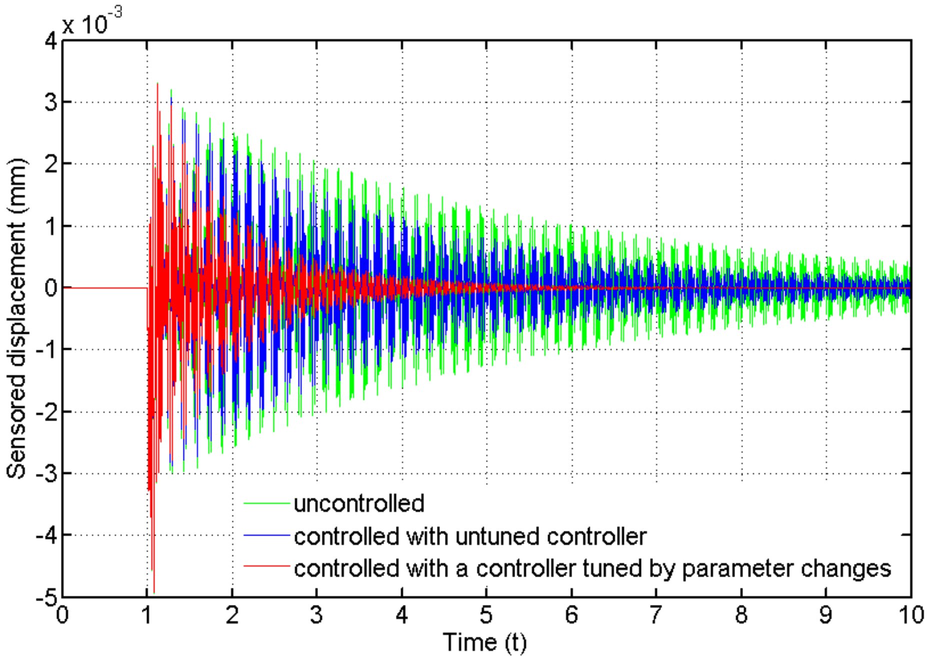

Figure 5.23.: Displacement plot from sensor 2 (case 7)

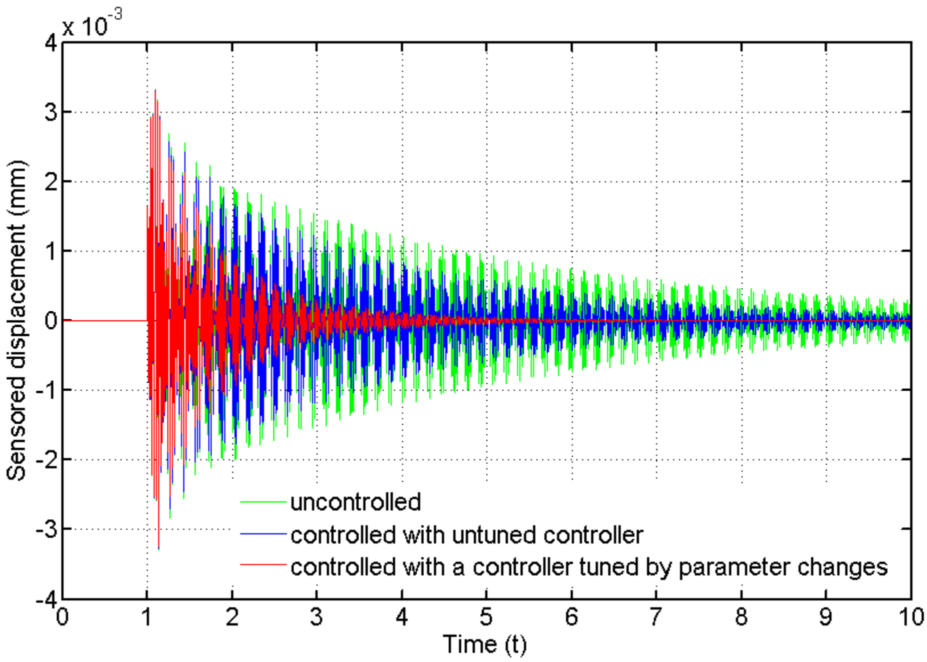

Figure 5.24.: Displacement plot from sensor 3 (case 7)

5.2.2. Solar array panel model

Model and parameter definition

As a more complicated model, a solar array panel model designed for a laboratory experiment is examined. The original target is 4m by 2.5m solar array panel being developed by EADS Astrium. This laboratory model is designed for preliminary designing and implementing of active damper; therefore it should have similar natural frequencies and mode shapes from the original panel while its size is small enough to be tested in laboratory. Although 4 panels will be packed together during launch, due to the similarity of the behavior, a single panel model is used. The model is scaled down to 1.5m by 1m and its configuration is shown in Fig. 5.26. To match natural frequencies, special panel material is designed: 5 layered sandwich composite. As illustrated in Fig. 5.27, it is made of glass fiber reinforced polymer (GFRP) facesheet, aluminum honeycomb core, and a steel layer in the middle. To adjust mode shape more correctly, dummy masses are applied in some regions.

4 parameters come from material properties, and 3 parameters come from geometrical properties: Elastic modulus of GFRP facesheet (E_x and E_y), shear modulus of GFRP facesheet (G_{xy}) and shear and elastic modulus of aluminum honeycomb core (E_c), thickness of facesheet (t_f), thickness of core (t_c), and thickness of steel layer (t_s). Additionally 3 nonstructural mass values (m_1, m_2, m_3) are also treated as parameter; totally 10 parameter are involved. The initial values of 10 parameters are shown in Table 5.10.

Parametric model reduction

For each parameters, $\pm 50\%$ change of initial values are used for parameterization. Same assumptions from previous cases are applied: 1) differential terms are assumed as a linear difference within $\pm 50\%$ variation, 2) depending on the characteristics of each parameter, it can be replaced in a different form (e.g. thickness). Physical and geometrical parameters are treated in the same way as in a truss example, and nonstructural masses are treated linearly.

E_x	21560 (MPa)	t_c	3 (mm)
E_y	21560 (MPa)	t_s	2 (mm)
G_{xy}	8290 (MPa)	m_1	200 (g)
E_c	1890 (MPa)	m_2	100 (g)
t_f	0.95 (mm)	m_3	80 (g)

Table 5.10.: Initial parameter values for solar array panel model

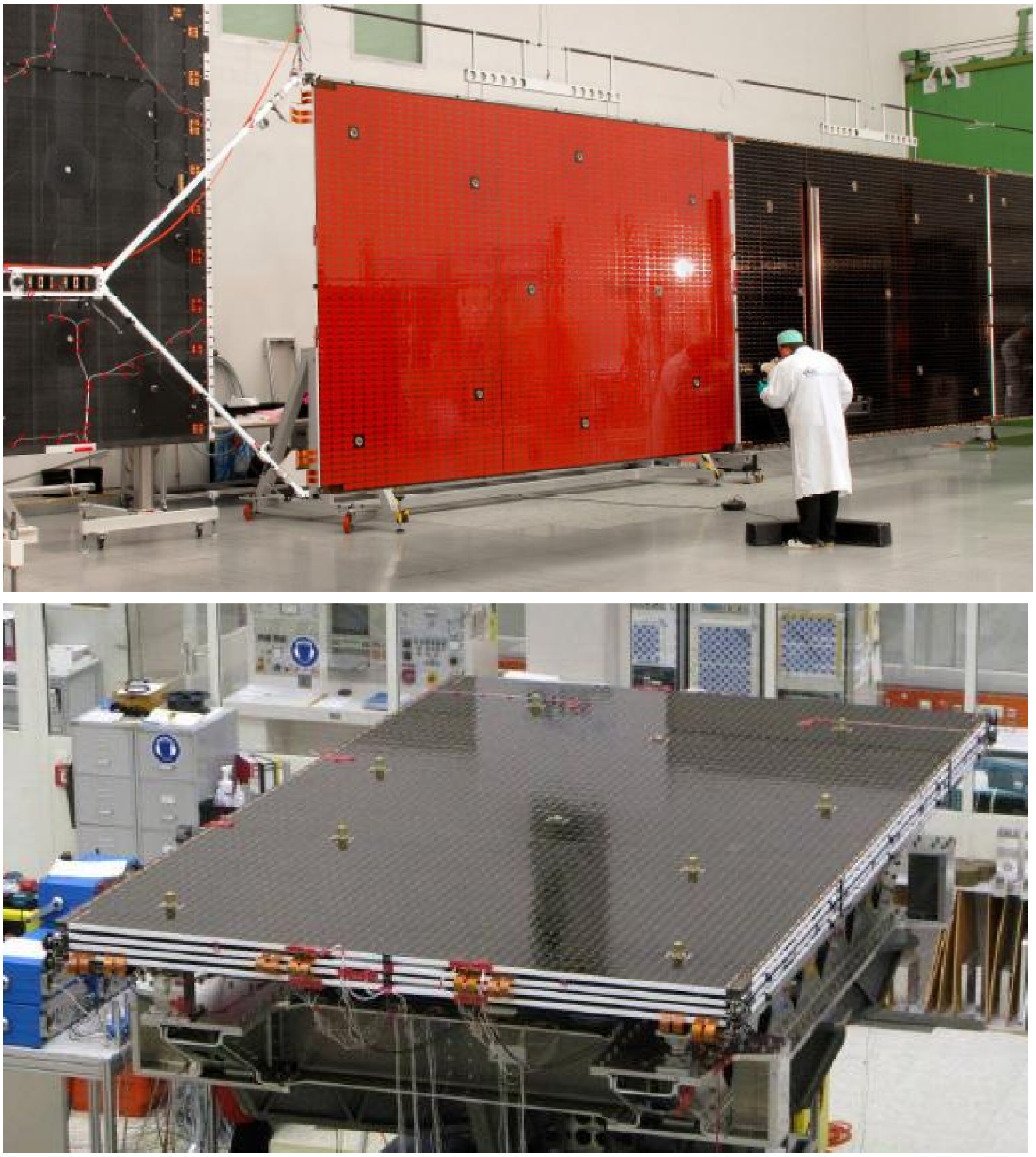

Figure 5.25.: Solar array panel structure from EADS

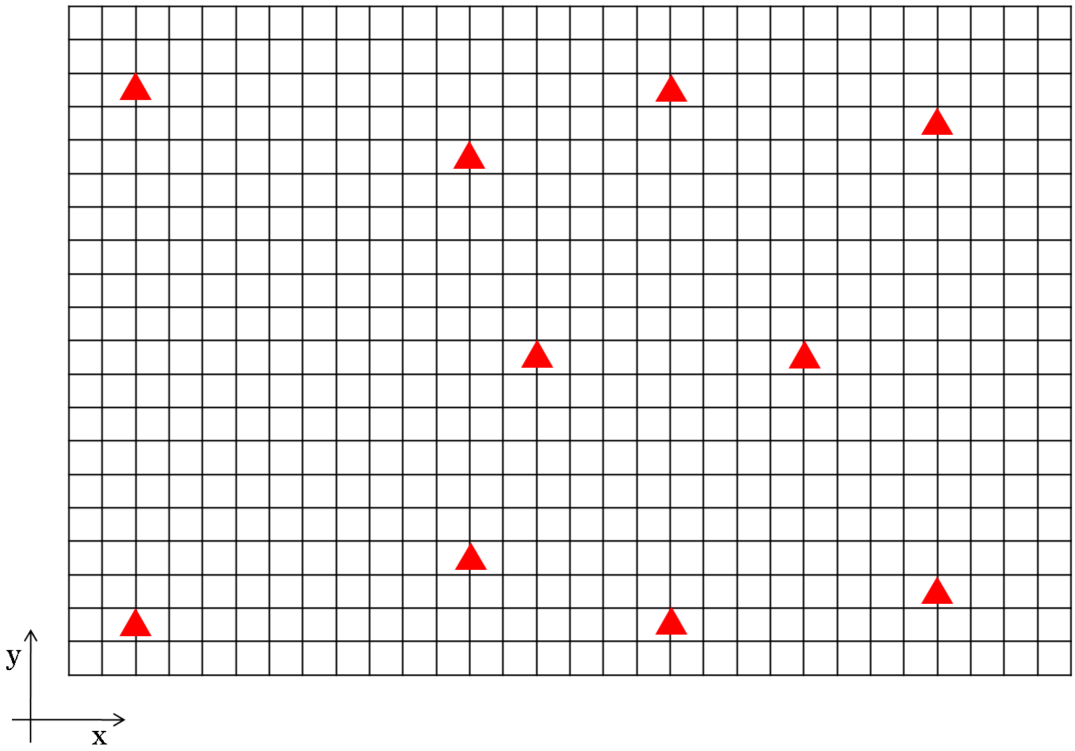

Figure 5.26.: Solar array panel model

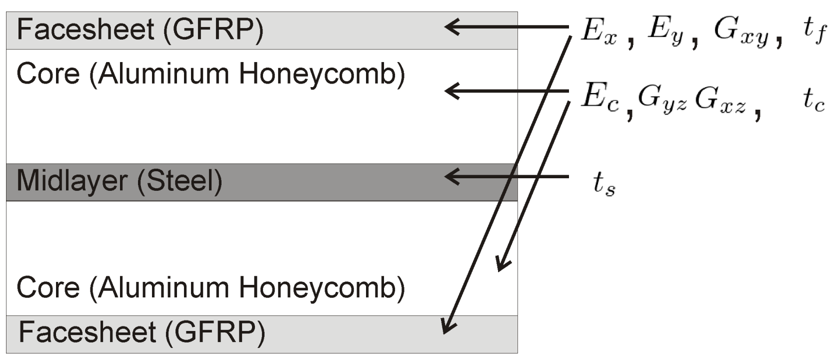

Figure 5.27.: A composite structure of solar panel model

Modal analysis results

The order is reduced from 11346 to 51. Examplary parameter cases are listed in Table 5.11. The eigen-frequencies and mode shapes are calculated from both the reduced model and ANSYS, and compared in Table 5.12 - Table 5.13 and in Fig. 5.28 - Fig. 5.29. The reduced model provides accurate results in eigen-analysis, also reflecting parameter changes very well. As an example, parameter case 11 and case 12 are taken. Additional graphs for other parameter cases are shown in Appendix B.3.

Vibration control

For large and complex structures showing complicated mode shapes, robust modern controllers such as linear quadratic state feedback regulator (LQR) are recommended. A large structure like solar panel includes some local modes; therefore which modes are important and should be controlled is another critical issue. Effective mass, introduced in Appendix A.2, is used to determine predominant modes. From the first to the tenth modes, the effective mass on z-axis, which is the axis perpendicular to the panel surface, are observed both from the reduced model and from ANSYS. As shown in Table 5.14 and Table 5.15, the results from both correspond to each other very well. Modes with the highest 5 effective mass values are selected and used for designing a controller: mode 1, 2, 3, 6, 10.

The locations of sensor and actuator are calculated by the same way used in truss structure; performance indexes (PIs) from controllability and observability gramians are used. Since the actuator is a patch type piezo actuator as shown in Fig. 5.30, actuator is modeled based on pin-force model as introduced in Appendix A.3. From the results shown in Table 5.16 and Table 5.17, the best locations for each mode are selected. Since the panel is symmetric on the x-axis, the PI values from each actuator location are also symmetric. Their actual positions on the panel are illustrated in Fig. 5.31 and Fig. 5.32.

The controller is designed based on the reduced model in modal space. Simulation test on SIMULINK platform is followed applying the controller to the full model. Because the size of full model in physical coordinate, 11346, is too large to run a simulation, a modal space model with the first 50 modes are used for simulation. As a controller, linear quadratic regulator (LQR), introduced in Appendix A.4, is used. Calculating gain factors for LQR is also done on the MATLAB using parameterized reduced model. SIMULINK model is drawn in Fig. 5.33. Simulation results with and without controller are compared in Fig. 5.34. The response is from the impulse force on the middle of the panel. The controller designed from reduced model successfully reduces the vibration both of the cases with and without parameter changes.

case number	parameter changes
case 0	$\Delta p_i = 0 \ (i = 1, 2, \cdots, 10)$
case 1	$\Delta p_1 = +40\%$
case 2	$\Delta p_2 = +40\%$
case 3	$\Delta p_3 = +40\%$
case 4	$\Delta p_4 = +40\%$
case 5	$\Delta p_5 = +40\%$
case 6	$\Delta p_6 = +40\%$
case 7	$\Delta p_7 = +40\%$
case 8	$\Delta p_8 = +40\%$
case 9	$\Delta p_9 = +40\%$
case 10	$\Delta p_{10} = +40\%$
case 11	$\Delta p_i = +20\% \ (i = 1, 2, \cdots, 10)$
case 12	$\Delta p_1 = -20\%$, $\Delta p_2 = -10\%$, $\Delta p_3 = +30\%$, $\Delta p_4 = -30\%$, $\Delta p_5 = +10\%$, $\Delta p_6 = +20\%$, $\Delta p_7 = -20\%$, $\Delta p_8 = +20\%$, $\Delta p_9 = +40\%$, $\Delta p_{10} = -40\%$

Table 5.11.: Parameter changes from each cases

case	mode		1	2	3	4	5	6	7	8	9	10	11	12	13	14	15	16
0	Freq.	FM	35.3	43.9	65.9	72.3	78.4	79.6	83.9	89.7	98.0	104.1	110.3	111.8	120.3	123.5	131.5	146.0
	(Hz)	RM	35.3	43.9	65.9	72.3	78.4	79.6	83.9	89.7	98.0	104.1	110.3	111.8	120.3	123.5	131.5	146.0
	MAC		1.00	1.00	1.00	1.00	1.00	1.00	1.00	1.00	1.00	1.00	1.00	1.00	1.00	1.00	1.00	1.00
1	Freq.	FM	35.6	46.2	72.1	76.8	82.1	84.2	88.6	90.0	97.8	110.0	114.5	117.8	125.5	126.2	137.7	152.5
	(Hz)	RM	35.6	46.3	72.2	76.9	82.2	84.4	88.8	90.2	98.0	110.2	114.7	118.2	125.8	126.4	138.0	152.7
	MAC		1.00	1.00	1.00	1.00	1.00	1.00	1.00	1.00	1.00	1.00	1.00	1.00	0.99	0.99	1.00	1.00
2	Freq.	FM	39.1	46.1	68.1	75.2	80.0	84.1	87.3	101.2	109.8	110.6	117.5	118.0	128.7	132.7	139.8	155.1
	(Hz)	RM	39.3	46.3	68.2	75.3	80.1	84.3	87.5	101.6	110.4	111.0	117.8	118.3	129.2	133.2	140.2	155.5
	MAC		1.00	1.00	1.00	1.00	1.00	1.00	1.00	1.00	1.00	1.00	1.00	1.00	1.00	1.00	1.00	1.00
3	Freq.	FM	36.7	45.7	67.5	75.3	82.5	84.9	88.0	91.6	101.1	107.0	114.0	115.4	125.3	131.5	136.9	153.3
	(Hz)	RM	36.8	45.8	67.6	75.4	82.6	85.0	88.2	91.7	101.3	107.2	114.2	115.6	125.5	131.7	137.0	153.5
	MAC		1.00	1.00	1.00	1.00	1.00	1.00	1.00	1.00	1.00	1.00	1.00	1.00	1.00	1.00	1.00	1.00
4	Freq.	FM	35.3	43.9	65.9	72.3	78.4	79.6	83.9	89.7	98.0	104.1	110.3	111.8	120.3	123.5	131.5	146.0
	(Hz)	RM	35.3	43.9	65.9	72.3	78.4	79.6	83.9	89.7	98.0	104.1	110.3	111.8	120.3	123.5	131.5	146.0
	MAC		1.00	1.00	1.00	1.00	1.00	1.00	1.00	1.00	1.00	1.00	1.00	1.00	1.00	1.00	1.00	1.00
5	Freq.	FM	40.6	50.5	75.9	83.2	90.1	91.8	96.5	103.3	112.5	120.3	127.0	129.2	139.2	142.6	152.0	169.1
	(Hz)	RM	40.8	50.7	76.2	83.5	90.5	92.2	96.9	103.7	113.0	120.8	127.5	129.7	139.7	143.1	152.6	169.7
	MAC		1.00	1.00	1.00	1.00	1.00	1.00	1.00	1.00	1.00	1.00	1.00	1.00	1.00	1.00	1.00	1.00
6	Freq.	FM	42.8	53.2	80.1	87.7	95.0	96.9	101.7	108.9	118.4	126.3	133.9	135.9	146.4	150.2	160.2	178.0
	(Hz)	RM	43.1	53.6	80.6	88.3	95.6	97.5	102.4	109.6	119.3	127.1	134.7	136.7	147.3	151.1	161.2	179.1
	MAC		1.00	1.00	1.00	1.00	1.00	1.00	1.00	1.00	1.00	1.00	1.00	1.00	1.00	1.00	1.00	1.00

Table 5.12.: Comparison of natural frequencies and mode shapes between reduced model and full model (case 0-6)

case	mode		1	2	3	4	5	6	7	8	9	10	11	12	13	14	15	16
7	Freq.	FM	36.6	45.5	68.3	74.9	81.2	82.5	86.9	92.9	101.8	109.5	114.4	117.0	125.9	128.9	136.8	152.4
	(Hz)	RM	36.9	45.8	68.9	75.5	81.8	83.2	87.6	93.7	102.6	110.4	115.3	118.0	126.9	129.9	137.9	153.7
	MAC		1.00	1.00	1.00	1.00	1.00	1.00	1.00	1.00	1.00	1.00	1.00	1.00	1.00	1.00	1.00	1.00
8	Freq.	FM	35.3	43.9	65.9	72.3	78.3	79.6	83.9	89.6	97.4	103.1	109.8	110.0	117.2	122.9	130.6	144.5
	(Hz)	RM	35.3	43.9	65.9	72.3	78.3	79.6	83.9	89.6	97.4	103.1	109.8	110.0	117.2	122.9	130.7	144.5
	MAC		1.00	1.00	1.00	1.00	1.00	1.00	1.00	1.00	1.00	1.00	1.00	1.00	1.00	1.00	1.00	1.00
9	Freq.	FM	35.3	43.9	65.9	72.3	78.4	79.6	83.9	89.7	98.0	104.1	110.3	111.8	120.3	123.5	131.5	146.0
	(Hz)	RM	35.3	43.9	65.9	72.3	78.4	79.6	83.9	89.7	98.0	104.1	110.3	111.8	120.3	123.5	131.5	146.0
	MAC		1.00	1.00	1.00	1.00	1.00	1.00	1.00	1.00	1.00	1.00	1.00	1.00	1.00	1.00	1.00	1.00
10	Freq.	FM	35.3	43.9	65.9	72.3	78.4	79.6	83.9	89.7	98.0	102.0	110.2	111.8	120.3	123.4	131.2	145.3
	(Hz)	RM	35.3	43.9	65.9	72.3	78.4	79.6	83.9	89.7	98.0	102.0	110.2	111.8	120.3	123.4	131.2	145.3
	MAC		1.00	1.00	1.00	1.00	1.00	1.00	1.00	1.00	1.00	1.00	1.00	1.00	1.00	1.00	1.00	1.00
11	Freq.	FM	45.3	56.2	84.6	92.6	100.3	102.4	107.5	115.1	124.9	133.3	141.5	143.5	154.6	158.7	169.4	188.3
	(Hz)	RM	44.0	54.5	82.0	89.8	97.3	99.3	104.3	111.8	121.6	129.4	137.2	139.2	149.9	153.9	164.2	182.4
	MAC		1.00	1.00	1.00	1.00	1.00	1.00	1.00	1.00	1.00	1.00	1.00	1.00	1.00	1.00	1.00	1.00
12	Freq.	FM	41.2	50.4	73.4	82.9	90.9	95.4	97.6	102.8	112.7	118.6	125.4	125.5	137.6	147.2	152.1	169.6
	(Hz)	RM	40.5	49.8	73.0	81.9	89.5	93.2	96.0	101.1	110.7	117.2	123.9	123.9	134.9	143.8	149.5	166.6
	MAC		1.00	1.00	1.00	1.00	1.00	0.99	0.99	1.00	1.00	1.00	1.00	1.00	1.00	1.00	1.00	0.98

Table 5.13.: Comparison of natural frequencies and mode shapes between reduced model and full model (case 7-12)

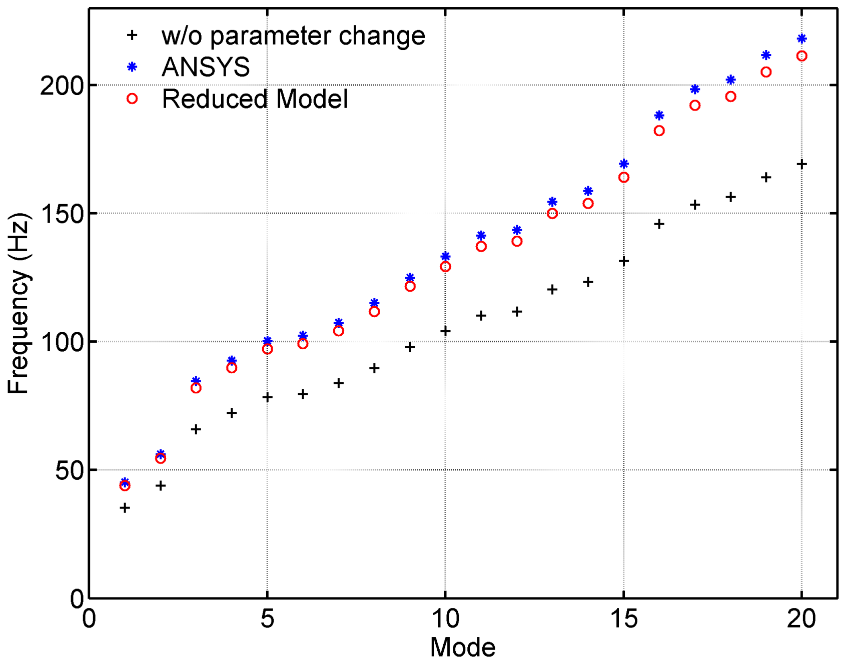

a) case 11

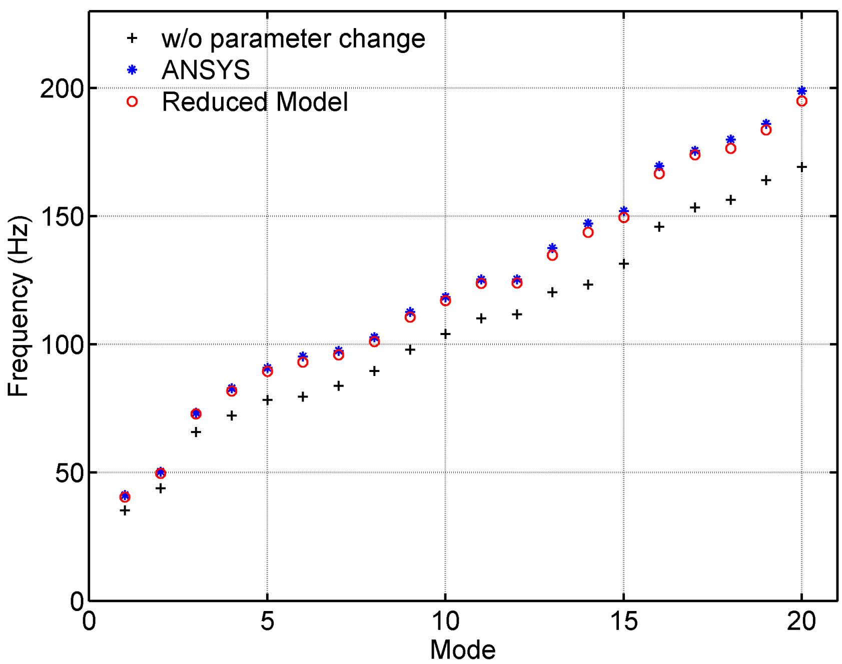

b) case 12

Figure 5.28.: Natural frequencies of solar panel model according to parameter cases

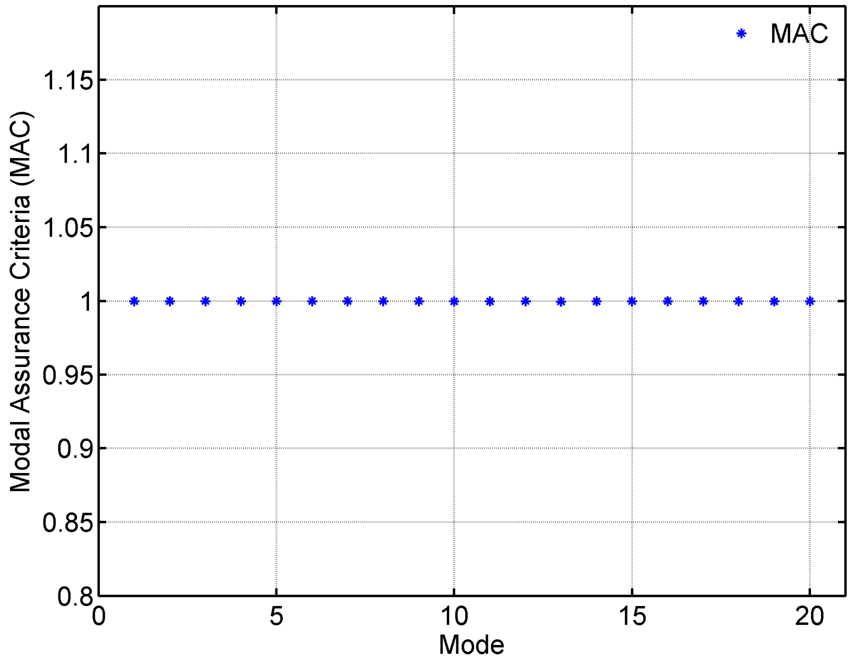

a) case 11

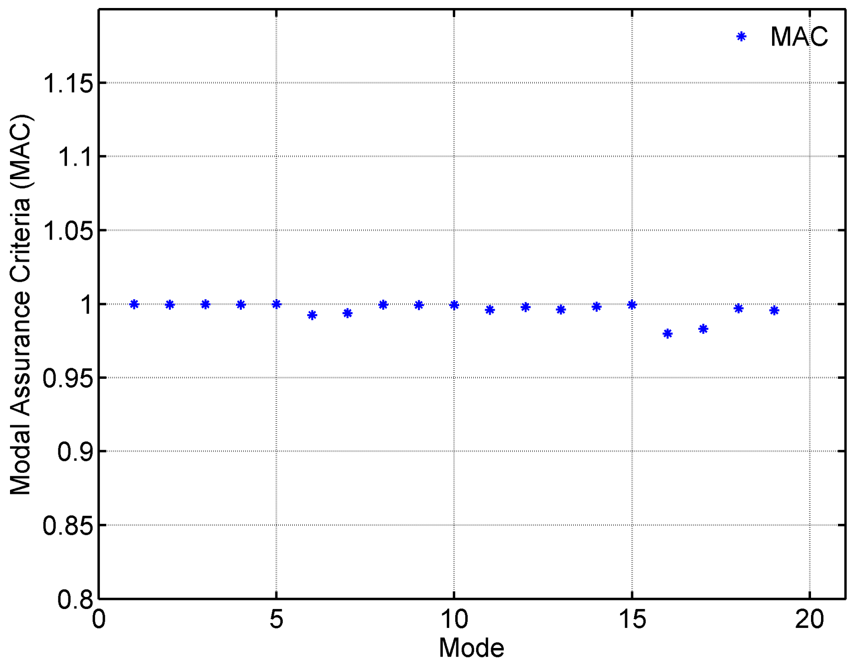

b) case 12

Figure 5.29.: MAC values between reduced and full model of solar panel model according to parameter cases

order	mode number		effective mass (kg)	
	FM	RM	FM	RM
1	1	1	5.93	5.72
2	10	10	4.16	4.94
3	3	3	3.29	3.30
4	2	2	2.55	2.66
5	6	6	0.99	0.79

Table 5.14.: Order of modes with highest effective mass on z-direction (case 11)

order	mode number		effective mass (kg)	
	FM	RM	FM	RM
1	1	1	4.48	4.27
2	3	3	2.34	2.38
3	2	2	1.91	1.99
4	10	10	0.96	1.63
5	6	6	0.67	0.50

Table 5.15.: Order of modes with highest effective mass on z-direction (case 12)

Figure 5.30.: Piezoelectric patch-type actuator

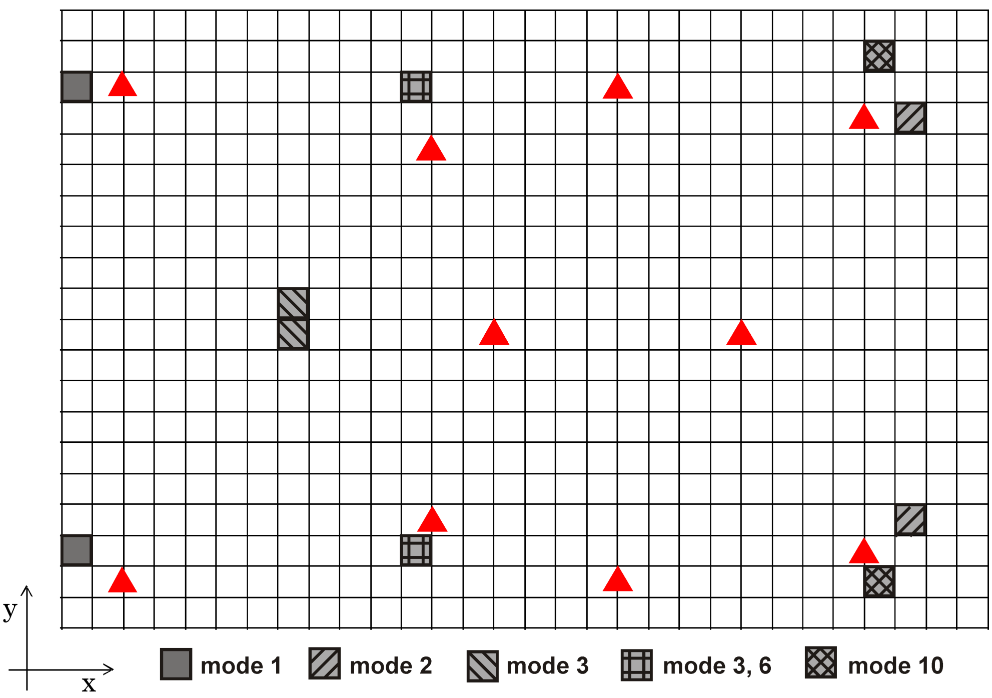

Figure 5.31.: Actuator locations for active damping of solar panel model (case 12)

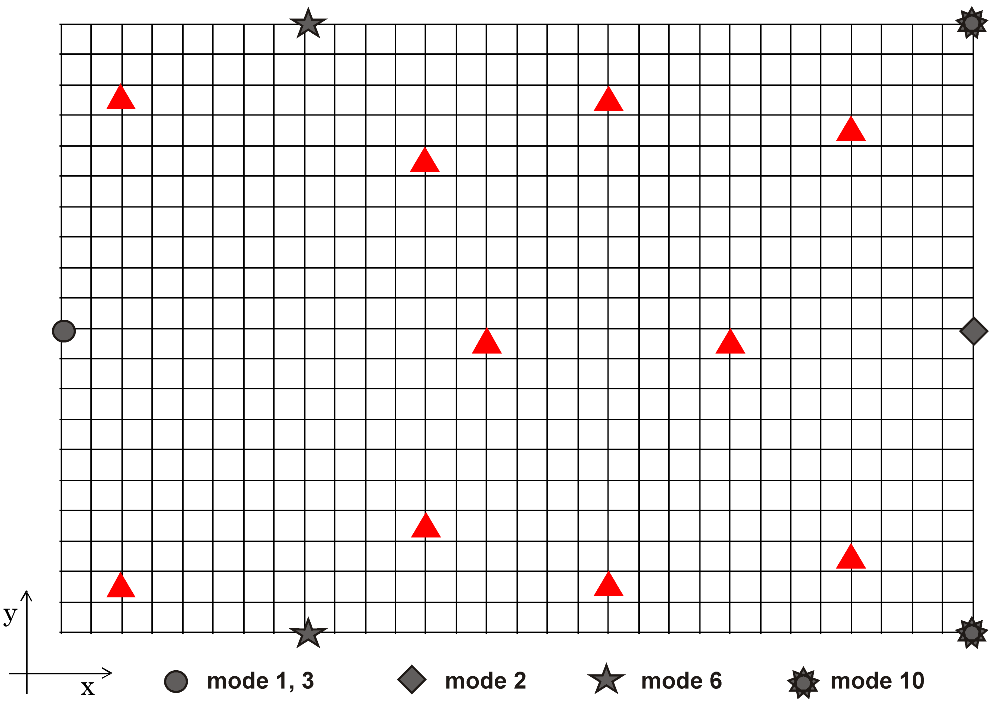

Figure 5.32.: Sensor locations for active damping of solar panel model (case 12)

		index number		PI value	
	order	FM	RM	FM	RM
mode 1	1	3, 18	3, 18	1.00	1.00
	2	62, 63	62, 63	0.79	0.67
	3	44, 45	44, 45	0.78	0.66
mode 2	1	487, 498	504, 517	1.00	1.00
	2	504, 517	487, 498	0.95	0.96
	3	503, 518	503, 518	0.13	0.10
mode 3	1	215, 226	215, 226	1.00	1.00
	2	142, 143	142, 143	0.71	0.69
	3	141, 144	141, 144	0.65	0.64
mode 6	1	215, 226	215, 226	1.00	1.00
	2	37, 52	196, 209	0.57	0.59
	3	196, 209	37, 52	0.49	0.48
mode 10	1	486, 499	486, 499	1.00	1.00
	2	487, 498	503, 518	0.52	0.54
	3	503, 518	487, 498	0.46	0.52

Table 5.16.: Highest performance index (PI) values and corresponding element numbers for actuator selection of solar panel model (case 12)

	order	index number		PI value	
		FM	RM	FM	RM
mode 1	1	181	181	1.00	1.00
	2	180, 182	180, 182	0.97	0.97
	3	179, 183	179, 183	0.90	0.90
mode 2	1	82	82	1.00	1.00
	2	81, 83	81, 83	0.98	0.98
	3	80, 84	80, 84	0.93	0.93
mode 3	1	181	181	1.00	1.00
	2	180, 182	180, 182	0.98	0.98
	3	179, 183	179, 183	0.93	0.93
mode 6	1	18, 146	18, 146	1.00	1.00
	2	17, 147	17, 147	0.99	0.98
	3	19, 145	19, 145	0.92	0.93
mode 10	1	2, 62	2, 62	1.00	1.00
	2	63, 101	63, 101	0.90	0.90
	3	64, 100	64, 100	0.81	0.80

Table 5.17.: Highest performance index (PI) values and corresponding node numbers for sensor selection of solar panel model (case 12)

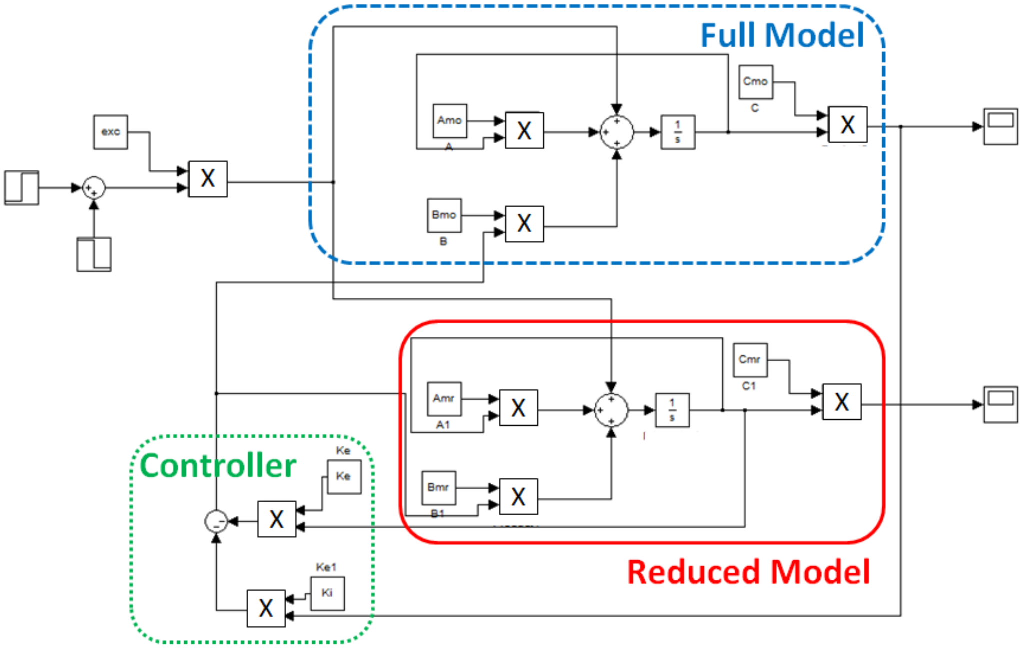

Figure 5.33.: Simulink model for vibration control of solar panel model

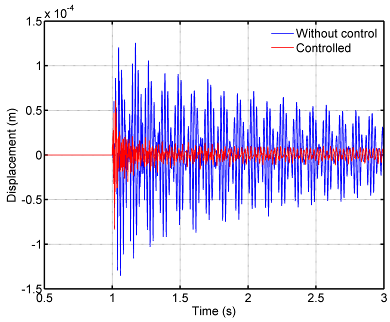

(a) sensor 1

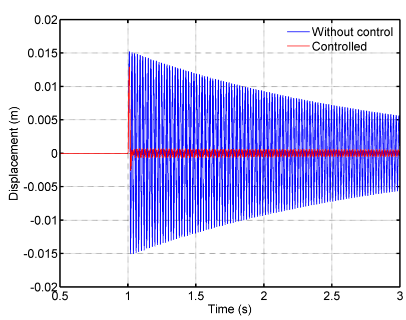

(b) sensor 2

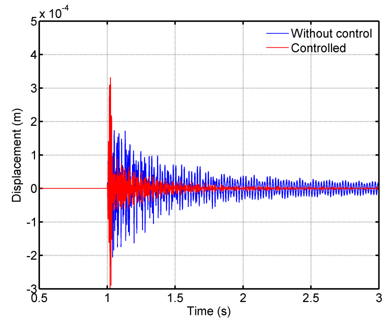

(c) sensor 3

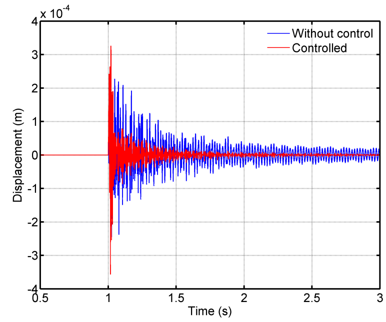

(d) sensor 4

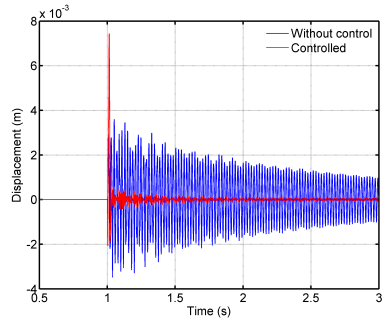

(e) sensor 5

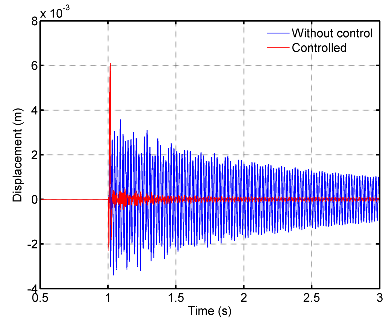

(f) sensor 6

Figure 5.34.: Displacement plot from sensors (case 12)

5.3. Structural design optimization

Many structural analyses are to be executed for designing a structure or a structural element such as a plate or a joint. According to its specific purpose (objective), boundary conditions and constraints, various types of design variables from material properties to the geometry of a structure are considered. Finding the optimal combination of all design variables achieving the best value for objective function, while satisfying a set of constraints, is called structural design optimization. Because of the complexity of structures in these days, optimization procedure should consider wide range of studies from material science to the control theory; therefore design optimization is commonly designated as multidisciplinary design optimization (MDO). MDO is a very promising and useful method especially in aerospace engineering where the optimal value among acute constraints is required. however, the computational cost to find the optimal value is not cheap. Although the exact amount of computation differs among different types of optimization algorithms, in general many times of functional evaluation is required varying design variables. As more design variables are included, the number of functional evaluation increases geometrically.
Consequently the more cost effective model is desired in MDO. A general reduced model can decrease computational efforts on each evaluation, however it cannot be used for the different design variables. It means that the model should be regenerated and re-reduced for every iteration, which is computationally not efficient at all and sometimes even worse. Parametric model order reduction (PMOR) can be a good solution here. The model is reduced as a function of parameters, which are design variables in optimization problems. Then each functional evaluation will be carried out on the reduced space only. Considering the high number of functional evaluation generally required in optimization problem, PMOR can give a promising prospect on computational efficiency in MDO.

5.3.1. Composite plate

As an elementary step, simple carbon-fiber reinforced polymer(CFRP) composite-Aluminum(Al) honeycomb sandwich plate under torsional load as shown in Fig. 5.35 is optimized. Two objectives which will be minimized are the deflection under the torsional load and the total mass of the plate. Design parameters are: the fiber volume fraction (V_f), the thickness of each layer (t), angles of fiber orientation (θ_1, θ_2), modulus of honeycomb core (E_c, G_{xz}, G_{yz}), and the thickness of the core (t_c). The key to a successful PMOR is knowing the effect of each parameter onto the system whether it is linear or quadratic or in other forms. Differently from the parameters tested in previous sections, which are modulus, thickness, and mass, design variables for a composite plate do not alter the structure in a simple formation. Instead, based on the composite theory, the design variables V_f, t, θ_1, θ_2 constitute a material with specific material properties E_x, E_y, and G_{xy}.

Since we have known the effects of above material properties and thickness as seen in section 4.4, the analysis is divided into two steps as shown in Fig. 5.36. The first step is based on rule of mixture and classical laminate theory (CLT) calculating

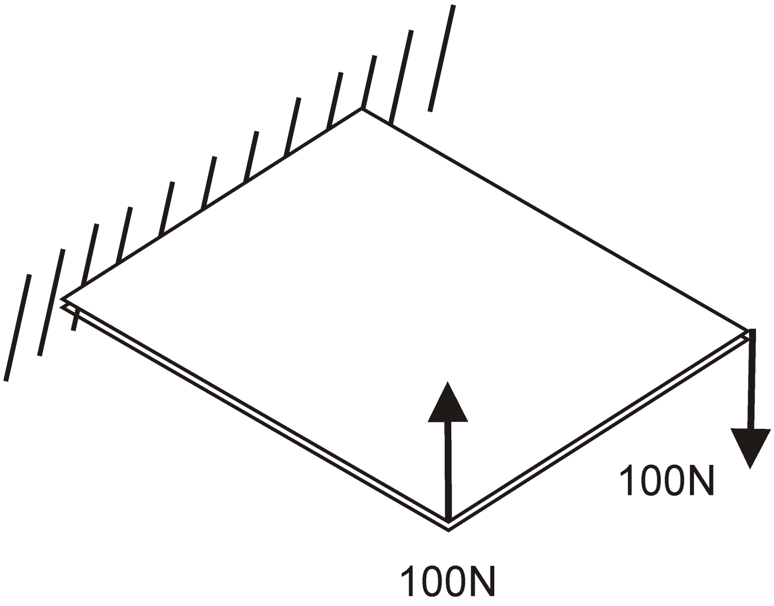

Figure 5.35.: Composite plate model under the torsional load

moduluses from CFRP facesheet; details are provided in Appendix A.5. This step can be done by simple matrix calculation, and does not require a model reduction since it is not computationally critical. The second step relates to the finite element (FE) model. Based on the material properties and thickness from the first step, FE model is generated and analyzed. PMOR will be held for the second step concerning material properties and thickness as parameters.

The optimization runs with parameterized reduced model, and the result will be compared with the result from ANSYS for verification. To simplify the task, the layup of the facesheet is assumed as $[0/90/\theta_1/\theta_2]_S$. And the fiber angles θ_1 and θ_2 are optimized first to minimize the deflection. After then other design parameters V_f, t, E_c, t_c are optimized to minimize the total mass taking the deflection as a constraint (maximum deflection should be less than 6.7mm). The upper and lower bounds and initial values are set as shown in Table 5.18. The order of the model is reduced from 16560 to 100.

	V_f (%)	t (mm)	θ_1 (deg)	θ_2 (deg)	E_c (GPa)	t_c (mm)
initial value	60	0.30	-30	30	1.9	17
lower bound	50	0.28	-90	0	1.0	8
upper bound	70	0.32	0	90	2.2	25

Table 5.18.: Initial values, upper and lower bounds for design variables of composite plate

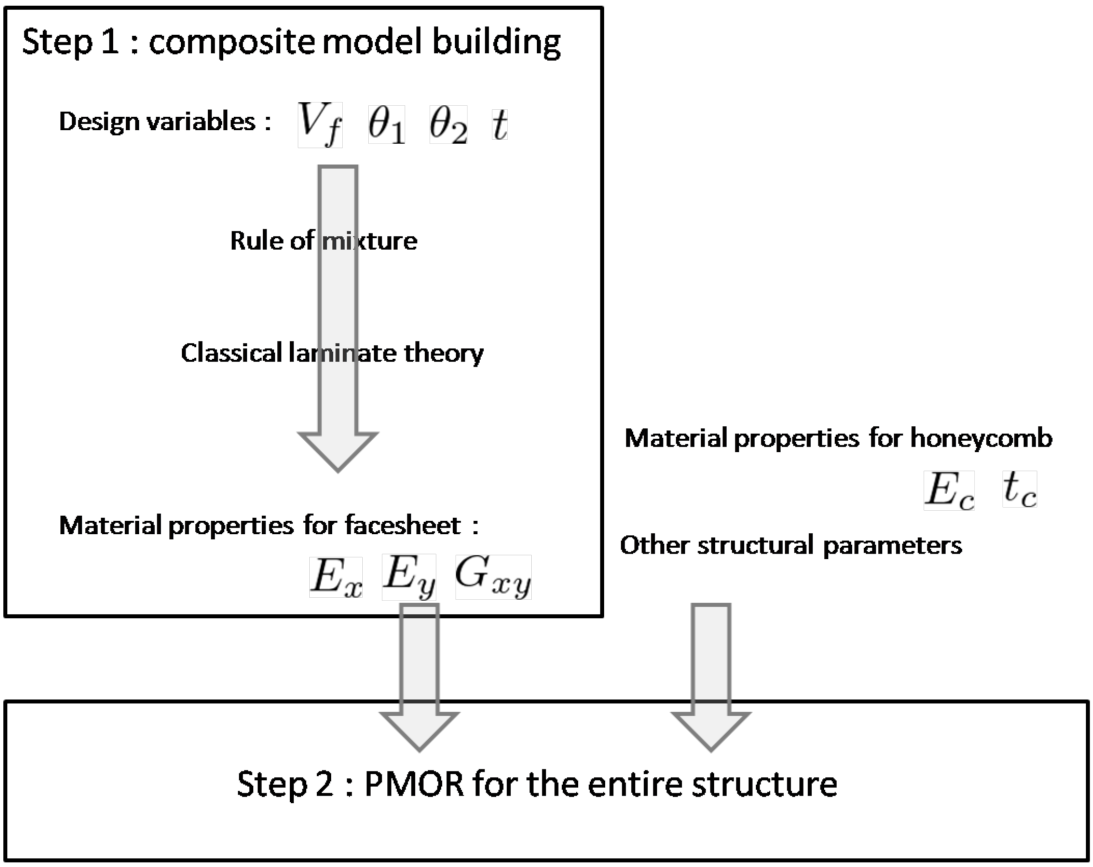

Figure 5.36.: A procedure of composite plate design optimization

Computational effort

During the optimization, matlab function $fmincon$, a optimization algorithm based on Sequential Quadratic Programming (SQP) method, is used. The optimal solutions from the reduced model and from the ANSYS are listed in Table 5.19. Clearly PMOR provides the same result as from calling and running ANSYS every time. The required computational time for each iteration is 0.06(s) for PMOR and 1.79 (s) for ANSYS.

	V_f (%)	t (mm)	θ_1 (deg)	θ_2 (deg)	E_c (GPa)	t_c (mm)
PMOR	70	0.28	-41.7	41.7	1.9	17.9
ANSYS	70	0.28	-41.4	41.4	1.8	18.0

Table 5.19.: Optimal solution of composite plate model from the reduced model and from the ANSYS

5.3.2. Mirror panel of the Overwhelming large (OWL) telescope

The second example is a more complex structure: designing of the mirror segments of the overwhelming large (OWL) telescope developed by the European Southern Observatory (ESO). The OWL telescope aims for a very large main mirror which can collect star light from distant places. The original design of OWL consisted of 3048 segments, half of which is shown in Fig. 5.37 [Pet05]. The diameter of entire mirror is 100m.

As the size of mirror larger, the manufacturing cost increases. The most critical point is the mass; many desirable consequences, for example simplified and cheaper support structures, smaller actuator for control, will be followed by lowering the mass, finally lowering the total cost of the telescope. Therefore optimization minimizing its areal mass, while still maintaining a sufficient accuracy of the optical surface under a gravity load of 1g $(9.8m/s^2)$ will be tried.
A mirror segment is modelled as a CFRP-Al honeycomb sandwich on the surface, and aluminum on the back supporting structure. The design variables are from the sandwich structure as in section 5.3.1. The initial values of design parameters and their upper and lower bounds are listed in Table 5.20. Fiber angles and lay-up type are optimized first to minimize the deformation of the surface (z_{RMS}) assuming that the total thickness of facesheet remains same regardless of number of layers. Type 1 with $[0/90/\theta_1/\theta_2]_S$ and type 2 with $[0/90/\theta_1/\theta_2/\theta_1]_S$ are considered. For the second optimization procedure, the objective function is an areal mass, and the constraint is the deformation of the surface (z_{RMS}) limited to 25nm. The order of the model is reduced from 14235 to 100.

Computational effort

The resultant optimum is shown in Table 5.21, both from the reduced model and from the ANSYS. Parameterized reduced model gives the same result as ANSYS does spending only 45.5 (s) of CPU time per each functional evaluation while ANSYS requires 492.1 (s).

	θ_1 (deg)	θ_2 (deg)	number of layer	t_f (mm)	t_c (mm)
initial value	0	90	8	3	17
lower bound	-90	0	8	1	14
upper bound	0	90	10	4	20

Table 5.20.: Initial values, upper and lower bounds for design variables of composite plate

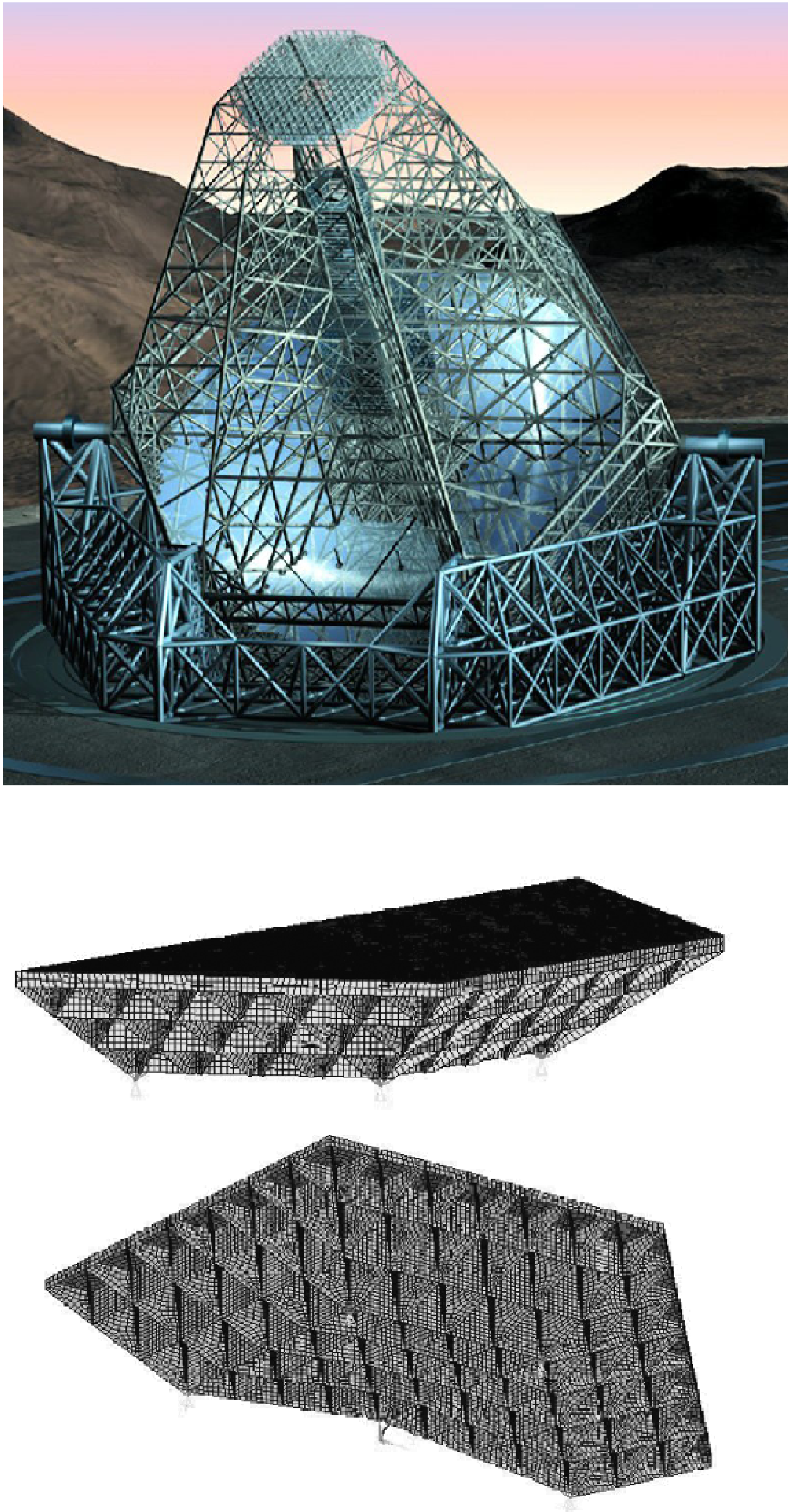

Figure 5.37.: A Mirror segment from overwhelmingly large (OWL) telescope

	θ_1 (deg)	θ_2 (deg)	number of layer	t_f (mm)	t_c (mm)
PMOR	-46.1	+46.1	10	2.8	14
ANSYS	-46.2	+46.8	10	2.9	14

Table 5.21.: Optimal solution of OWL telescope model from the reduced model and from the ANSYS full model

6. Conclusion

In recent decades model order reduction (MOR) and parametric model order reduction (PMOR) are investigated in various fields of study. For structural models such as large finite element (FE) models, MOR based on modal space are preferred because one can predict its physical behavior after the reduction. In control engineering, singular value decomposition (SVD) based methods are preferred because of the preservation of stability and existence of error bound. Multibody system, circuit design, and micro-electro-mechanical system (MEMS) preferred Krylov subspace method since it can handle very large size models which SVD based methods cannot. Krylov method is often implemented to the FE model as eigen-analysis for modal transformation needs high computational effort.

For PMOR, most of studies are focusing on rational reduction or model reduction with a few system parameters. In this case parameters can be directly extracted from the first order dynamic equation in state space; therefore relatively simple formulation can be applied. However, when a large and complex FE model with various physical or geometrical parameters are concerned, the application of formerly developed theories (as shown in chapter 3) is not straight forward. Those parameters are directly related to the structural matrices, mass and stiffness matrices, not to the state space model. Therefore, inversions and multiplications required when they are turned into a state space form makes the method highly complicated accompanying with very high computational effort. It is also observed that sometime the accuracy of reduced model is limited by a low level. This dissertation contributes to solve those problems as well as to investigate practically efficient PMOR for large FE models.

The method driven in chapter 4 aims for the realization of mathematically developed method, and the examination of its effectivity. Four main objectives are achieved; 1) the parameter change can be directly applied to the reduced model, 2) the reduced model gives fairly accurate results compared to the original model, 3) the reduced model can reflect parametric effects well, 4) the controller designed from parametrized reduced model works well. Both static and dynamic models are developed and tested by numerical examples of space structures: large reflector for static case, active truss structure and solar array panel model for dynamic case. The nature of FE model, superposition of matrices from single elements, makes parameter handling easier; however it also causes some technical difficulties in application of theory, which are solved through the two-step Arnoldi method and the deflation. A disadvantage of block Arnoldi algorithm, larger reduction space, is also solved by the deflation process. In dynamic analysis, reordering process corrects the error caused by integrating infinite summation term. Applying LU decomposition method into PMOR algorithm instead of direct inversion, computational efficiency is even increased. Computational time and order is compared to show it.

The parametric effectivenss in this method is calculated by finite difference from two FE models. Therefore lineary affecting parameters or polynomially affecting parameters such as thickness can be well treated. However, if the parameters are nonlinearly affecting the structure, reduced model will not be accurate. One alternative way is transforming those parameters into linearly affecting parameters as done in composite plate example in section 5.3.1. The other remained problem is nonlinearities in the system. Even though the parameters are linearly formulated, the reduced model may not properly reflect the nonlinear terms in the system. To compensate this part, adaptation of interpolation based method seems worth to investigate as a future work.

A. Appendix 1 : Theoretical background for numerical examples

A.1. Actuator and sensor location based on performance index

For the better efficiency of actuation, the location which can transfer more energy into the system is desirable; and for sensing, the location where more energy is detectable is more desirable. Hac and Liu[HL93] presented expectation of total energy in the form of equation (A.1).

$$E_i = \beta_{ii}/4\zeta_i\omega_i \quad \text{:expectation of total energy of the } i\text{th mode} \tag{A.1}$$

where $\beta_{ij} = \sum_{q=1}^{q} \Phi_i\left(P_q\right)\Phi_j\left(P_q\right)$

Φ_i : eigen function of ith mode

P_q : actuator location, q number of actuators

ζ_i : damping ratio on ith mode

ω_i : natural frequency on ith mode

As a criterion of actuator location, following performance index PI' is suggested in [HL93].

$$PI' = 2\left(\sum_{i=1}^{n} E_i\right)\sqrt[n]{\prod_{i=1}^{n}\left(E_i\right)} \tag{A.2}$$

If the damping ration ζ_i is small enough and the natural frequencies of the structure are well spaced, then equation (A.3) is satisfied.

$$\lambda_{c,2i-1} = \lambda_{c,2i} = E_i \tag{A.3}$$

$$\text{where} \quad \lambda_c\text{: eigenvalues of the controllability gramian} \tag{A.4}$$

Therefore following performance index is finally suggested as a criterion for actuator location.

$$PI = \left(\sum_{i=1}^{2n} \lambda_{c,i}\right)\sqrt[2n]{\prod_{i=1}^{2n}\left(\lambda_{c,i}\right)} \tag{A.5}$$

Applying same methodology to the obeservability gramian and energy index from it, a criterion for sensor location is suggested as in equation (A.6).

$$PI = \left(\sum_{i=1}^{2n} \lambda_{o,i} \right) \sqrt[2n]{\prod_{i=1}^{2n} (\lambda_{o,i})} \tag{A.6}$$

$$\text{where} \quad \lambda_o\text{: eigenvalues of the controllability gramian} \tag{A.7}$$

A.2. Effective mass

Since ealry 70's, the concept of effective mass has been used for identifying predominant modes. Effective mass is a moving mass value when the structure is exposured to a unit base excitation on a single direction under a certain mode. It is measured as a modal reaction force to the unit base acceleration. Each of modal effective mass is assumed to vibrate on a certain mode only; therefore the summation of effective mass of all modes are teh same as a total mass of the structure. On the other word, effective mass represents the contribution of each mode for the movement on a certain degree of freedom. Consequently, the mode which has high effective mass value on the interested degree of freedom(d.o.f), it can be assumed as predominant mode on that d.o.f.
Effective mass can be derived as in equation (A.8).

$$M_i^{eff} = \frac{L_i^T L_i}{m_{ii}} = \frac{\left(\varphi^T M \psi_i\right)\left(\psi_i^T M \varphi\right)}{\psi_i^T M \psi_i} \tag{A.8}$$

where ψ_i : ith mode shape
φ : rigid body mode
L_i : mass modal participation vector on mode i

Note that effective mass values are not influenced by the normalization of mode shape.

A.3. Actuator modeling for piezo-patch actuator

After a trade-off study about active damping concept for solar array panel, as a part of solar array panel project under EADS Astrium, piezo-electric patch is chosen as an actuator. It has a high power speicific volume or mass ration (power divided by volume or mass); so suitable to space application. Acceptable temperature range (-20 $+120\,^\circ$ C) and hysteresis ($\sim 10\%$) make piezoceramic (PZT) patches desirable than other smart materials such as shape memory alloy or piezoelectric polymer. Since PZT has high stiffness, it can generate high force on the base structure to modify its behavior. High bandwidth and load bearing capabiliy are also merits of PZT. As it is made in patch type, it can be integrated very well onto the structure, especially to a panel without adding any spatial problems. Due to above advantages, piezoceramic material is widely used in space application as an actuator. However, because of its electro-mechanical property, modeling its behavior is complicated. Deppoling of ceramic under high electric field, nonlinearity between strain and electric field, hysterisis, and dependency on mechanical load and temperature increase the complexity of PZT modeling. However, under a certain electric field range, linearized model is acceptable and widely used. Linear theory of piezoelectricity is summarized in equation (A.9).

$$\begin{Bmatrix} S \\ D \end{Bmatrix} = \begin{bmatrix} s^E & d \\ d & \varepsilon^T \end{bmatrix} \begin{Bmatrix} T \\ E \end{Bmatrix} \tag{A.9}$$

S : strain

D : dielectric displacement (charge per unit area)

T : stress

E : electric field

s^E : compliance matrix

d : piezoelectric constants

ε^T : permittivity constants

Based on the electrical and mechanical constitutive equation, there are several modeling methods to integrate PZT actuator into the base structure. Thermo elastic analogy treats a strain due to electric field as a thermal strain. It is easily applicable, but it contains high modeling error and cannot be applied to the structure exposured under an actual thermal loading. Blocking force model uses the approximated force generated by elongation of piezo patch. It can be applied both on static and dynamic application but still contains some errors. In reality the force from actuator is always smaller than blocking force because the base structure is elastic, when piezo-patch generates force, some part of the force is consumed to deform a base structure. In the blocking force model, this effect is neglected and the base structure is assumed to be rigid. Finally, equivalent force model, so called pin-force model, is suggested to consider the deformation of the base structure as well.

In the pin-force model, the bonding between the actuator and the base structure is assumed as a perfect bonding. Under this condition, the shear stress caused by bending deformation is concentrated on the edge of the actuator behaving like a pin connection with force and moment as drawn in Fig. A.1 [CR94].

Using the classical laminate theory (CLT), the components of stiffness matrices $[A]$, $[B]$, and $[D]$ matrices are obtained as in equation (A.10)

$$\begin{aligned}
[A] &= \textstyle\sum_k [A_k] = \sum_k \left[\bar{Q}_k\right] (z_{k+1} - z_k) \\
[B] &= \textstyle\sum_k [B_k] = \frac{1}{2} \sum_k \left[\bar{Q}_k\right] \left(z_{k+1}^2 - z_k^2\right) \\
[D] &= \textstyle\sum_k [D_k] = \frac{1}{3} \sum_k \left[\bar{Q}_k\right] \left(z_{k+1}^3 - z_k^3\right)
\end{aligned} \tag{A.10}$$

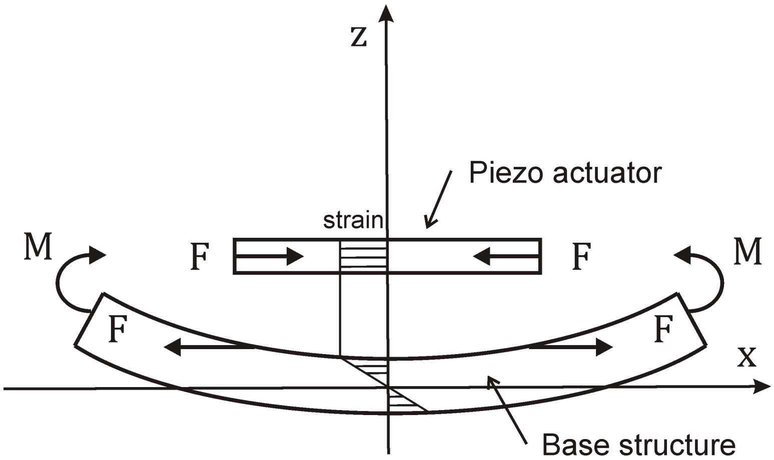

Figure A.1.: Pin-force model for piezoelectric patch actuator

- $[A]$: matrix of in plane stiffnesses that relates in-plane deformation with in-plane forces
- $[B]$: matrix of coupling stiffnesses that relates in-plane deformation with moments and curvatures with in-plane forces
- $[D]$: matrix of rotational stiffnesses that relates curvature with applied moments

From the equivalent force condition as shown in equation (A.11)-(A.12), the force and moment generated by piezo-patch actuator can be modeled by equation (A.13) [Loc01].

$$\begin{gathered}\int_{plate}\{\sigma\}\,dz + \int_{act}\{\sigma\}\,dz = 0 \text{ for the force}\\ \int_{plate}\{\sigma\}\,z\,dz + \int_{act}\{\sigma\}\,z\,dz = 0 \text{ for the moment}\end{gathered} \tag{A.11}$$

$$\begin{bmatrix}[A_{plate}] & [B_{plate}]\\ [B_{plate}] & [D_{plate}]\end{bmatrix}\begin{Bmatrix}\{\varepsilon^0\}\\ \{\chi\}\end{Bmatrix} = -\begin{bmatrix}[A_{act}] & [B_{act}]\\ [B_{act}] & [D_{act}]\end{bmatrix}\begin{Bmatrix}\{\varepsilon^0\}\\ \{\chi\}\end{Bmatrix} + \begin{bmatrix}[A_{act}]\\ [B_{act}]\end{bmatrix}\{\Lambda\}$$

$$\begin{aligned}&\varepsilon^0 \quad \text{: stiffness from actuator}\\ &\chi \quad \text{: stiffness from total structure}\\ &\Lambda = \begin{cases}[d]_t \dfrac{V}{t_a} & \text{: actuator layer}\\ 0 & \text{: plate}\end{cases}\end{aligned} \tag{A.12}$$

$$\begin{Bmatrix} \{F_{act}\} \\ \{M_{act}\} \end{Bmatrix} = \left(\begin{bmatrix} [A_{act}] & [B_{act}] \\ [B_{act}] & [D_{act}] \end{bmatrix} \begin{bmatrix} [A_{tot}] & [B_{tot}] \\ [B_{tot}] & [D_{tot}] \end{bmatrix}^{-1} - 1 \right) \begin{bmatrix} [A_{act}] \\ [B_{act}] \end{bmatrix} \Lambda$$

act : stiffness from actuator (A.13)

tot : stiffness from total structure

The advantage of pin-force model as well as blocking force model is that the actuator does not need to be integrated in a complex FE model. Instead, the existance of actuator is counted in acuation force modeling as in equation (A.13), and only external force and moment are applied to the base structure. It provides much more computational efficiency especially when the base structure is large and complex, and when the location of actuator is changed. The limitation of pin-force model is the thickness ratio between the patch actuator and the base structure. In general, when the base structure is more than five time thicker than the patch actuator, pin-force model gives accurate approximation as shown in Fig. A.2 [CR94].

The distribution of force on each node is from the weight factor shown in Fig. A.3; 0.5 on the corner, 1 on the middle of the edge.

A.4. Controller design

The type of controller is selected based on the target structure. For the relatively simple structures such as active truss structure, more direct way is preferred such as positive position feedback (PPF) control by filtering chosen modes. For the complex structures, modern control theory such as Linear Quadratic Regulator (LQR) is preferred in order to keep a system robust.
For a dynamic system in state space as shown in equation (A.14), if $\{A, B\}$ is controllable, state x can be sent to zero within a finite time from any initial state $z(t_0) = z_0$.

$$\dot{z} = Az + Bu \tag{A.14}$$

A finite energy input make this possible can be described as $u = -Lz$. As L becomes larger, z can be zero faster; however large L represents large input energy for control Therefore trade-off between fast decay and control energy is required. Linear Quadratic Regulator (LQR) problem is designing optimal control input u minimizing quadratic summation J of those two factors.

$$J = \frac{1}{2} \int_0^\infty \left(x^T Q x + u^T R u \right) dt \tag{A.15}$$

where $Q(\geq 0)$, $R(\geq 0)$ are weighting matrices

For the solar panel model, LQR controller is used. Since the aim is vibration control, weighting factor for state, Q, is decided very large value.

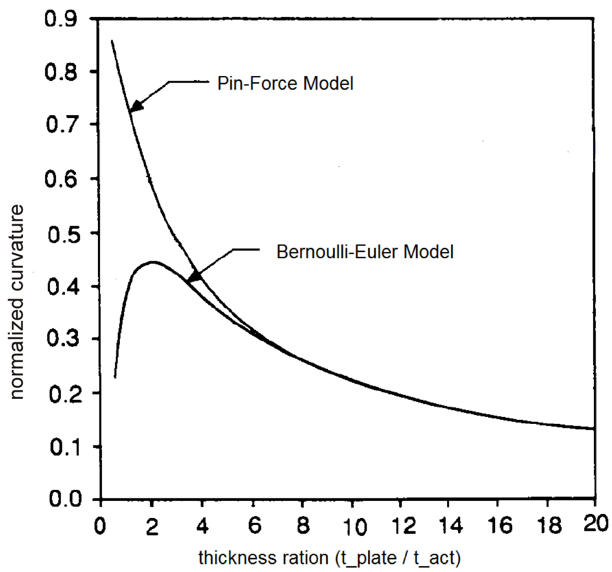

Figure A.2.: Comparison of Bernoulli-Euler model and pin-force model according to the thickness ratio

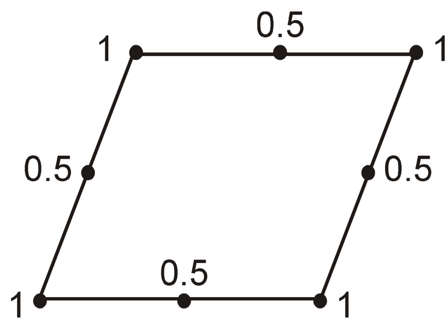

Figure A.3.: Weighting factor for an element in pin-force model (actuator)

A.5. Composite modeling

A composite refers a mixture of two different materials to have advantages from both sides. Generally it consists of a ductile material (matrix) and a material with high strength and stiffness (filler/fiber). The main puprpose of designing a composite is to make a material with better performance and lower mass; therefore both materials are taken from low density materials. Among the various kinds of composite depending on which matrix and filler types are used, fiber reinforced polymer is most commonly used. As a filler, graphite (carbon) fiver, and glass fiber are popular. The strength and stiffness of a composite are decided by the types and amount of fiber in the resin, arrangement and lay-up. Fundamental methods to calculate the material properties of a composite from the properties of matrix and fibers are the rule of mixture and classical laminate theory.

A perfect bonding between fiber and matrix is assumed; then the strains from both matrix and fiber are same as shown in equation (A.16).

$$\sigma_x = V_f\,\sigma_{fx} + V_m\,\sigma_{mx} = (V_f\,E_f + V_m\,E_m)\;\epsilon_x \tag{A.16}$$

V_f : fiber volume fraction
V_m : matrix volume fraction , $1 - V_f$
E_f : Young's modulus of fiber
E_m : Young's modulus of matrix
σ_{fx} : stress on fiber
σ_{mx} : stress on matrix
ϵ_x : strain

Therefore the Young's modulus of the entire structure E_x can be expressed as in equation (A.17), which is called rule of mixture.

$$E_x = V_f\,E_f + V_m\,E_m \tag{A.17}$$

With similar manners other properties are driven as in equation (A.18)[TH80].

$$\begin{aligned} \text{Poisson's ratio}: &\quad \nu_x = V_f\,\nu_f + V_m\,\nu_m \\ \text{Elastic modulus } E_y: &\quad \frac{1}{E_y} = \frac{V_f}{E_f} + \frac{V_m}{E_m} \qquad \text{(A.18)} \\ \text{Shear modulus } E_s: &\quad \frac{1}{E_s} = \frac{V_f}{G_f} + \frac{V_m}{G_m} \end{aligned}$$

(A.19)

Figure A.4.: Matrix-fiber composite

Rule of mixture determines material properties of each layer according to the axis of fiber alignment. When the layers with various fiber angle orientations are piled up, the material properteis of the total laminates are also different. Their flexibility in designing is one of the major advantages of composite structures.

A classical laminate theory (CLT) combines the properties of each layer based on equilibrium equations, compatibility conditions, and Hook's law. A perfect bond between single laminas and Kirchhoff hypothesis are assumed. A stiffness matrix Q^k from a single lamina with fiber angle α_k can be transformed into a global coordinate as shown in equation (A.20).

$$\begin{bmatrix} \bar{Q_{11}}^k & \bar{Q_{12}}^k & \bar{Q_{13}}^k \\ \bar{Q_{21}}^k & \bar{Q_{22}}^k & \bar{Q_{23}}^k \\ \bar{Q_{31}}^k & \bar{Q_{32}}^k & \bar{Q_{33}}^k \end{bmatrix} = \begin{bmatrix} m^2 & n^2 & 2mn \\ n^2 & m^2 & -2mn \\ -mn & mn & m^2-n^2 \end{bmatrix} \begin{bmatrix} Q_{11}^k & Q_{12}^k & Q_{13}^k \\ Q_{21}^k & Q_{22}^k & Q_{23}^k \\ Q_{31}^k & Q_{32}^k & Q_{33}^k \end{bmatrix} \begin{bmatrix} m^2 & n^2 & 2mn \\ n^2 & m^2 & -2mn \\ -mn & mn & m^2-n^2 \end{bmatrix}^T$$

$$\bar{Q}^k = T^k \, Q^k \, \left(T^k\right)^T \tag{A.20}$$

,where $m = \cos\alpha_k$ and $n = \sin\alpha_k$

The resultant force-momentum equation after piling up is shown in equation (A.21). CLT is valid only for thin laminates such that the span is at least ten times larger than the thickness, and the transverse deflection is small.

$$\left\{\begin{array}{c} N_x \\ N_y \\ N_{xy} \\ \hline M_x \\ M_y \\ M_{xy} \end{array}\right\} = \left[\begin{array}{ccc|ccc} A_{11} & A_{12} & A_{16} & B_{11} & B_{12} & B_{16} \\ A_{21} & A_{22} & A_{26} & B_{21} & B_{22} & B_{26} \\ A_{61} & A_{62} & A_{66} & B_{61} & B_{62} & B_{66} \\ \hline B_{11} & B_{12} & B_{16} & D_{11} & D_{12} & D_{16} \\ B_{21} & B_{22} & B_{26} & D_{21} & D_{22} & D_{26} \\ B_{61} & B_{62} & B_{66} & D_{61} & D_{62} & D_{66} \end{array}\right] \left\{\begin{array}{c} \epsilon_x^0 \\ \epsilon_y^0 \\ \gamma_{xy}^0 \\ \hline \kappa_x \\ \kappa_y \\ \kappa_{xy} \end{array}\right\} \tag{A.21}$$

$$\begin{aligned} [A] &= \textstyle\sum_k \left[A^k\right] = \sum_k \left[\bar{Q}^k\right] (z_{k+1} - z_k) \\ [B] &= \textstyle\sum_k \left[B^k\right] = \frac{1}{2} \sum_k \left[\bar{Q}^k\right] \left(z_{k+1}^2 - z_k^2\right) \\ [D] &= \textstyle\sum_k \left[D^k\right] = \frac{1}{3} \sum_k \left[\bar{Q}^k\right] \left(z_{k+1}^3 - z_k^3\right) \end{aligned}$$

B. Appendix 2 : Additional results

B.1. Results from static analysis and control

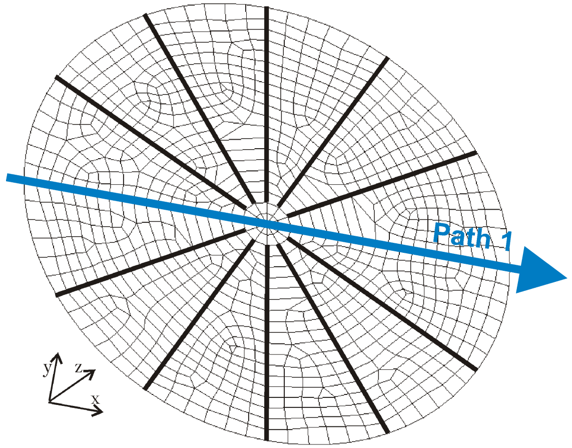

(a) A path to observe

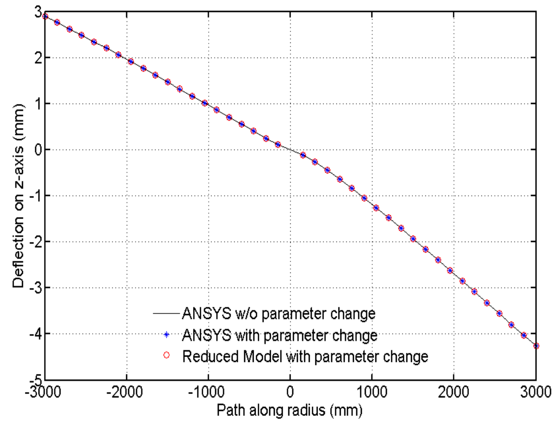

(b) case 0

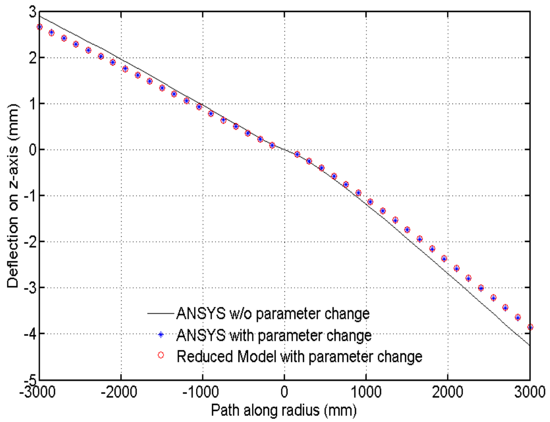

(c) case 1

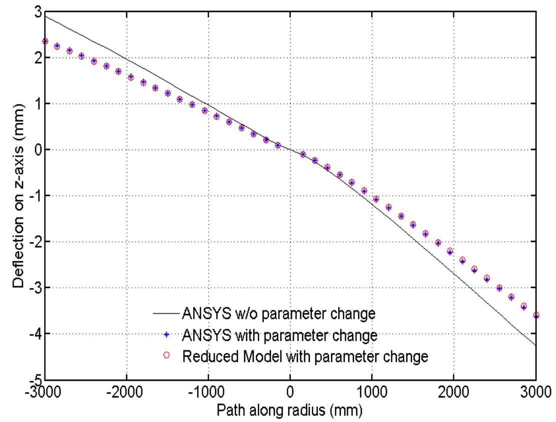

(d) case 2

Figure B.1.: Deflection plots on cross sectional area along the path shown in (a), with corresponding paramter cases

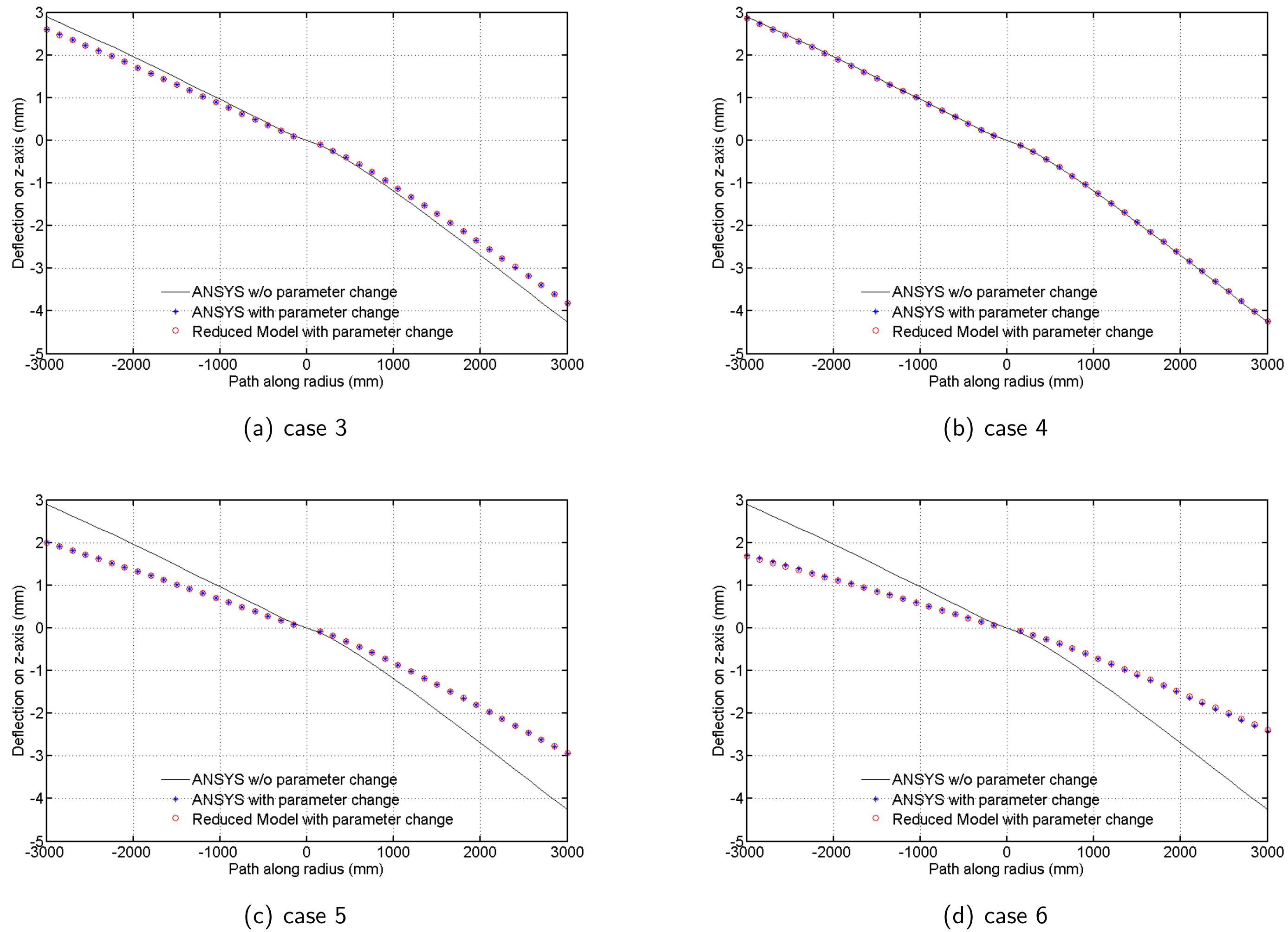

(a) case 3

(b) case 4

(c) case 5

(d) case 6

Figure B.2.: Deflection plots on cross sectional area along the path shown in (a), with corresponding paramter cases

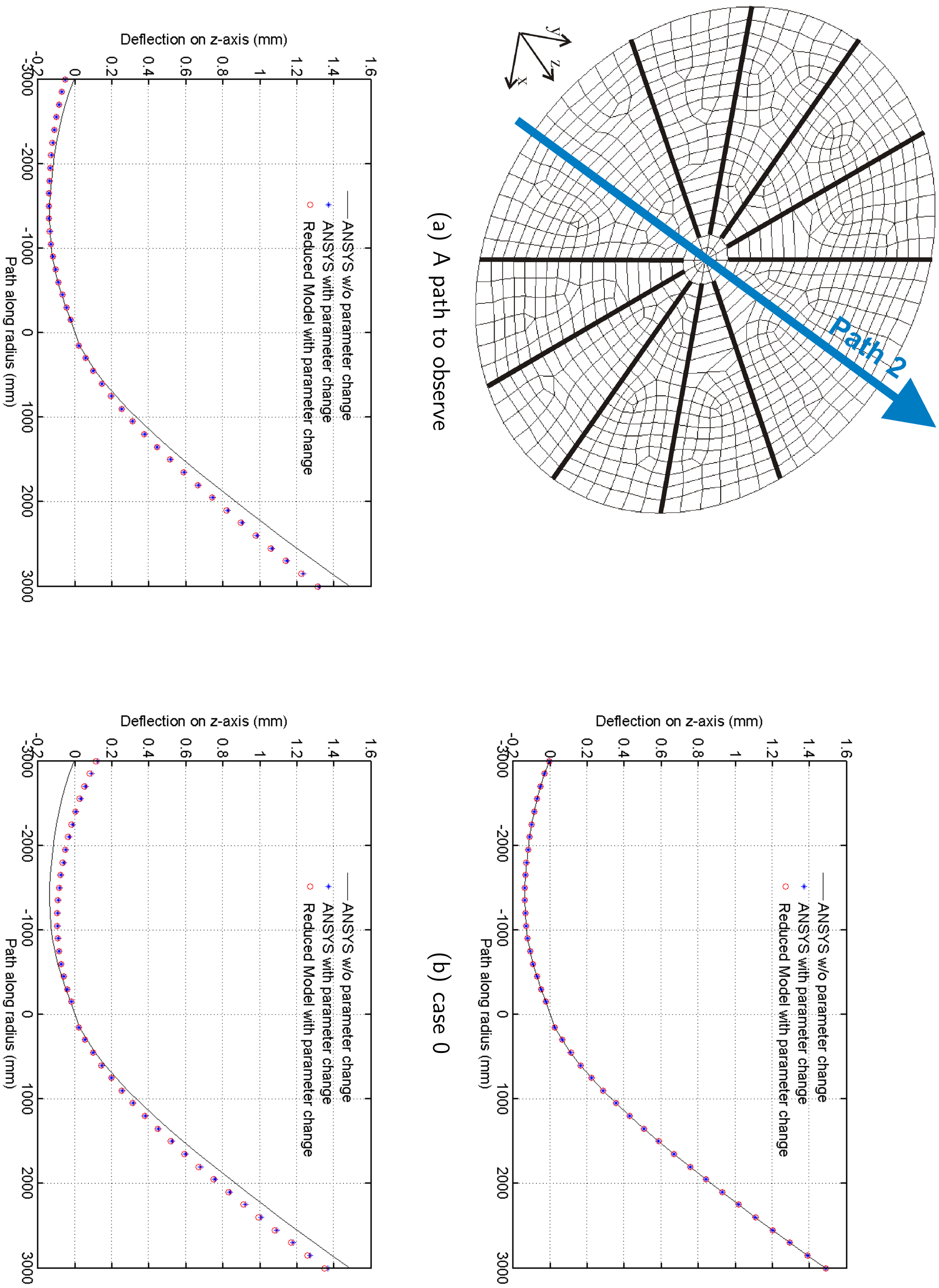

(a) A path to observe

(b) case 0

(c) case 1

(d) case 2

Figure B.3.: Deflection plots on cross sectional area along the path shown in (a), with corresponding paramter cases

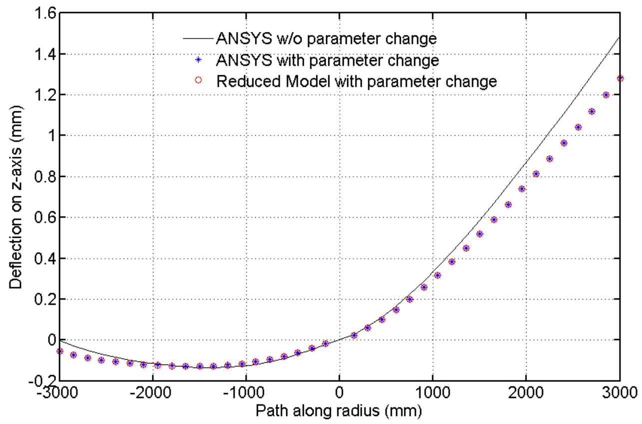

(a) case 3

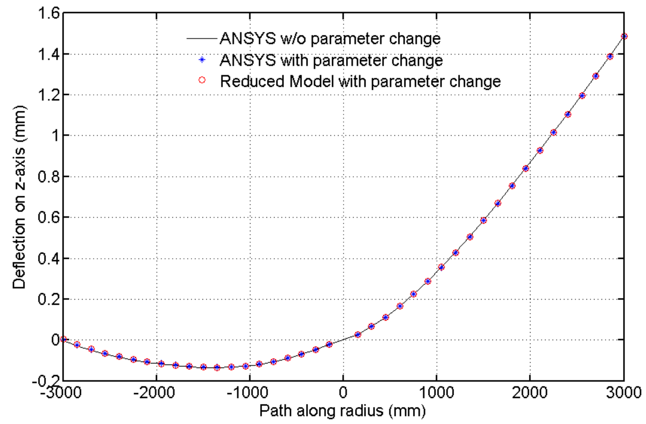

(b) case 4

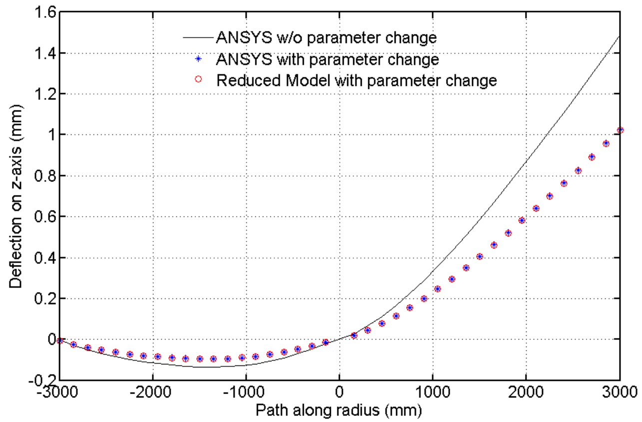

(c) case 5

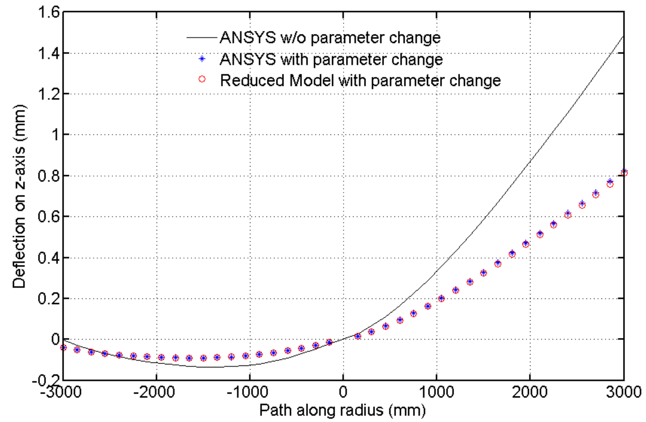

(d) case 6

Figure B.4.: Deflection plots on cross sectional area along the path shown in (a), with corresponding paramter cases

B.2. Results from dynamic analysis of truss structure

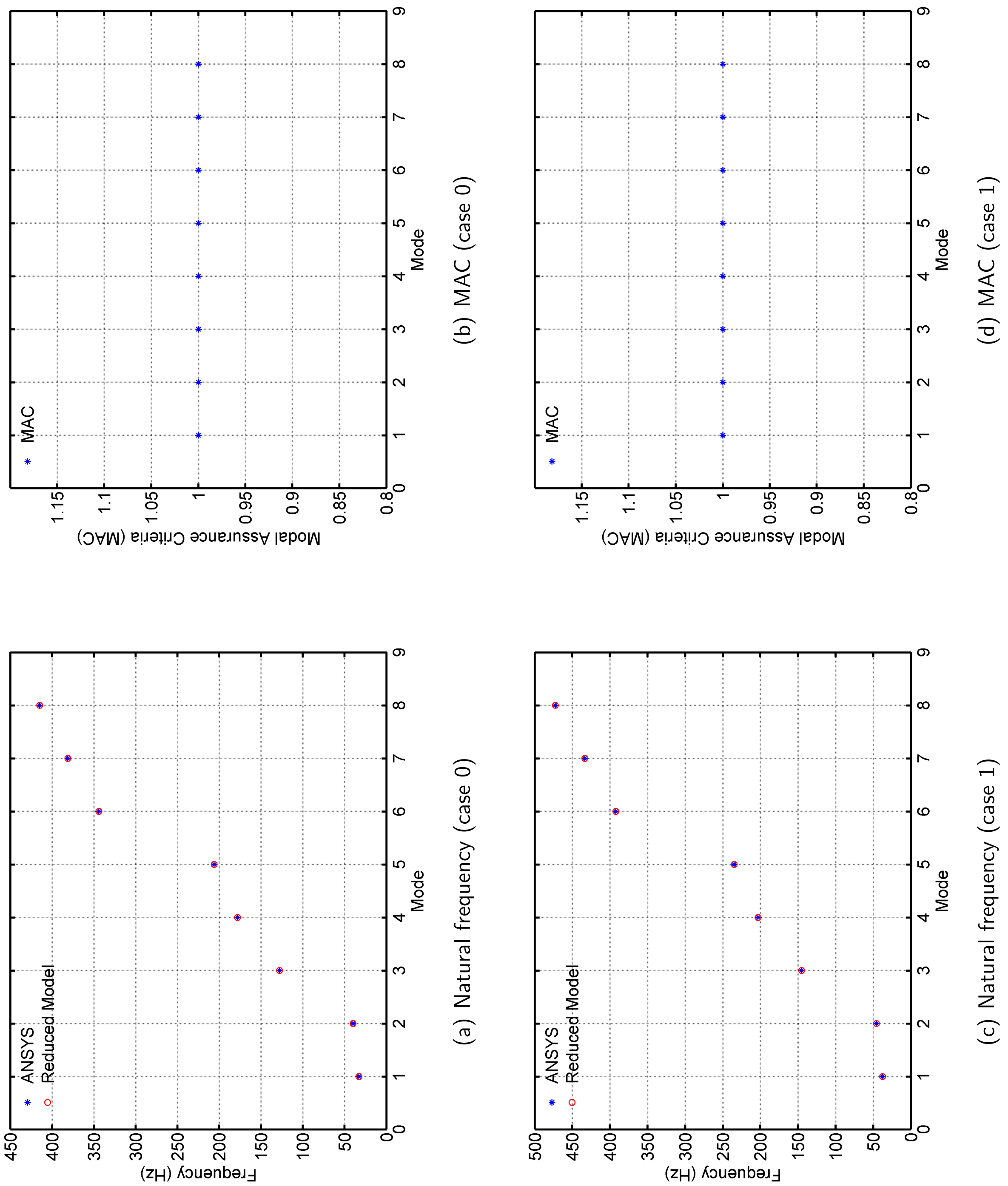

Figure B.5.: Comparison of natural frequencies and MAC values of active truss structure (case 0-1)

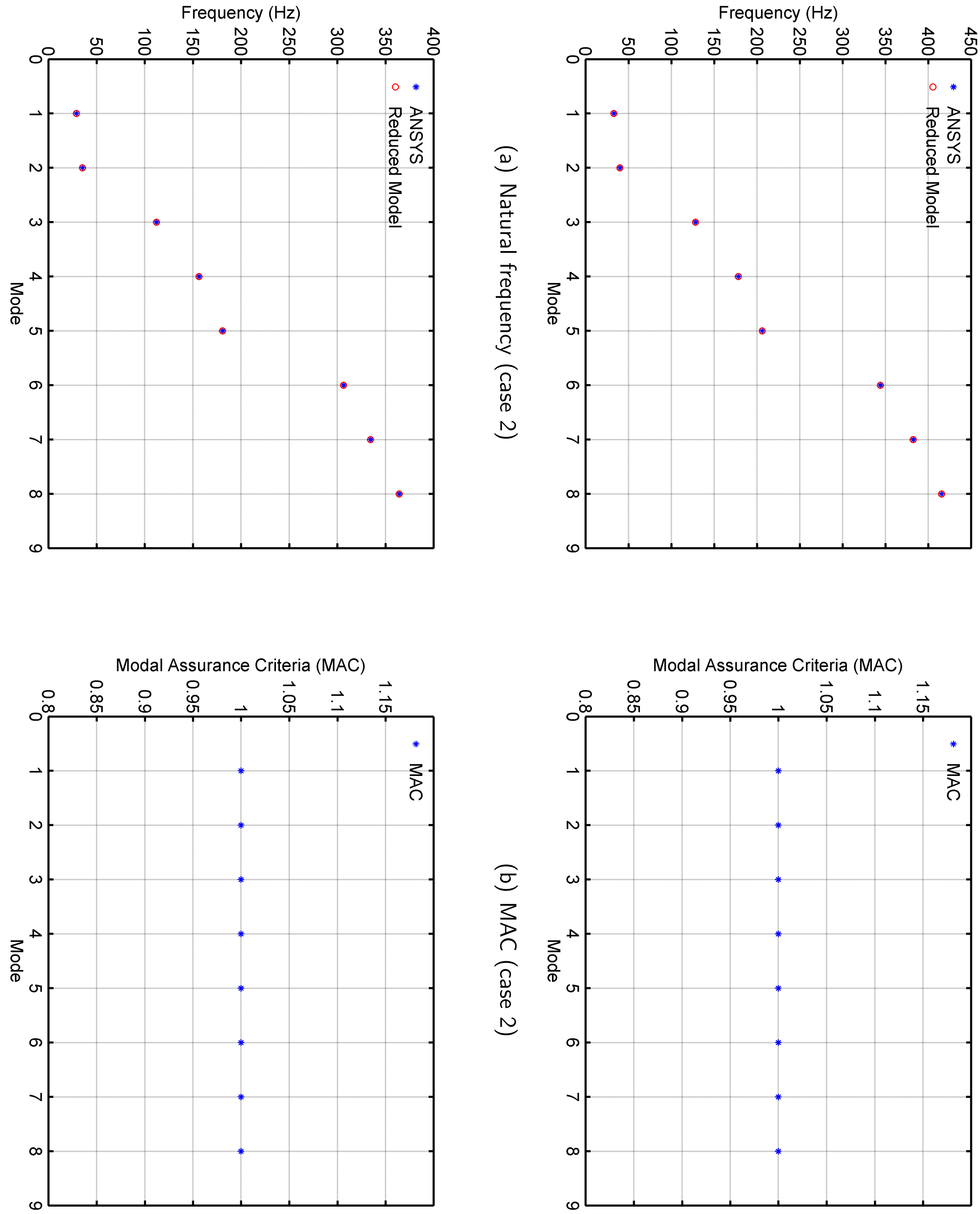

(a) Natural frequency (case 2)

(b) MAC (case 2)

(c) Natural frequency (case 3)

(d) MAC (case 3)

Figure B.6.: Comparison of natural frequencies and MAC values of active truss structure (case 2-3)

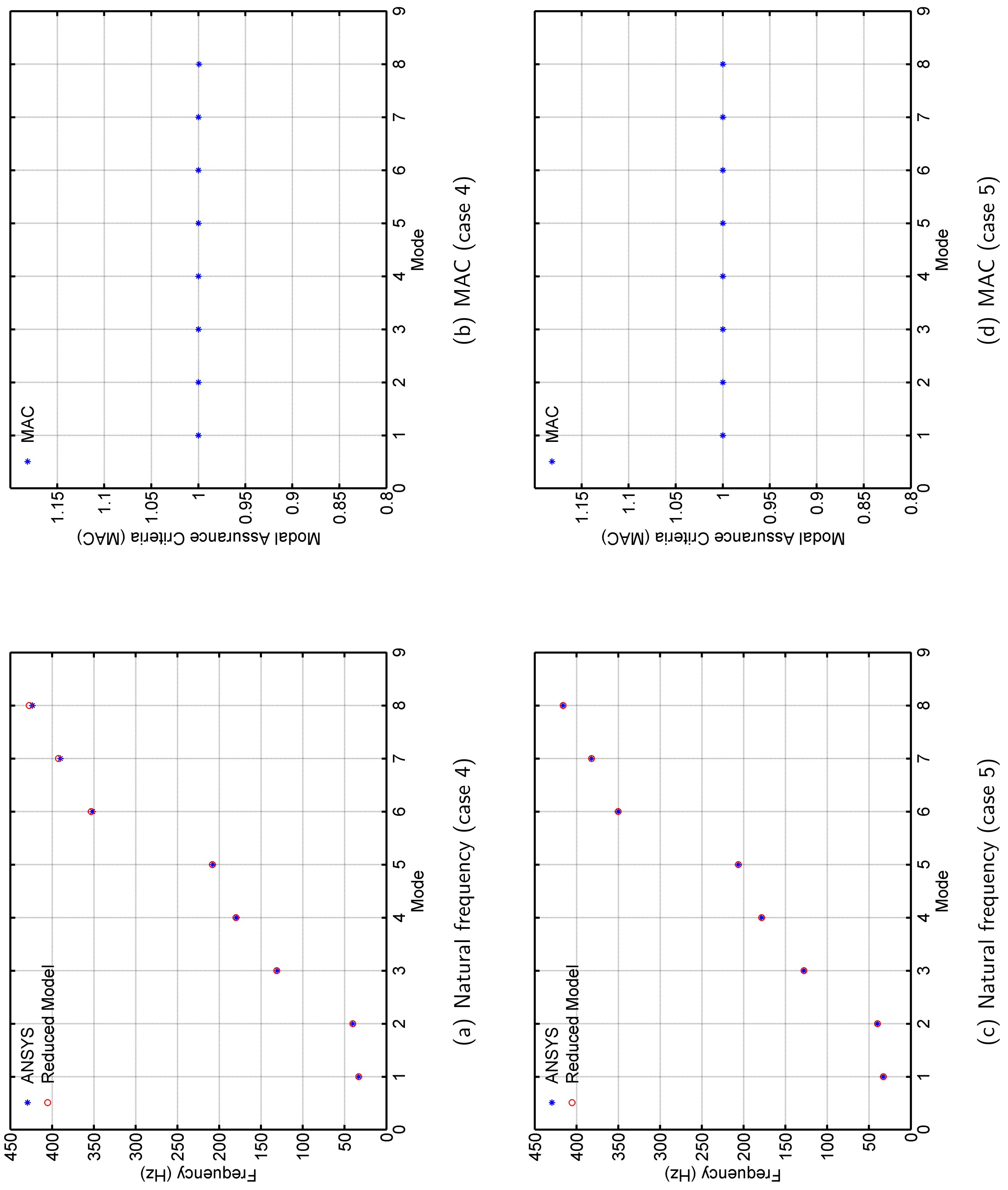

(a) Natural frequency (case 4)

(b) MAC (case 4)

(c) Natural frequency (case 5)

(d) MAC (case 5)

Figure B.7.: Comparison of natural frequencies and MAC values of active truss structure (case 4–5)

B.3. Results from dynamic analysis of solar panel model

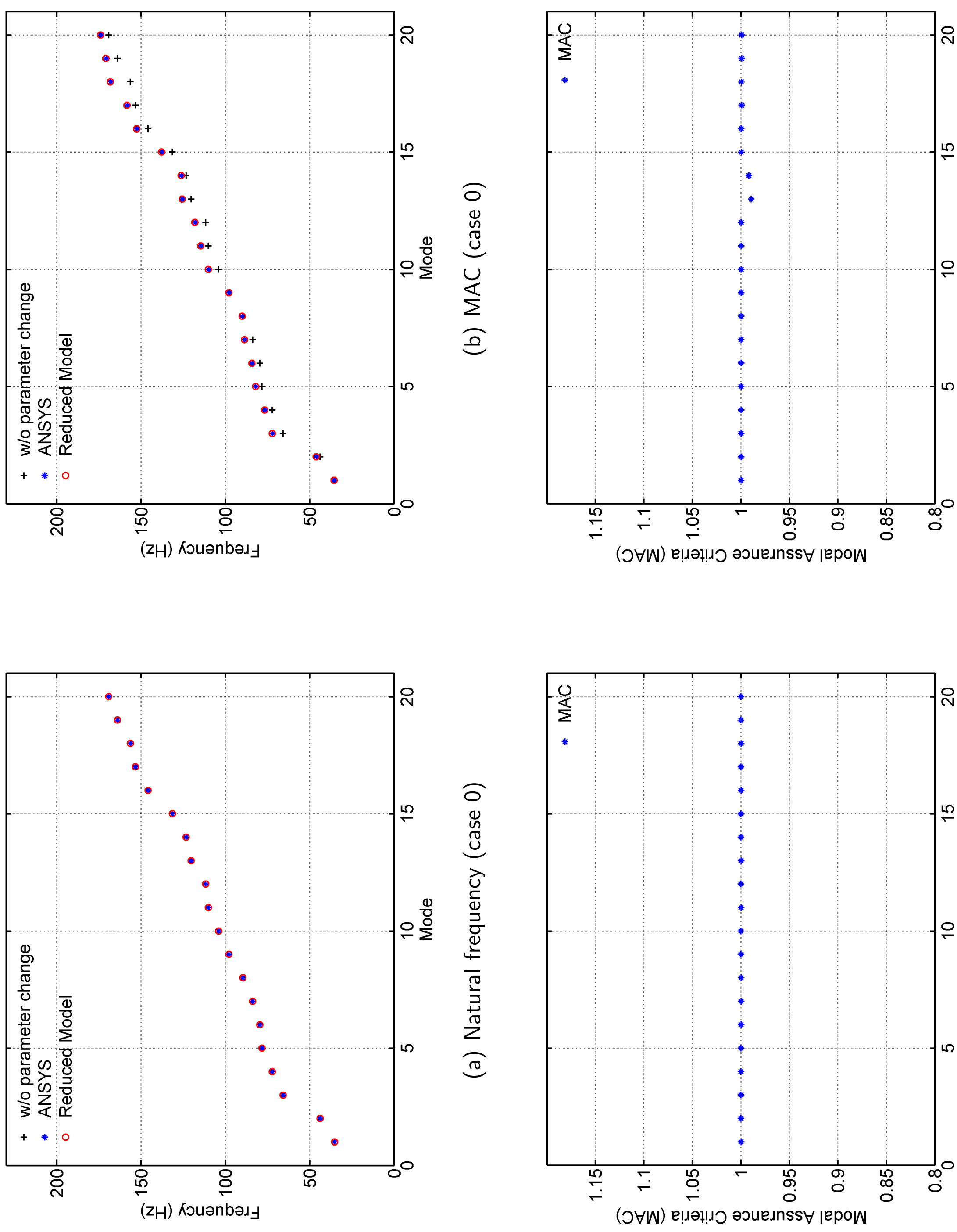

Figure B.8.: Comparison of natural frequencies and MAC values of solar panel model (case 0-1)

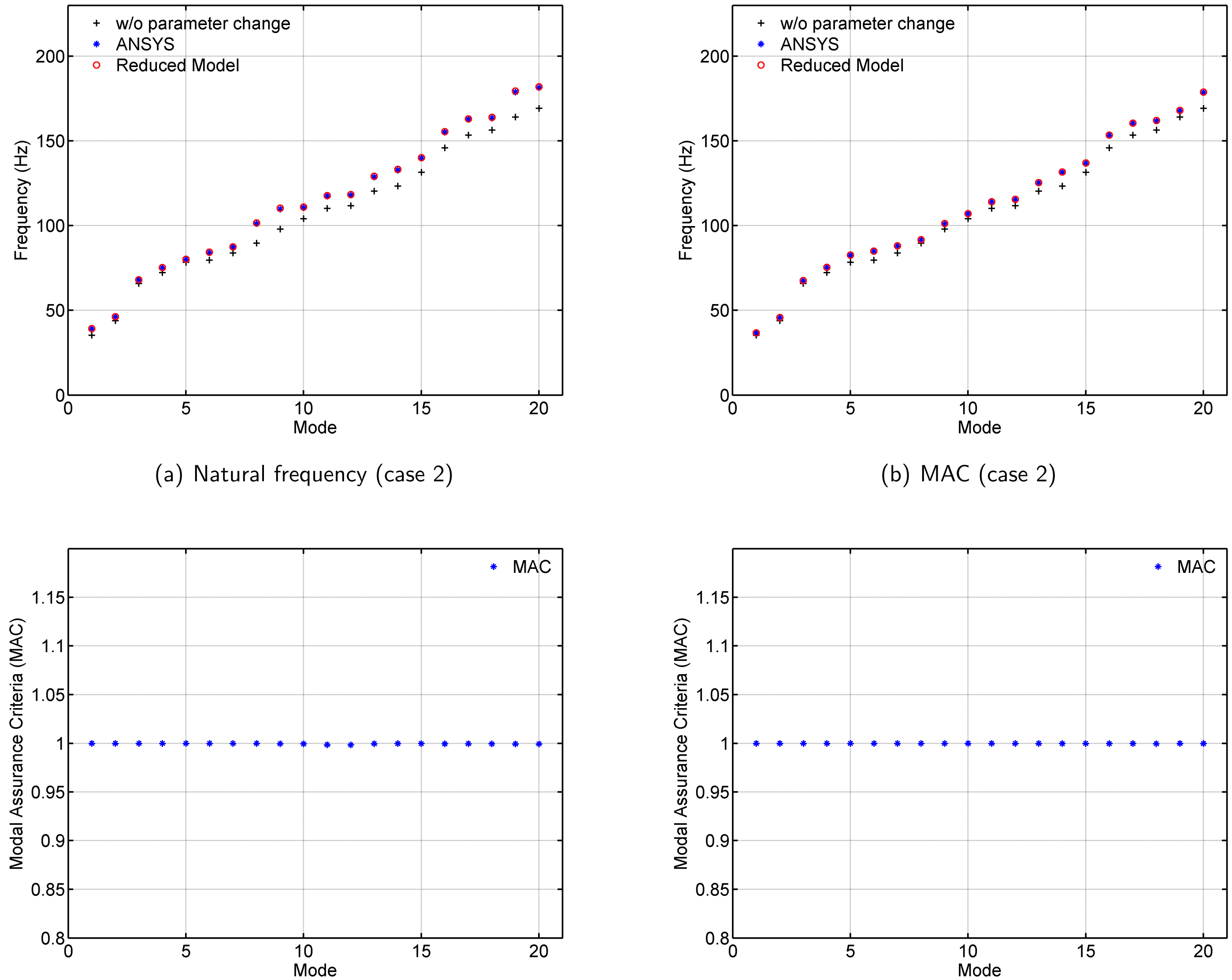

(a) Natural frequency (case 2)

(b) MAC (case 2)

(c) Natural frequency (case 3)

(d) MAC (case 3)

Figure B.9.: Comparison of natural frequencies and MAC values of solar panel model (case 2-3)

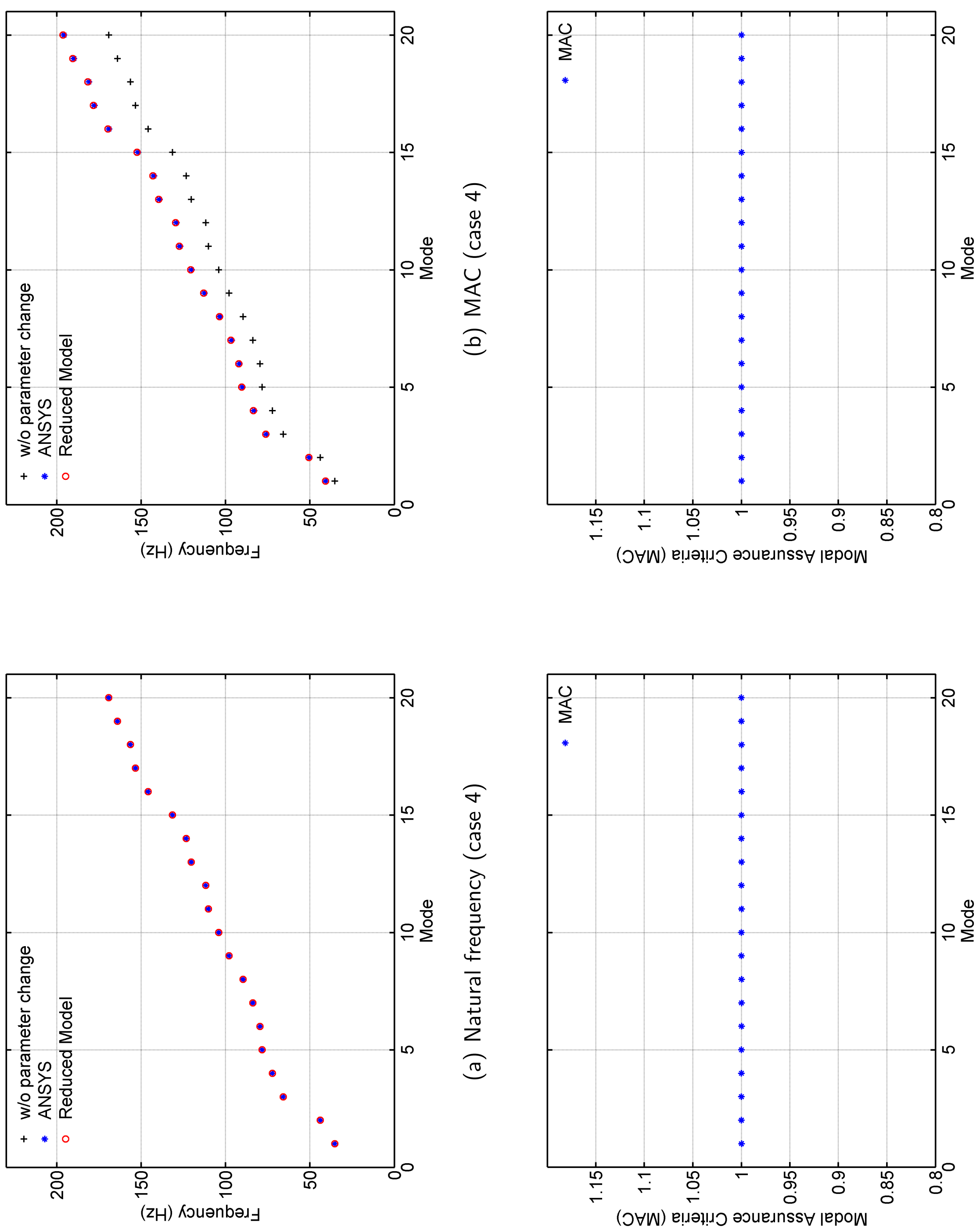

Figure B.10.: Comparison of natural frequencies and MAC values of solar panel model (case 4–5)

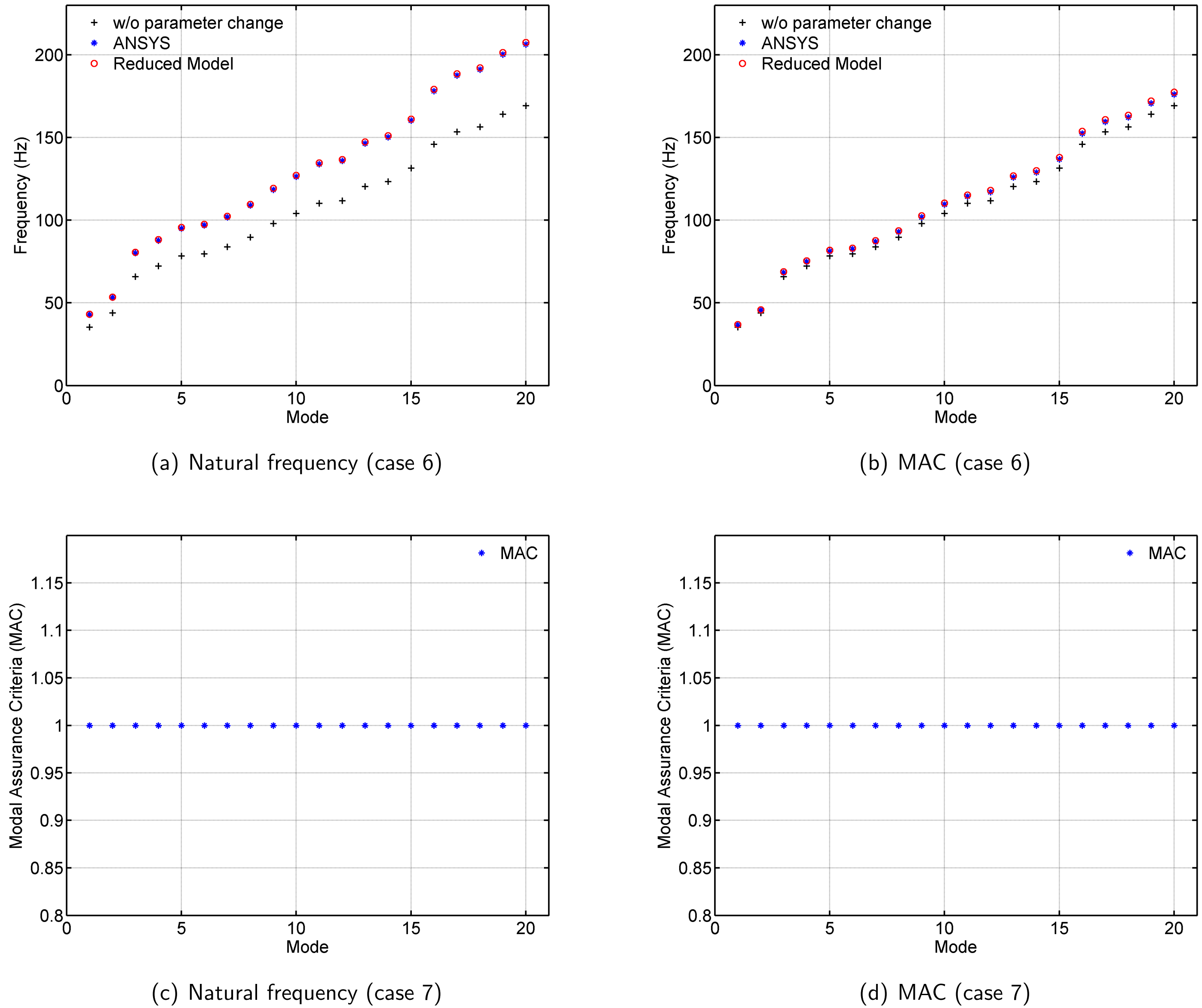

(a) Natural frequency (case 6)

(b) MAC (case 6)

(c) Natural frequency (case 7)

(d) MAC (case 7)

Figure B.11.: Comparison of natural frequencies and MAC values of solar panel model (case 6-7)

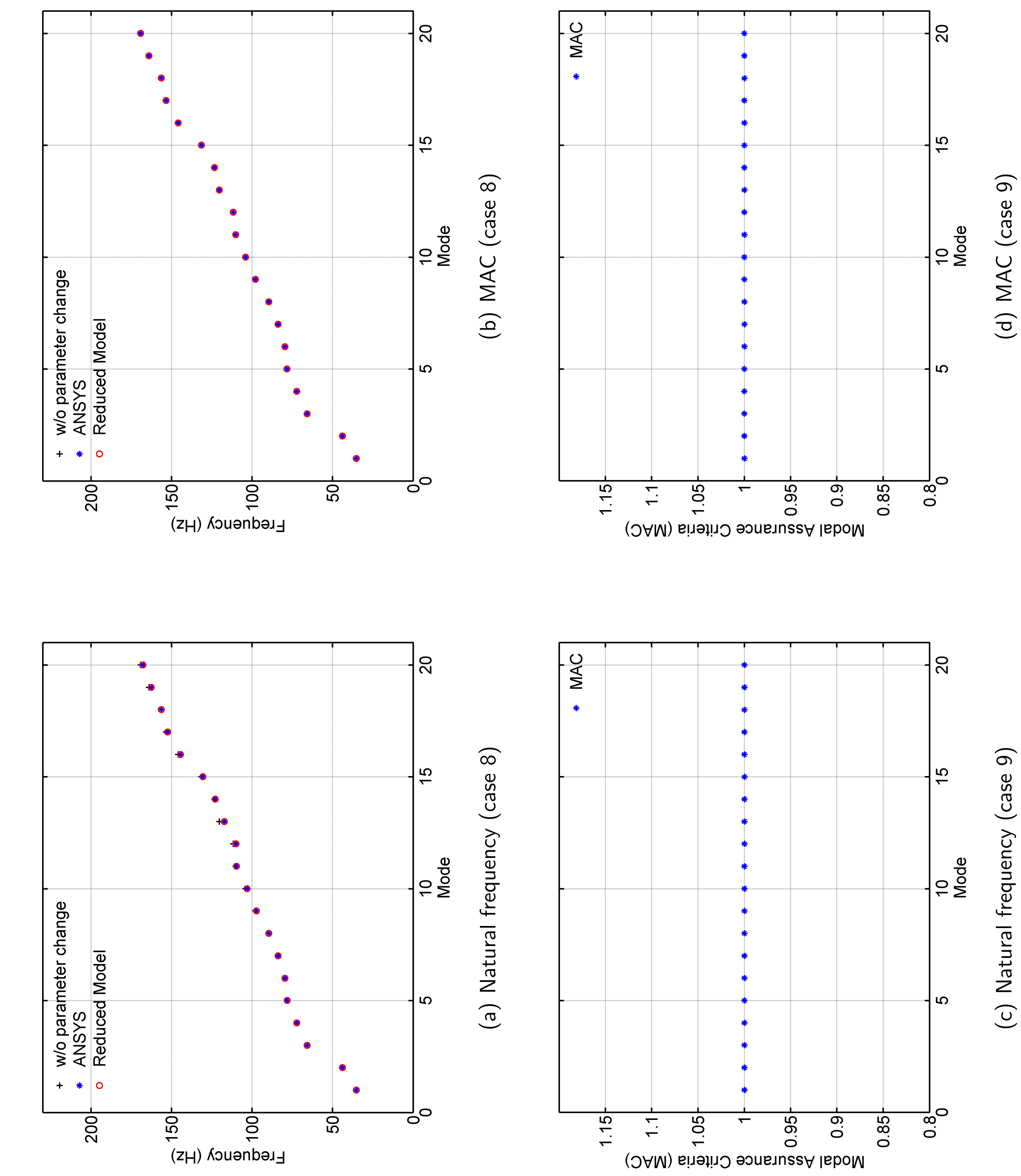

(a) Natural frequency (case 8)

(b) MAC (case 8)

(c) Natural frequency (case 9)

(d) MAC (case 9)

Figure B.12.: Comparison of natural frequencies and MAC values of solar panel model (case 8-9)

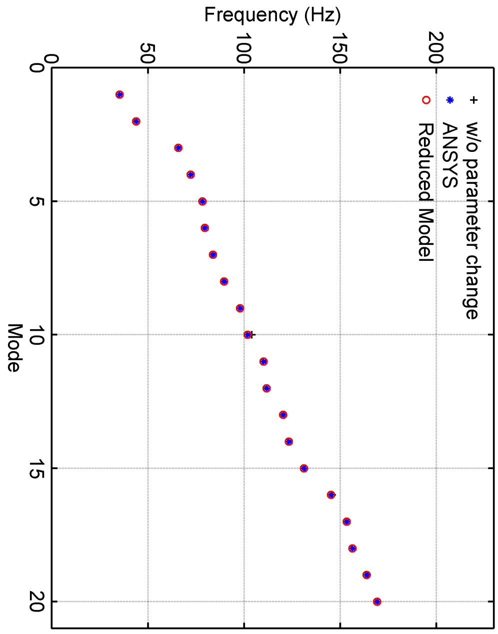

(a) Natural frequency (case 10)

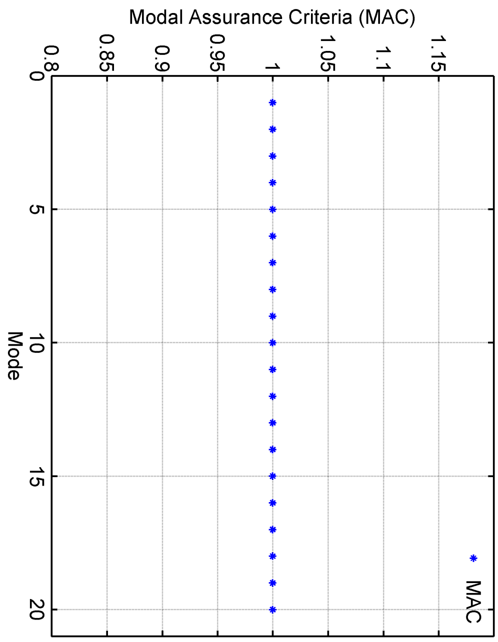

(b) MAC (case 10)

Figure B.13.: Comparison of natural frequencies and MAC values of solar panel model (case 10)

B.4. Vibration control of solar panel model with parameter case 11

		index number		PI value	
	order	FM	RM	FM	RM
mode 1	1	3, 18	3, 18	1.00	1.00
	2	44, 45	44, 45	0.74	0.61
	3	28, 29	28, 29	0.73	0.59
	4	62, 63	62, 63	0.66	0.55
mode 2	1	504, 517	504, 517	1.00	1.00
	2	487, 498	487, 498	0.95	0.94
	3	550, 551	419, 420	0.16	0.12
	4	471, 482	550, 551	0.15	0.12
mode 3	1	142, 143	215, 226	1.00	1.00
	2	215, 226	142, 143	0.96	0.86
	3	122, 123	122, 123	0.90	0.78
	4	141, 144	141, 144	0.88	0.77
mode 6	1	215, 226	215, 226	1.00	1.00
	2	196, 209	196, 209	0.69	0.69
	3	248, 259	37, 52	0.43	0.41
	4	37, 52	248, 259	0.41	0.36
mode 10	1	486, 499	486, 499	1.00	1.00
	2	503, 518	503, 518	0.56	0.53
	3	487, 498	487, 498	0.51	0.52
	4	504, 517	504, 517	0.49	0.47

Table B.1.: Highest performance index (PI) values and corresponding element numbers for actuator selection of solar panel model (case 11)

	order	index number FM	index number RM	PI value FM	PI value RM
mode 1	1	181	181	1.00	1.00
	2	180, 182	180, 182	0.97	0.97
	3	179, 183	179, 183	0.90	0.90
mode 2	1	82	82	1.00	1.00
	2	81, 83	81, 83	0.98	0.98
	3	80, 84	80, 84	0.92	0.92
mode 3	1	181	181	1.00	1.00
	2	180, 182	180, 182	0.98	0.98
	3	179, 183	179, 183	0.93	0.93
mode 6	1	18, 146	18, 146	1.00	1.00
	2	17, 147	17, 147	0.97	0.97
	3	19, 145	19, 145	0.95	0.95
mode 10	1	2, 62	2, 62	1.00	1.00
	2	63, 101	63, 101	0.90	0.89
	3	64, 100	64, 100	0.79	0.79

Table B.2.: Highest performance index (PI) values and corresponding node numbers for sensor selection of solar panel model (case 11)

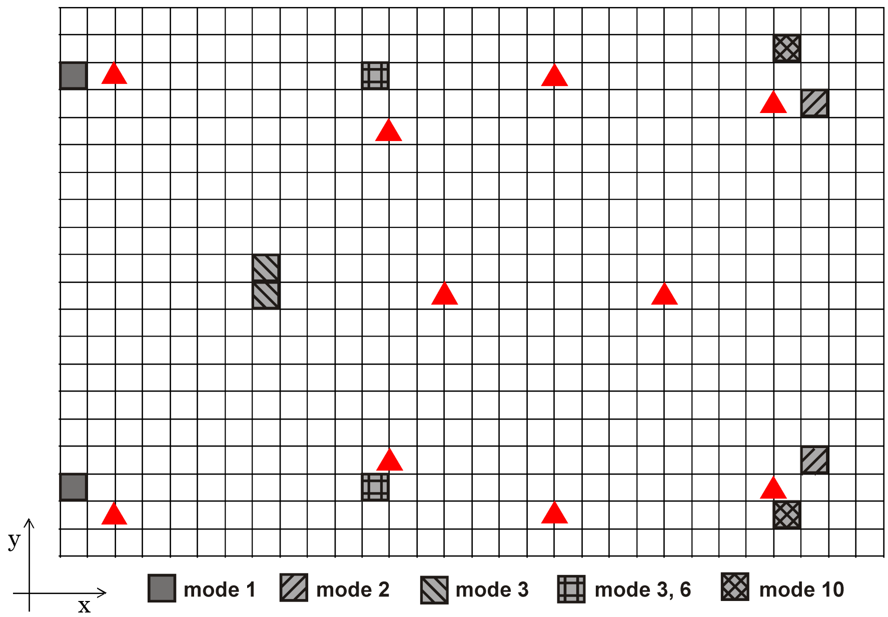

Figure B.14.: Actuator locations for active damping of solar panel model (case 11)

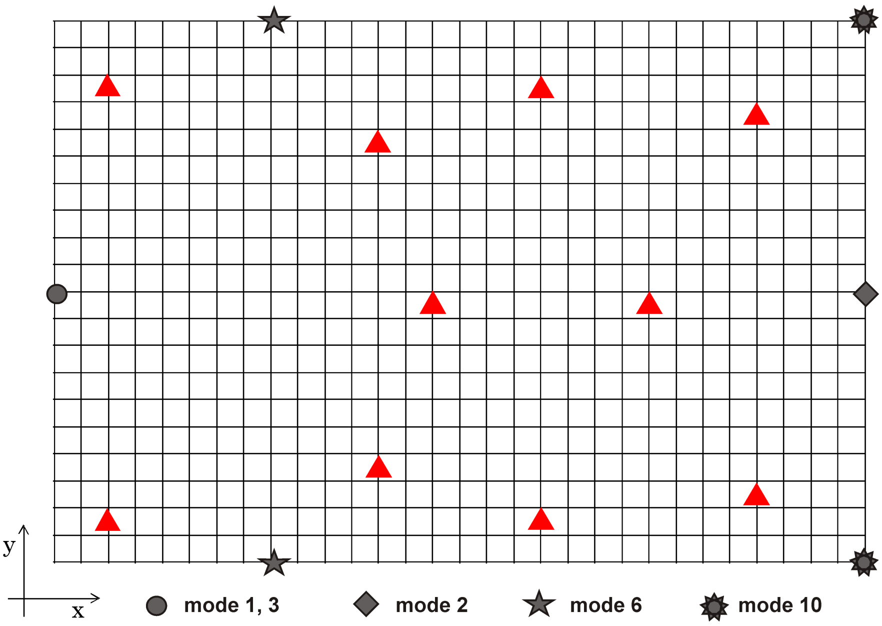

Figure B.15.: Sensor locations for active damping of solar panel model (case 11)

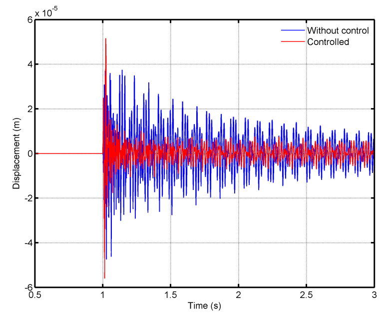

(a) sensor 1

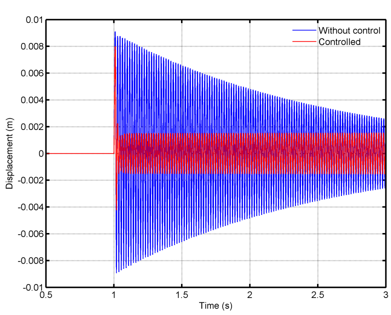

(b) sensor 2

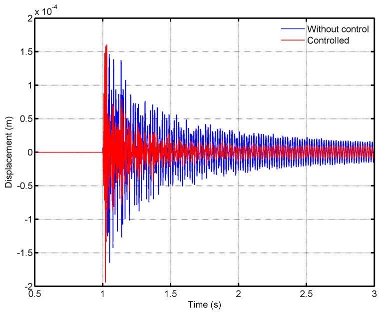

(c) sensor 3

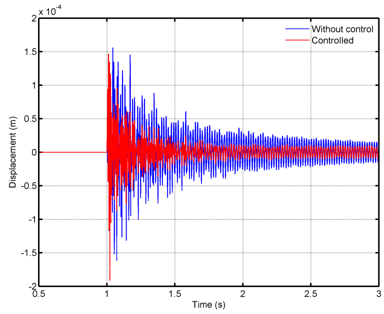

(d) sensor 4

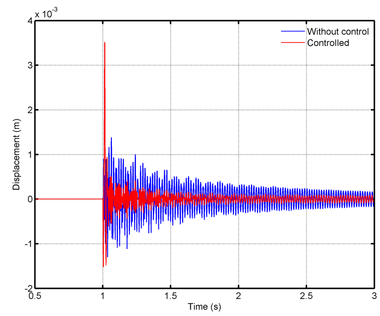

(e) sensor 5

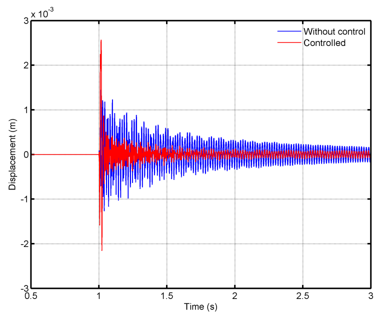

(f) sensor 6

Figure B.16.: Displacement plot from sensors (case 11)

Bibliography

[ACCF09] D. Amsallem, J. Cortial, K. Carlberg, and C. Farhat. An on-line method for interpolating linear reduced-order structural dynamics models. *Proceedings of 50th AIAA/ASME/ASCE/AHS/ASC Structures, Structural Dynamics, and Materials Conference*, page published online, 2009. 1.2.2, 3.4.2

[ANS07] Ansys, inc. theory reference. Release 11.0 Documentation for ANSYS, 2007. 4.4.2

[Arn51] W. E. Arnoldi. The principle of minimized iterations in the solution of the matrix eigenvalue problem. *Quarterly of Applied Mathematics*, 9:17–29, 1951. 1.2.1

[ASG01] A. C. Antoulas, D. C. Sorensen, and S. Gugercin. A survey of model reduction methods for large-scale systems. *Structured Matrices in Operator Theory, Numerical Analysis, Control, Signal and Image Processing*, (280):193–219, 2001. 1.2.1

[BD05] B. Bond and L. Daniel. Parameterized model order reduction of nonlinear dynamical systems. *Proceedings of International Conference on Computer Aided Design*, 6(10):487–494, November 2005. 1.2.2

[Ben06] P. Benner. Numerical linear algebra for model reduction in control and simulation. *GAMM Mitteilungen*, 29(2):275–296, 2006. 1.2.1

[Bol94] D. L. Boley. Krylov space methods on state-space control models. *Circuits, Systems, and Signal Processing*, 13(6):733–758, November 1994. 1.2.1

[BS05] Z. Bai and Y. Su. Soar: a second-order arnoldi method for the solution of the quadratic eigenvalue problem. *SIAM Journal on Matrix Analysis and Applications*, 26(3):640–659, 2005. 1.2.1

[CB68] R. R. Craig and M. C. Bampton. Coupling of substructures for dynamic analyses. *AIAA Journal*, 6(7):1313–1319, July 1968. 1.2.1

[CLF06] C. C. Chu, M. H. Lai, and W. S. Feng. Mimo interconnects order reductions by using the multiple point adaptive-order rational global arnoldi algorithm. *IEICE transactions on electronics*, 89(6):792–802, June 2006. 1.2.1

[CR94] Z. Chaudhry and C. A. Rogers. The pin-force model revisited. *Journal of Intelligent Material Systems and Structures*, 5:347–354, 1994. A.3, A.3

[DSC$^+$04] L Daniel, O. C. Siong, L. S. Chay, K. H. Lee, and J. White. A multiparameter moment-matching model-reduction approach for generating geometrically parameterized interconnect performance models. *IEEE Transactions on Computer-Aided Design of Integrated Circuits and Systems*, 23(5):678–693, May 2004. 1.2.2, 3.3, 3.3, 3.3, 3.3.2, 3.3.3, 5.1.1

[DVW09] J. Degroote, J. Vierendeels, and K. Willcox. Interpolation among reduced-order matrices to obtain parameterized models for design, optimization and probabilistic analysis. *International Journal for Numerical Methods in Fluids*, page published online, 2009. 1.2.2, 3.4.2

[Enn84] D. F. Enns. Model reduction with balanced realization: An error bound and a frequency weighted generalization. In *Proceedings of 23rd Conference on Decision and Control*, December 1984. 1.2.1

[ESL$^+$06] R. Eid, B. Salimbahrami, B. Lohmann, E. B. Rudnyi, and J. G. Korvink. Parametric order reduction of proportionally damped second order systems. In *Technical Reports on Automatic Control*, volume 1, October 2006. 4.3

[FGEM93] R. W. Freund, M. H. Gutknecht, M. El, and Nachtigal N. M. An implementation of the look-ahead lanczos algorithm for non-hermitian matrices. *SIAM Journal on Scientific Computing*, 14(1):137–158, January 1993. 1.2.1

[FI01] B.F. Farrell and P.J. Ioannou. Accurate low dimensional approximation of the linear dynamics of fluid flow. *Journal of the Atmospheric Sciences*, 58(18):2771–2789, 2001. 1.2.1

[FK98] B. F. Feeny and R. Kappagantu. On the physical interpretation of proper orthogonal modes in vibrations. *Journal of Sound and Vibration*, 211(4):607–616, 1998. 1.2.1

[FKRK05] L. H. Feng, D. Koziol, E. B. Rudnyi, and J. G. Korvink. Parametric model order reduction for scanning electrochemical microscopy: Fast simulation of cyclic voltammogram. In *Proceedings of 6th International conference on thermal and mechanical simulation and experiments in microelectronics and microsystems, EUROSIME 2005*, pages 18–20, 2005. 1.2.2

[Fla90] C. C. Flanigan. Implementation of the irs dynamic reduction method in msc/nastran. In *MSC/NASTRAN World Users Conference*, March 1990. 1.2.1

[FR95] P. Feldmann and Freund R. Efficient linear circuit analysis by pade approximation via the lanczos process. *IEEE Transactions on Computer-aided Design of Integrated Circuits and Systems*, 14(5):639–649, 1995. 1.2.1, 2.3.1

[FRK05] L. H. Feng, E. B. Rudnyi, and J. G. Korvink. Preserving the film coefficient as a parameter in the compact thermal model for fast electrothermal simulation. *IEEE Transactions on Computer-Aided Design* *of Integrated Circuits and Systems*, 24(12):1838–1847, December 2005. 1.2.2

[GAB01] S. Gugercin, A. C. Antoulas, and N. Bedrossian. Approximation of international space station 1r and 12a models. *Proceedings of the 40th IEEE Conference on Decision and Control*, 3:1515–1516, December 2001. 1.2.1

[GAB08] S. Gugercin, A. C. Antoulas, and C. A. Beattie. h_2 model reduction for large-scale linear dynamic systems. *SIAM Journal on Matrix Analysis and Applications*, 30(2):609–638, 2008. 1.2.2

[Gaw98] W. K. Gawronski. *Dynamics and Control of Structures - A Modal Approach*. Springer, New York, USA, 1998. 1.2.1, 2.2, 5.2.1

[Gil06] Eduardo Gildin. *Model and Controller Reduction of Large-Scale Structures Based on Projection Methods*. Ph.d. thesis, Faculty of Graduate School of The University of Texas at Austin, Texas Austin, USA, 2006. 1.2.2

[GKN+03] P. K. Gunupudi, R. Khazaka, M. S. Nakhla, T. Smy, and D. Celo. Passive parameterized time-domain macromodels for high-speed transmission-line networks. *IEEE Transactions on Microwave Theory and Techniques*, 51(12):2347–2354, December 2003. 3.3.1

[GL] S. Gugercin and J. R. Li. Smith-type methods for balanced truncation of large-sparse systems. In P. Benner, V. L. Golub, G. H. Mehrman, and D. C. Sorensen, editors, *Dimension Reduction of Large-scale Systems*, pages 49–82. Springer, Berlin/Heidelberg. 2.2

[GL83] W. B. Gragg and A. Lindquist. On the partial realization problem. *Linear Algebra and Its Applications*, 50:277–319, 1983. 1.2.1

[GLO81] G. H. Golub, F. T. Luk, and M. L. Overton. A block lanczos method for computing the singular values and corresponding singular vectors of a matrix. *ACM Transactions on Mathematical Software*, 7(2):149–169, June 1981. 1.2.1

[Glo84] K. Glover. All optimal hankel-norm approximations of linear multivariable systems and their l-infinity error bounds. *International Journal of Control*, 39(6):1115–1193, June 1984. 1.2.1

[GN00] P. Gunupudi and M. Nakhla. Multi-dimensional model reduction of vlsi interconnects. In *Proceedings of IEEE Custom Integrated Circuits Conference*, pages 499–502, 2000. 3.3.1

[GS99] I. T. Georgiou and I. B. Schwartz. Dynamics of large scale coupled structural mechanical systems: A singular perturbation proper orthogonal decomposition approach. *SIAM Journal on Applied Mathematics*, 59(4):1178–1207, 1999. 1.2.1

[GSA03] S. Gugercin, D. C. Sorensen, and A. C. Antoulas. A modified low-rank smith method for large-scale lyapunov equations. *Numerical Algorithms*, 32(1):27–55, 2003. 1.2.1, 2.2

[Guy65] R. J. Guyan. Reduction of stiffness and mass matrices. *AIAA Journal*, 3(2):380, 1965. 1.2.1, 1.2.1

[Hexa] Hexcel carbon fiber data sheets. http://www.hexcel.com/Products/Downloads/Carbon Fiber Data Sheets/. 5.1.1

[Hexb] Hexweb honeycomb attributes and properties. http://www.hexcel.com/NR/rdonlyres/599A3453-316D-46D6-9AEE-C337D8B547CA/0/HexwebAttributesandProperties.pdf. 5.1.1

[HL93] A. Hać and L. Liu. Sensor and actuator location in motion control of flexible structures. *Journal of Sound and Vibration*, 167(2):239–261, 1993. A.1, A.1

[KCJ88] H. M. Kim and R. R. Craig Jr. Structural dynamics analysis using an unsymmetric block lanczos algorithm. *International Journal for Numerical Methods in Engineering*, 26(10):2305 – 2318, 1988. 1.2.1

[KF00a] R. Kappagantu and B. F. Feeny. Part 1: Dynamical characterization of a frictionally excited beam. *Nonlinear Dynamics*, (22):317–333, 2000. 1.2.1

[KF00b] R. Kappagantu and B. F. Feeny. Part 2: Proper orthogonal modal modeling of a frictionally excited beam. *Nonlinear Dynamics*, (23):1–11, 2000. 1.2.1

[Lan50] C. Lanczos. An iteration method for the solution of the eigenvalue problem of linear differential and integral operators. *Journal of Research of the National Bureau of Standards*, 45(4):255–282, October 1950. 1.2.1

[LBW07] Y. Lin, L. Bao, and Y. Wei. Model-order reduction of large-scale second-order mimo dynamical systems via a block second-order arnoldi method. *International Journal of Computer Mathematics*, 84(7):1003–1019, July 2007. 1.2.1

[LE09] B. Lohmann and R. Eid. Efficient order reduction of parametric and nonlinear models by superposition of locally reduced models. In *Methoden und Anwendungen der Regelungstechnik, Erlangen-Münchener Workshops*, 2009. 1.2.2, 3.4.1, 3.4.1

[LHPW87] A. J. Laub, M. T. Heath, C. C. Paige, and R. C. Ward. Computation of system balancing transformations and other applications of simultaneous diagonalization algorithms. *IEEE Transactions on Automatic Control*, 32(2):115–122, February 1987. 2.2

[LK05] A. T. Leung and R. Khazaka. Parametric model order reduction technique for design optimization. *Proceedings of IEEE International Sym-*

posium on Circuits and Systems (ISCAS), 2:1290– 1293, May 2005. 3.3.3

[LLL+01] Y. C. Liang, W. Z. Lin, H. P. Lee, S. P. Lim, K. H. Lee, and D. P. Feng. A neural-network-based method of model reduction for the dynamic simulation of mems. *Journal of Micromechanics and Microengineering*, (11):226–233, 2001. 1.2.1

[Loc01] G. Locatelli. *Piezo-actuated adaptive structures for vibration damping and shape control - modeling and testing*. Ph. d. dissertation, Fakultät für Maschinenwesen, Technische Universität München, München, Germany, 2001. A.3

[LS96] R. B. Lehoucq and D. C. Sorensen. Deflation techniques for an implicitly restarted arnoldi iteration. *SIAM Journal on Matrix Analysis and Applications*, 17(4):789 – 821, October 1996. 1.2.1

[LV] J. Lampe and H. Voss. *Second order Arnoldi reduction: application to some engineering problems*, chapter Report 93. 1.2.1

[MB] M. Müller and H. Baier. Structural modeling interface for the eso integrated modeling toolbox (user manual). Lehrstuhl fü Leichtbau, Technische Universität München. 5

[MM03] M. M. Mansour and A. Mehrotra. Model-order reduction based on prony's method. In *Proceedings of Automation and Test in Europe Conference and Exhibition (DATE'03)*, March 2003. 1.2.1

[Moo81] B. C. Moore. Principle component analysis in linear systems: Controllability, and observability, and model reduction. *IEEE Transacttions on Automatic Control*, 26(1):17–32, February 1981. 1.2.1

[MRG+05] C. Moosmann, E. B. Rudnyi, A. Greiner, J. G. Korvink, and M. Hornung. Parameter preserving model order reduction of a flow meter. *Technical Proceedings of Nanotechnology Conference and Trade Show*, 3:684–687, May 2005. 1.2.2

[MVB01] X. Ma, A. F. Vakakis, and L. A. Bergman. Karhunenloéve modes of a truss: Transient response reconstruction and experimental verification. *AIAA JOURNAL*, 39(4):687–696, 2001. 1.2.1

[OCP98] A. Odabasioglu, M. Celik, and L. Pileggi. Prima: passive reduced-order interconnect macromodeling algorithm. *IEEE Transactions on Computer-aided Design of Integrated Circuits and Systems*, 17(8):645–654, 1998. 1.2.1

[Pet05] Oegmundur Petersson. *Optimisation of the OWL telescope main mirror segments*. Master thesis, Faculty of Mechanical Engineering, Technical University Munich, Boltzmannstr. 15, 85748 Garching, GERMANY, 2005. 5.3.2

[PR90] L. Pillage and R. Rohrer. Asymptotic waveform evaluation for timing analysis. *IEEE Transactions on Computer-aided Design of Integrated Circuits and Systems*, 9(4):352–366, 1990. 1.2.1

[PS05] J. R. Phillips and L. M. Silveira. Poor man's tbr: A simple model reduction scheme. *IEEE Transactions on Computer-Aided Design of Integrated Circuits and Systems*, 24(1):43–55, January 2005. 1.2.2

[RFS+] E. B. Rudnyi, L. H. Feng, M. Salleras, S. Marco, and J. G. Korvink. Error indicator to automatically generate dynamic compact parameteric thermal models. In *Proceedings of 11th International workshop on thermal investigation of ICs and systems*, pages 139–145, September. 1.2.2

[RS98] A. Ruhe and D. Skoogh. Rational krylov algorithms for eigenvalue computation and model reduction. *Proceedings of Applied Parallel Computing Large Scale Scientific and Industrial Problems, 4th International Workshop, PARA*, 1541:491–502, 1998. 1.2.2

[Ruh84] A. Ruhe. Rational krylov sequence methods for eigenvalue computation. *Linear Algebra and its Applications*, 58:391–405, 1984. 1.2.2

[Sal05] B. Salimbahrami. *Structure Preserving Order Reduction of Large Scale Second Order Models*. Ph. d. dissertation, Fakultät für Maschinenwesen, Technische Universität München, München, Germany, 2005. 1.2.1

[SBLK03] B. Salimbahrami, T. Bechtold, B. Lohmann, and J. G. Korvink. Two-sided arnoldi algorithm and its application in order reduction of mems. In *Proceedings of 4th MATHMOD, Vienna*, February 2003. 1.2.1, 2.3.2

[SHS06] G. Shi, B. Hu, and C. J. R. Shi. On symbolic model order reduction. *IEEE Transactions on Computer-Aided Design of Integrated Circuits and Systems*, 25(7):1257–1272, July 2006. 1.2.2, 3.2

[Sir87] L. Sirovich. Turbulence and the dynamics of coherent structures - part 1: Coherent structures. *Quarterly of Applied Mathematics*, 45(3):561–571, October 1987. 1.2.1

[SKEW99] L. M. Silveira, M. Kamon, I. Elfadel, and J. White. A coordinate-transformed arnoldi algorithms for generating guaranteed stable reduced-order models of rlc circuits. *Computer Methods in Applied Mechanics and Engineering*, 169(3-4):377–389, February 1999. 1.2.1

[SL99] R. D. Slone and R Lee. Matrix pade via lanczos for fem problems. In *Proceedings of Antennas and Propagation Society International Symposium*, August 1999. 1.2.1

[TH80] S. W. Tsai and H. T. Hahn. *Introduction to composite materials*. Technomic Publishing Company, Lancaster, Pennsylvania, USA, 1980. A.5

[VS87] C. Villemagne and R. L. Skelton. Model reductions using projection formulation. *International Journal of Control*, 46(6):2141–2169, 1987. 1.2.1

[WM01] D. S. Weile and E. Michielssen. Analysis of frequency selective surfaces using two-parameter generalized rational krylov model-order reduction. *IEEE Transactions of Antennas and Propagation*, 49(11):1539–1549, November 2001. 1.2.2

[WMSW02] T. Wittig, I. Munteanu, R. Schuhmann, and T. Weiland. Two-step lanczos algorithm for model order reduction. *IEEE Transactions on Magnetics*, 38(2):673–676, 2002. 1.2.1

[WP02] K. Willcox and J. Peraire. Balanced model reduction via the proper orthogonal decomposition. *AIAA Journal*, 40(11):2323–2330, November 2002. 1.2.1

[YB09] E. J. Yoo and H. Baier. Parametric model order reduction techniques for simulating active shape and vibration control of the large space structures. In *Proceedings of European Conference on Spacecraft Structures, Materials, and Mechanical Testing*, September 2009. 1.2.1, 4.5

[YRS04] R. Yu, S. Roberts, and I. Sharf. Model order reduction of structural dynamics of a very large optical telescope. In *Proceedings of SPIE Conference*, volume 5497, 2004. 1.2.1

[ZP07] Z. Zhu and J. Phillips. Random sampling of moment graph: A stochastic krylov-reduction algorithm. In *Proceedings of Design, Automation Test in Europe Conference Exhibition (DATE)*, pages 1502–1507, 2007. 3.3.2, 3.3.2